Identification of Arhgap28, a New Regulator of Stress Fibre Formation in Cells Assembling a Fibrous Extracellular Matrix

A thesis submitted to The University of Manchester for the degree of Doctor of Philosophy in Cell Biology in the Faculty of Life Sciences

2012

Ching-Yan Chloé Yeung

CONTENTS

Word count: 29, 378

LIST OF FIGURES

LIST OF TABLES

Chapter 2. Methods and Materials

Chapter 3. Identification of a Candidate Regulator of Actin Reorganisation

Chapter 5. Study of Arhgap28 Function in the *Arhgap28^{gt}* Reporter Mouse and *Arhgap28^{del}* Knockout Mouse

LIST OF ABBREVIATIONS

2D, 3D	two-dimensional, three-dimensional
aa	amino acid residues
Arhgap28^{gt}	*Arhgap28 gene trap* allele
Arhgap28^{del}	*Arhgap28 del7-9* allele
d	day(s) from which cells are seeded into fibrin gels, before tendon constructs are formed
DAVID	Database for Annotation, Visualisation and Integrated Discovery
dChip	DNA-Chip Analzer (analysis software for normalising microarray readouts)
DLC	deleted in liver cancer (a RhoGAP)
DMEM	Dulbecco's modified Eagle's medium containing 4500 mg/l D-glucose, non-essential amino acids and 110 mg/l sodium pyruvate
E	embryonic day, day(s) post-coitum
ECM	extracellular matrix
ES cell	embryonic stem cell
FCS	foetal calf serum
F-actin	filamentous-actin
GAP	GTPase activating protein
GDI	guanine nucleotide dissociation inhibitors
GDP	guanosine diphosphate
GST	glutathione S-transferase
GTP	guanosine triphosphate
GTPase	guanosine triphosphatase
hMSC	human mesenchymal stem cell
KOMP	Knockout Mouse Project
LPA	lysophosphatidic acid
MLC	myosin light chain
MMP	matrix metalloproteinase
P	postnatal day
PAK	p21-activated kinase
PBS	phosphate-buffered saline
PCA	principal component analysis
PCR	polymerase chain reaction
PFA	paraformaldehyde
qPCR	quantitative PCR
ROCK	Rho-associated kinase
RT	reverse transcription
SEM	standard error of mean
siRNA	small interfering RNAs
T	day(s) from which tendon constructs are fully formed
TEM	transmission electron microscopy
V5	unique epitope tag (GKPIPNPLLGLDST)
WASP	Wiskott–Aldrich syndrome protein
WAVE	Wiskott-Aldrich syndrome protein verprolin homologous
Y27632	chemical inhibitor of ROCK

ABSTRACT

The motivation for this PhD thesis was to understand the molecular basis of how cells regulate the formation of an organised and mechanically strong extracellular matrix (ECM). In tendon this process begins during embryogenesis with the appearance of bundles of narrow-diameter (~30 nm) collagen fibrils that are parallel to the tendon long axis. At the onset of collagen fibrillogenesis, the cells elongate, the fibrils are constrained within plasma membrane channels with their ends contained in tension-sensitive actin-stabilised plasma membrane protrusions. The mechanism by which actin is reorganised during cell elongation and the formation of tension-sensitive plasma membrane protrusions is poorly understood. The small GTPase RhoA is the major regulator of actin reorganisation into stress fibres, which have been implicated in mechanotransduction, ECM assembly and remodelling. The hypothesis tested by this PhD thesis was that the organisation and tensioning of extracellular collagen fibrils is generated on a blueprint of tensioned actin filaments within the cell. Rho activity is regulated specifically by Rho GTPase activating proteins (RhoGAPs). By comparing the global gene expression of tendon tissues at different developmental stages, Arhgap28, a novel RhoGAP, which is expressed during tendon development but not during postnatal maturation, was identified.

Arhgap28 belongs to a large family of RhoGAPs containing the closely related members, Arhgap6 and Arhgap18, which have previously been shown to regulate RhoA and stress fibre formation. Arhgap28 expression was upregulated in embryonic fibroblasts cultured in a 3D, tensioned embryonic tendon-like construct compared to monolayer culture. Arhgap28 expression was further enhanced during the development of mechanical strength and stiffness of the tendon constructs, but downregulated when the tension in tendon constructs was released. Overexpression of a C-terminal V5-tagged Arhgap28 protein caused a reduction in RhoA activation and disruption of stress fibre assembly. Modulation of Rho signalling using lysophosphatidic acid and Y27632 showed that collagen remodelling by cells in collagen gels and tendon constructs is regulated by RhoA signalling. A tissue-wide qPCR analysis identified Arhgap28 in several tissues including tendon, bone, and skin. An Arhgap28 reporter mouse (*Arhgap28*^{gt}) and an Arhgap28 knockout mouse (*Arhgap28*^{del}) were also studied to investigate the role of Arhgap28 in tissue organisation *in vivo*. *Arhgap28*^{gt} mice showed Arhgap28 expression in bones at E18.5. Homozygous *Arhgap28*^{del} mice were viable, appeared normal but expressed a truncated Arhgap28 transcript, which if translated, would produce a protein lacking the RhoGAP domain. Therefore, it was hypothesised that knockout mice were normal due to compensation from another RhoGAP. Overexpression of Arhgap6 in Arhgap28-null bone tissues was confirmed. Upregulation in RhoA expression was also detected, further suggesting that Arhgap28 regulates RhoA. Interestingly, a microarray comparison of bone tissues from wild type and Arhgap28-null mice showed that genes linked to bone dysplasia are downregulated in Arhgap28-null bone. Together, these results suggest that formation of a strong and organised collagen ECM is mediated by RhoA-generated cellular tension and that Arhgap28 and Arhgap6 might be co-regulators of this process.

LAY ABSTRACT

Discovery of Arhgap28, a Molecule Involved in Controlling Cell Forces Important in Making a Strong Tendon

Movements of the body such as running or gripping a door handle require strong tissue types such as muscle, bone, tendon, ligament and cartilage. These tissues make up the musculoskeletal system. Their ability to transmit and withstand mechanical loading is because of a rope-like protein called collagen, which surrounds the cells. Collagen is important as it allows tissues of the body to endure the constant forces of being pulled, pushed and squashed. In bone tissue, these fibrils are woven together to allow calcium to bind, which creates strong bone that can bear the weight of the body. The collagen ropes or 'fibrils' in tendon are bundled together like a rope so that tendons can be stretched repetitively without breaking. How the collagen fibrils are organised is linked to the function of the tissue. A disadvantage of having such a unique and strong tissue structure is that once damaged, the collagen fibrils do not fully repair, often resulting in poor healing and long-term recovery. It is estimated that the annual cost of tendon injury in the UK is £25 billion. Scientists led by Professor Karl Kadler at the University of Manchester want to understand how organisation of collagen fibrils is established during the formation of musculoskeletal tissues, so that new medical treatments to improve tissue healing may be developed.

As a starting point, the scientists began studying tendon tissue. Since 2004, they have discovered that the cells that live in tendon are responsible for organising the collagen fibrils into non-crisscrossing, straight strands. They found that the cell scaffolding plays important roles in the organisation of collagen fibrils and in generating pulling forces used to make tendons strong. This PhD project investigated the idea that the organisation of the scaffolding inside the cell is responsible for determining the arrangement of the collagen fibrils outside the cell. Scientists found a gene called Arhgap28 that is more prevalent in cells when they make tendon tissues. Experiments showed that Arhgap28 could prevent the cell scaffolding from generating pulling forces. Scientists now think that Arhgap28 controls how the cell is able to touch and pull on fibrils so that they can be arranged correctly and produce a tissue that is not too stiff and not too loose. Further understanding of Arhgap28 would pave the way for improved therapeutics for musculoskeletal injuries in the future.

DECLARATION

No portion of the work referred to in the thesis has been submitted in support of an application for another degree or qualification of this or any other university or other institute of learning.

COPYRIGHT STATEMENT

i. The author of this thesis (including any appendices and/or schedules to this thesis) owns certain copyright or related rights in it (the "Copyright") and she has given The University of Manchester certain rights to use such Copyright, including for administrative purposes.

ii. Copies of this thesis, either in full or in extracts and whether in hard or electronic copy, may be made **only** in accordance with the Copyright, Designs and Patents Act 1988 (as amended) and regulations issued under it or, where appropriate, in accordance with licensing agreements which the University has from time to time. This page must form part of any such copies made.

iii. The ownership of certain Copyright, patents, designs, trade marks and other intellectual property (the "Intellectual Property") and any reproductions of copyright works in the thesis, for example graphs and tables ("Reproductions"), which may be described in this thesis, may not be owned by the author and may be owned by third parties. Such Intellectual Property and Reproductions cannot and must not be made available for use without the prior written permission of the owner(s) of the relevant Intellectual Property and/or Reproductions.

iv. Further information on the conditions under which disclosure, publication and commercialisation of this thesis, the Copyright and any Intellectual Property and/or Reproductions described in it may take place is available in the University IP Policy (see http://www.campus.manchester.ac.uk/medialibrary/policies/intellectual-property.pdf), in any relevant Thesis restriction declarations deposited in the University Library, The University Library's regulations (see http://www.manchester.ac.uk/library/aboutus/regulations) and in the University's policy on presentation of Theses.

ACKNOWLEDGEMENTS

First and foremost, I would like to thank my supervisor, Karl Kadler. Thank you for being my personal cheerleader and the best supervisor in the world (a fact!). Thank you for never saying 'no' and for giving me free rein in this exciting project.

A massive thank you to all members of the Kadler lab, past and present, for accompanying me on this wonderful Arhgap28 journey. Special thanks to Sue Taylor for looking out for me; Zoher Kapacee for being my mentor from day one; Yinhui Lu for teaching me how to make EM beautiful; David Holmes for introducing me to the biophysics; and to Liz Canty-Laird and Toby Starborg for their endless knowledge on tendons. Thanks to Sarah Al Youha and Amanda Patist for being great friends.

A huge thank you to all support staff of the Biological Support Facility, especially Mike Jackson, Emma Owen, Ian Townsend and Raymond Hodgkiss. Many thanks to Ray Boot-Handford and Mike Briggs for their advice on the animal work. Thanks to Dr Leo Zeef of the Bioinformatics Facility who performed the statistical analysis of the microarrays. Thanks also to Leanne Wardleworth and Michal Smiga of the Genomic Technology Facility who performed the RNA quality control and microarray chip hybridisation. Thanks to colleagues in the Wellcome Trust Centre for Cell-Matrix Research for helpful discussions. I would like to acknowledge the Biotechnology and Biological Sciences Research Council for funding my PhD and the Wellcome Trust for funding awarded to the Kadler lab and the Electron Microscopy Facility.

Thanks to Simon Foulcer, Douglas Dyer, Louise Kung, Luke Bonser and Peter Bell, these last four years have been full of laughter, holidays and extravagant meals! Thanks to Simon for simply being the bestest best friend. Thanks to Kipper for helping me to see the good in everything. Thanks to Lou for her continuing encouragement. Thanks to Luke for his positive thinking. Thanks to Pete for the music and crazy stores.

Thanks to Emma Chiu, Lorivic Lignes, Levan Tieu, Si-Mung Man and Alex Cheung for being amazing and loving friends, especially during these past 4 years, even though they have no idea what it is I actually do! Thanks to Lily Stanley, Laura Kusinski, Carole Beachill and Jennifer Ridley for their continuing support. Thanks to Amanda Gallagher and Swapna Vaddi for taking me under their wings. Thanks to Emma Lawrence for being punctual; Rowann Bowcutt for her great leadership; Liam Ridge for providing great chats; and Davina Whitnall for answering all my questions.

I would also like to acknowledge Elizabeth Lyon, and also Bastian Hengerer because they were great teachers who planted in me the interest in science.

Last but definitely not the least, to my mum, my dad and my darling sister Jemma: Thank you for everything!

THE AUTHOR

Chloé Yeung was awarded an Upper Second Class for BSc (Hons) Biomedical Sciences with Industrial Experience (2003-2007) from The University of Manchester. From 2005-2006, a one-year sandwich placement was undertaken in Biberach-an-der-Riß, Germany at Boehringer-Ingelheim, one of the 20 leading pharmaceutical companies in the world. She worked under the supervision of Bastian Hengerer in the Parkinson's Disease group, where she studied the effects of siRNA knockdown on the Nrf2-Keap1 regulatory pathway on oxidative stress. Chloé then continued her research into cell biology at Manchester and was awarded a Distinction for MRes in Tissue Engineering for Regenerative Medicine (2007-2008).

During her PhD, she has presented talks and posters at two Gordon Research Conferences (GRCs) for Collagen and two British Society for Matrix Biology meetings. She has also organised Get Connected! – the Wellcome Trust Centre for Cell-Matrix Research Meeting in conjunction with the 22nd UK Adhesion Society Meeting and the Italian Associazione di Biologia Cellulare e del Differenziamento Meeting at the University of Manchester, 13th to 15th September 2010, and the first Gordon-Kenan Research Seminar in conjunction with the 40th GRC for Collagen held at Colby Sawyer College, New Hampshire, 16th to 22nd July 2011.

Some of the work done during her PhD that is not described in this thesis has contributed to the following publications:

Bayer ML, **Yeung CYC**, Kadler KE, Qvortrup K, Baar K, Svensson RB, Magnusson SP, Krogsgaard M, Koch M, Kjaer M. 2010. Adult human tendon fibroblasts initiate embryonic-like collagen fibrillogenesis when cultured under linear tension. *Biomaterials*. **31**, 4889-4897.

Kapacee Z, **Yeung CYC**, Lu Y, Crabtree D, Holmes, DF, Kadler KE. 2010. Synthesis of embryonic tendon-like tissue by human marrow stromal/mesenchymal stem cells requires a three-dimensional environment and transforming growth factor beta 3. *Matrix Biology*. **29**, 668-77.

CHAPTER 1

INTRODUCTION

1. Introduction

1.1 Relevance of the study

The ability of vertebrate connective tissues to withstand cycles of mechanical loading during everyday activities such as walking and running is a direct attribute of an extracellular matrix (ECM) comprising well-organised collagen fibrils. As will be discussed below, fibrillar collagen account for upwards of 90% of the mass of skeletal tissues, are indeterminate in length, are elaborately arranged in three-dimensions (3D), and are the major source of tensile strength in vertebrates. However, it is poorly understood how the fibrils are aligned to the mechanical axis of the tissue. The ability of collagen fibrils to transmit force is exemplified in bone and tendon. In bone the fibrils are the protein scaffold for mineralisation, which builds the skeleton for attachment of muscles. In tendon, the fibrils are the primary tensile element that transmits force from muscle to bone. The payoff for high tensile mechanical properties is poor healing capabilities. Tendon is particularly difficult to heal. It is estimated that the annual cost of tendon injury to the UK industry is £25 billion (The Royal College of Surgeons of England, 2010), which is largely explained by the slow rate of healing of the collagenous matrix and long-term physiology. There is therefore an unmet clinical need to understand how cells generate organised arrays of collagen fibrils. This PhD thesis tests the hypothesis that the long-range organisation of extracellular collagen fibrils is generated on a blueprint of tensioned actin filaments within the cell. If true, genes responsible for ECM-associated actin reorganisation should be highly expressed during embryonic tissue morphogenesis when the organisation of the ECM is established. The approach was to perform a genome-wide search for actin regulatory genes in embryonic tendon, of which the parallelism of the fibrils is established exclusively during late embryonic development. The approach identified Arhgap28, a

novel RhoGTPase activating protein (GAP) that is present in bone and tendon and is able to regulate RhoA-dependent actin reorganisation.

1.2 Tendon development

Tendon is a highly organised tissue composed of predominantly type I collagen. Type I collagen is a triple helical molecule made of two α1(I) chains (encoded by the COL1A1 gene) and one α2(I) chain (COL1A2). The collagen molecules assemble into fibrils that are bundled into fibres (see review by Kadler *et al.*, 1996). The bundles are organised into fascicles, which then make up a tendon unit (Kastelic *et al.*, 1978). The main cell type in tendon is the fibroblast, which is elongated to ~50 μm in length, ~5 μm in diameter during embryonic growth (Humphries *et al.*, 2008), and aligns with the collagen fibrils, parallel to the tendon long axis (Richardson *et al.*, 2007). Although soluble collagen molecules can spontaneously self-assemble into fibrils in a neutral salt solution at 37°C (Gross *et al.*, 1952, Jackson and Fessler, 1955), this self-assembly model is not sufficient for explaining how collagen matrices are deposited in a diverse range of elaborate patterns to serve the purpose of different tissues, such as the parallel bundles of collagen fibrils in tendon tissue. Early work by Trelstad (1979) and supported by Birk (1985, 1986) suggested that collagen fibrils are in close contact with the cell surface in membrane recesses. Extended 3D reconstructions of serial transmission electron microscopy (TEM) images of tendon cells later identified plasma membrane projections and intracellular fibril-containing compartments that are co-aligned with the actin cytoskeleton (Canty *et al.*, 2004, 2006). Taken together these 3D electron microscopy data hint at a role of the actin cytoskeleton in collagen fibril assembly and alignment.

1.2.1 Protrusions of the plasma membrane

Patterning of the tendon matrix occurs during embryonic development; starting from embryonic day (or days post coitum) E13.5 in the developing mouse embryo, when bundles of parallel narrow (~30 nm) collagen fibrils can be observed in the ECM. At the time of collagen fibrillogenesis, embryonic tendon cells form two major types of protrusions with their plasma membrane that can be observed by TEM (see Fig. 1). The first type of membrane protrusions extends laterally across the width of the tendon and form channels in the ECM that contain the collagen fibrils (see Fig. 1A, arrows in inset). These plasma membrane-formed ECM channels were found to be stabilised by cadherin-11-containing cell-cell junctions (Richardson *et al.*, 2007). Delivery of small interfering RNAs (siRNAs) targeting cadherin-11 into dissected embryonic chick tendons by electroporation resulted in loss of cell-cell junctions and ECM channels (Richardson *et al.*, 2007). The loss of ECM channels was coupled with disruption of the parallel organisation of collagen bundles suggesting that these ECM channels are involved in maintaining the parallel organisation of collagen fibrils.

Upon closer inspection of transverse TEM images, membrane-bound collagen fibril-containing compartments can be observed inside the cell, and double membrane compartments encapsulating one or two collagen fibrils can be seen close to the cell surface (Birk and Trelstad, 1985, 1986). Using 3D reconstruction of serial TEM images, the compartments at the cell surface have been characterised as finger-like protrusions of the plasma membrane, called fibripositors, which extend from intracellular fibril containing compartments called fibricarriers into the ECM (Canty *et al.*, 2004; see Fig. 1B). Fibripositors are actin-stabilised, tension-sensitive structures and their appearance corresponds with the establishment of the tendon matrix,

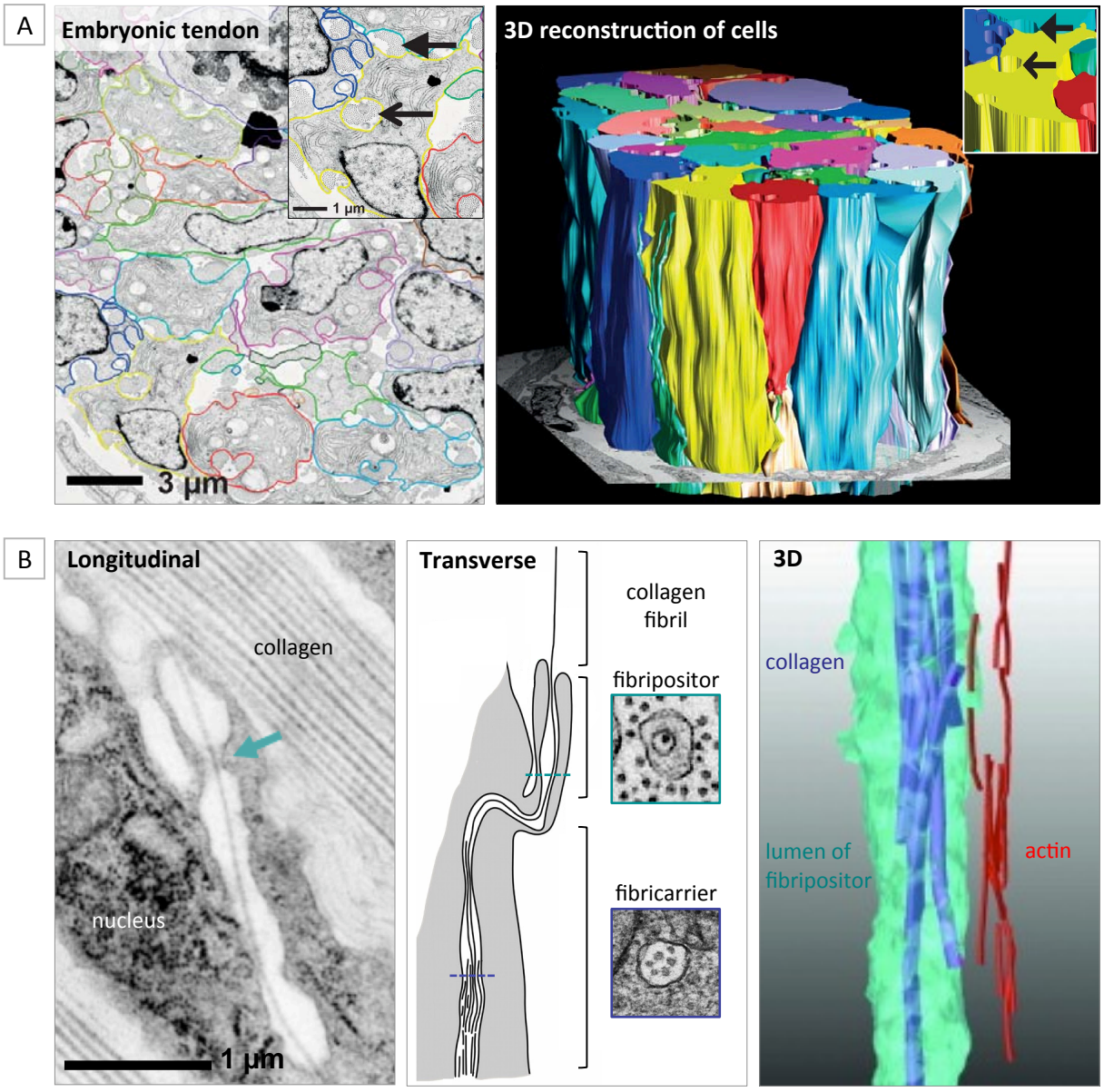

Figure 1

Specialised cell shape and actin-stabilised fibripositors in embryonic tendon cells.

Ultrastructure of embryonic tendon examined by TEM and 3D reconstruction. **(A)** Image of a transverse section with the plasma membrane of each cell traced. Reconstruction of information from serial sections produced a 3D model showing elongated cells. Arrows point to ECM channels formed by cadherin 11-stabilised plasma membranes of the same (open arrow) and adjacent cells (closed arrow). **(B)** Fibripositors as seen in a longitudinal section (green arrow points to pinch points occasionally observed in the lumen of the fibripositor), in a schematic diagram with representative images of a transverse section across a fibripositor and fibricarrier, and in a 3D reconstruction showing actin filaments aligned parallel to the long axis of the tendon. Figure made using data from Richardson *et al.*, 2007, Canty *et al.*, 2004, Canty *et* al., 2006, Starborg *et al.*, 2008.

indicating a link between the cell and the organisation of a collagen ECM (discussed below).

1.2.2 Matrix alignment is stabilised by actin

Similar to the collagen fibrils in the ECM, fibripositors are aligned parallel to the tendon long axis. Reconstruction studies of embryonic tendon showed that fibripositors contain intracellular actin filaments that are also aligned along the long axis of tendon, as represented in Fig. 1B (Canty *et al.*, 2006). Incubation of dissected embryonic chick tendons with cytochalasin B, an actin depolymerising agent, caused a significant reduction in the number of fibripositors as well as disorganisation of the collagen-rich ECM (Canty *et al.*, 2006). This finding shows that fibripositors are stabilised by actin and suggests that the organisation of the tendon matrix is also dependent on actin. To test if microtubules are also required for matrix organisation, tendons were incubated with nocodazole or colchicine, compounds which block microtubule polymerisation. However, no obvious effects on the occurrence of fibripositors or the parallelism of collagen fibrils was observed (Canty *et al.*, 2006).

In postnatal tendons, fibripositors are rare but can be found abundantly in areas containing newly synthesised narrow-diameter collagen fibrils after injury (Wong *et al.*, 2009), which might suggest that they are involved in deposition of new collagen. Interestingly, fibripositors and matrix organisation are not linked to collagen processing or secretion. Treatment with cytochalasin did not affect collagen synthesis, but treatment with nocodazole or colchicine delayed procollagen secretion (Canty *et al.*, 2006). These data suggest that actin-stabilised fibripositors are involved in the organisation rather than the deposition of collagen fibrils in the ECM.

1.2.3 Matrix alignment requires cell-generated tension

Embryonic tendon fibroblasts cultured in monolayer lack fibripositors. However, fibripositors are present when these cells are cultured into a 3D fibrin gel-based culture system, where the cells then generate tension (Kapacee *et al.*, 2008, Kalson *et al.*, 2010). Tendon cells isolated from embryonic tendons and adult tendons, or human mesenchymal stem cells (hMSCs) seeded in this 3D culture system in the presence of L-ascorbate for 7-14 days, will synthesise a tensioned embryonic tendon-like tissue construct, which includes fibripositors and an ECM containing narrow-diameter collagen fibrils (Kapacee *et al.*, 2008, Bayer *et al.*, 2010, Kapacee *et al.*, 2010). When tension is released in tendon constructs, the parallelism of the collagen fibrils is lost (Kapacee *et al.*, 2008), suggesting that the organisation of the tendon ECM is linked to mechanotransduction mechanisms, which requires the integrity of the actin cytoskeleton. Interestingly, the number of fibripositors is also reduced in untensioned tendon constructs and dissected tendons in culture, which lack tension (Canty *et al.*, 2006; Kapacee *et al.*, 2008). It is still unclear what the role of fibripositors is but the correlation between the appearance of fibripositors and an aligned collagen-rich matrix is interesting because fibripositors bear striking similarities to cell-matrix adhesions in that they make contact with the ECM, they are stabilised by actin and they are tension-sensitive (discussed in section 1.3 below). However, the existence of cell-matrix adhesion molecules within fibripositors has yet to be established.

1.3 Actin cytoskeleton and cell-matrix adhesions in matrix assembly

Cell-matrix adhesions enable bi-directional signalling between the cell and its extracellular environment (for reviews, see Green and Yamada, 2007, Askari *et al.*, 2009). They are integrin-containing protein complexes formed at the plasma

membrane and link proteins in the ECM to the actin cytoskeleton. Integrins are heterodimeric receptors of ECM proteins and when activated, signal through adapter molecules (including vinculin, tensin and α-actinin) to transmit signals to the actin cytoskeleton. Cell-matrix adhesions are readily observed in cells in culture and are also present *in vivo* (Cukierman *et al.*, 2001, Cukierman *et al.*, 2002). The role of cell-matrix adhesions in linking the actin cytoskeleton for matrix assembly and mechanotransduction in tendon tissue formation has not been fully explored but their role has been characterised in other cell types.

The assembly of a collagen-rich ECM has been shown to be dependent upon fibronectin assembly (reviewed by Kadler *et al.*, 2008). For example, fibronectin-null fibroblasts can only assemble collagen fibrils in the presence of soluble fibronectin (Velling *et al.*, 2002). In addition, overexpression of collagen-binding integrins, α2β1 and α11β1, in these fibronectin-null fibroblasts enhanced collagen fibrillogenesis in the presence of fibronectin (Velling *et al.*, 2002). In contrast, inhibitory antibodies to α2β1 integrins in vascular smooth muscle cells can inhibit type I collagen fibril assembly (Li *et al.*, 2003). Antagonising fibronectin-binding integrin α5β1 can also inhibit the remodelling of collagen gels (Sottile *et al.*, 2007). Together, these findings suggest that cells can directly mediate collagen fibril assembly via fibronectin assembly and integrins.

Adapter molecules such as vinculin transmit signals from integrins to the actin cytoskeleton. Cells isolated from vinculin knockout mouse embryos are less adherent to collagen and are unable to penetrate 3D collagen gels (Mierke *et al.*, 2010). The invasiveness of vinculin-expressing cells in collagen gels has been demonstrated to be

due to direct interaction between vinculin and actin stress fibres, which generates cell traction via the actomyosin machinery (Humphries *et al.*, 2007, Mierke *et al.*, 2008, Mierke *et al.*, 2010). Cellular tension generated by cell-matrix adhesions is critical for the assembly and remodelling of a fibronectin matrix and the same mechanisms may also be involved in collagen fibril assembly. Tensin can bind directly to integrins and actin (Davis *et al.*, 1991, Lo *et al.*, 1994, Miyamoto *et al.*, 1995). It is mostly localised to unique cell-matrix adhesions called fibrillar adhesions, which mediate fibronectin fibrillogenesis (Pankov *et al.*, 2000, Zamir *et al.*, 2000; discussed in section 1.3.1 below). α-actinin cross-links actin filaments and is required for the maturation of cell-matrix adhesions (Laukaitis *et al.*, 2001, Choi *et al.*, 2008). Knockdown of α-actinin causes loss of contractile stress fibres that connect cell-matrix adhesions and prevents maturation of focal adhesions into fibrillar adhesions and subsequently, inhibits fibronectin remodelling (Oakes *et al.*, 2012). These data show that adhesion to the ECM proteins and the ability to remodel ECM requires functional signalling from cell-matrix adhesion to initiate reorganisation of the actin cytoskeleton. How contractile actin stress fibres mediate the assembly of fibronectin at fibrillar adhesions and how a similar mechanism is required for the development of mechanical strength of tendon tissue will be discussed below.

1.3.1 Actomyosin contractility in assembly of a strong ECM

Cellular contractility is essential for mechanotransduction and contributes to development of biomechanics of tissues (Wozniak and Chen, 2009). Contractility is mediated via the assembly of contractile actin stress fibres containing non-muscle myosin (described in section 1.4.2). Inhibition of actomyosin contractility prevents maturation of focal complexes into larger focal adhesions, leading to a rapid loss of

vinculin, paxillin and tyrosine phosphorylation from mature focal adhesions that are required for signalling (Zamir *et al.*, 1999, Riveline *et al.*, 2001, Zaidel-Bar *et al.*, 2003). The same mechanism required for focal adhesion maturation is also required for the translocation of fibronectin-bound integrins in fibrillar adhesions along actin stress fibres, a process that is believed to stretch folded fibronectin dimers to facilitate its assembly (Pankov *et al.*, 2000, Zamir *et al.*, 2000, Ohashi *et al.*, 2002). The dynamic reorganisation of the actin cytoskeleton into stress fibres required for fibronectin assembly is regulated by signalling from Rho guanosine triphosphatases (GTPases; Yoneda *et al.*, 2007, Zhong *et al.*, 1998).

The actin cytoskeleton also plays an important role in the organisation of collagen fibrils in the tendon matrix (Canty *et al.*, 2006). More recently, actomyosin-forces have also been implicated in the development of a strong tendon tissue. Mechanical strength and stiffness of fully formed tendon constructs formed by embryonic chick tendon cell improve over 10 days in culture (Kalson *et al.*, 2010). No improvement in mechanical strength was observed 7 days after tendon constructs were treated with Triton X-100, which indicated that intact membranes are required for this process. Incubation of tendon constructs with chemical inhibitors to actin polymerisation (cytochalasin) or cell contractility (non-muscle myosin II inhibitor - blebbistatin) resulted in a loss of mechanical integrity without affecting procollagen processing or collagen secretion (Kalson *et al.*, 2010), suggesting that the loss of mechanical strength was not due to reduced collagen synthesis. Interestingly, increase in mechanical strength and stiffness of tendon constructs did not correlate with an increase in cell number, which suggested that the actomyosin-generated forces causes changes to the properties of the ECM, which are maintained in the absence of cellular activity (Kalson

et al., 2010). Perhaps, in a mechanism similar to fibronectin assembly, the cells 'stretch out' and align collagen fibrils to form a uniform ECM, improving mechanical properties.

Major actin reorganisation events are required for the generation of plasma membrane protrusions, mechanotransduction and actomyosin contractility – processes demonstrated to be important in tendon formation. How these events are regulated to produce a mechanically strong and organised tendon tissue is unknown and signalling by Rho GTPases, which are key regulators of the actin cytoskeleton organisation, is predicted to be involved. Understanding how actin reorganisation in tendon is regulated would be beneficial for designing strategies for improving healing and reducing scarring of fibrous tissues.

1.4 Rho GTPases

Rho is one of five subfamilies (Ras, Rho, Rab, Ran and Arf) of the Ras superfamily that has over 150 members for the regulation of many aspects of cell biology, such as proliferation, cytoskeleton reorganisation, differentiation and gene expression (for reviews on Rho-mediated processes, see Aspenstrom *et al.*, 2004, Heasman and Ridley, 2008). Rho GTPases are about 20-25 kDa and cycle between active, guanosine triphosphate (GTP)- and inactive, guanosine diphosphate (GDP)-bound states, represented in Fig. 2 (see Wennerberg *et al.*, 2005 for a review). Small GTPases have high binding affinity for GDP and GTP so the dissociation rate of GDP is slow and the exchange of GDP for GTP is accelerated by guanine nucleotide exchange factors (GEFs; reviewed by Vetter and Wittinghofer, 2001). Although they are called GTPases, their ability to hydrolyse GTP is slow. GTPase activating proteins (GAPs) can specifically enhance the intrinsic ability of GTPases to hydrolyse GTP to GDP (reviewed by

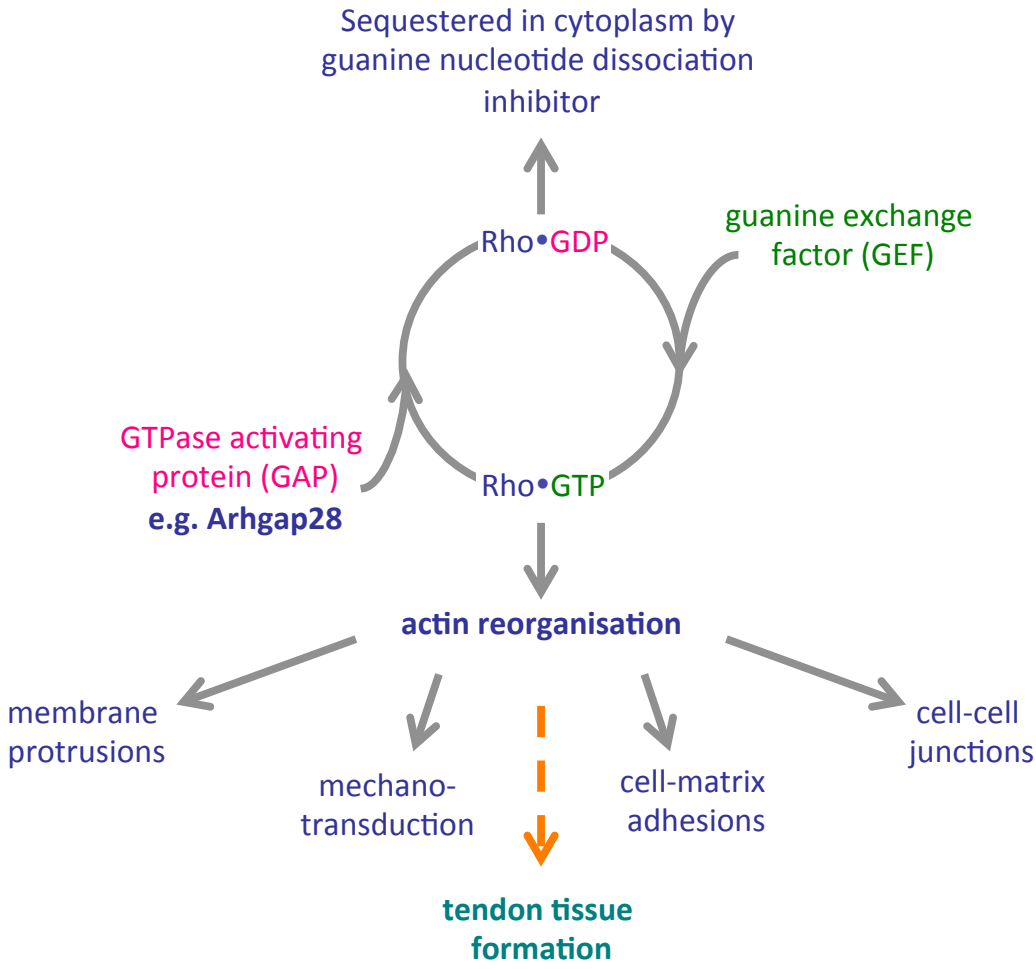

Figure 2
Schematic representation of Rho GTPase signalling regulation.
Rho GTPases are inactive when bound to GDP. The exchange of GDP for GTP is catalysed by GEFs and GAPs catalyse the hydrolysis of GTP to GDP. When bound to GTP, Rho GTPases can activate downstream effectors to co-ordinate reorganisation of the actin cytoskeleton for numerous cellular processes. We hypothesise that the putative RhoGAP, Arhgap28, is important in the regulation of actin cytoskeleton reorganisation during tendon ECM assembly.

Tcherkezian and Lamarche-Vane, 2007). An additional class of regulatory proteins involved in regulating small GTPase signalling is guanine nucleotide dissociation inhibitors (GDIs), which prevent GDP dissociation and/or masks lipid moiety on GTPases (Garcia-Mata *et al.*, 2011). This section of the Introduction will focus on the Rho subfamily of GTPases, highlighting the role of RhoGAPs regulating Rho signalling.

1.4.1 Signalling of the Rho subfamily

There are 22 mammalian genes that encode the members of the Rho subfamily and these are divided into subgroups according to similarities in the amino acid sequences (listed in Fig. 3A). The RhoA-related subgroup: RhoA, RhoB and RhoC; the Rac1-related subgroup: Rac1, Rac2, Rac3 and RhoG; the Cdc42-related subgroup: Cdc42, TC10 (or RhoQ) and TCL (TC10-like or RhoJ); and the RhoD-related subgroup: RhoD and Rif (or RhoF) belong to the classical or typical category. This term refers to the canonical mechanisms of GTPase regulation by GEFs and GAPs as described above. The atypical category contains Rho members that are regulated by alternative mechanisms independent of GEFs and GAPs (see list of atypical Rho GTPases in Fig. 3A). For example, RhoH remains in an active, GTP-bound state because it lacks hydrolytic activity and is resistant to nucleotide exchange and RhoGAP activity (Li *et al.*, 2002). This is due to two amino acid substitutions at highly conserved residues (see Fig. 3B for the substitutions in RhoH, and in Rnds). Instead, RhoH activity is regulated at the transcriptional level and by Rho GDIs via its isoprenyl lipid (farnesyl-isoprenoid) modification (Li *et al.*, 2002, Roberts *et al.*, 2008).

All classical Rho GTPases contain an N-terminal GTPase domain and a C-terminal CAAX motif (where C is cysteine, A is any aliphatic amino acid and X is a variable; see Fig 3B).

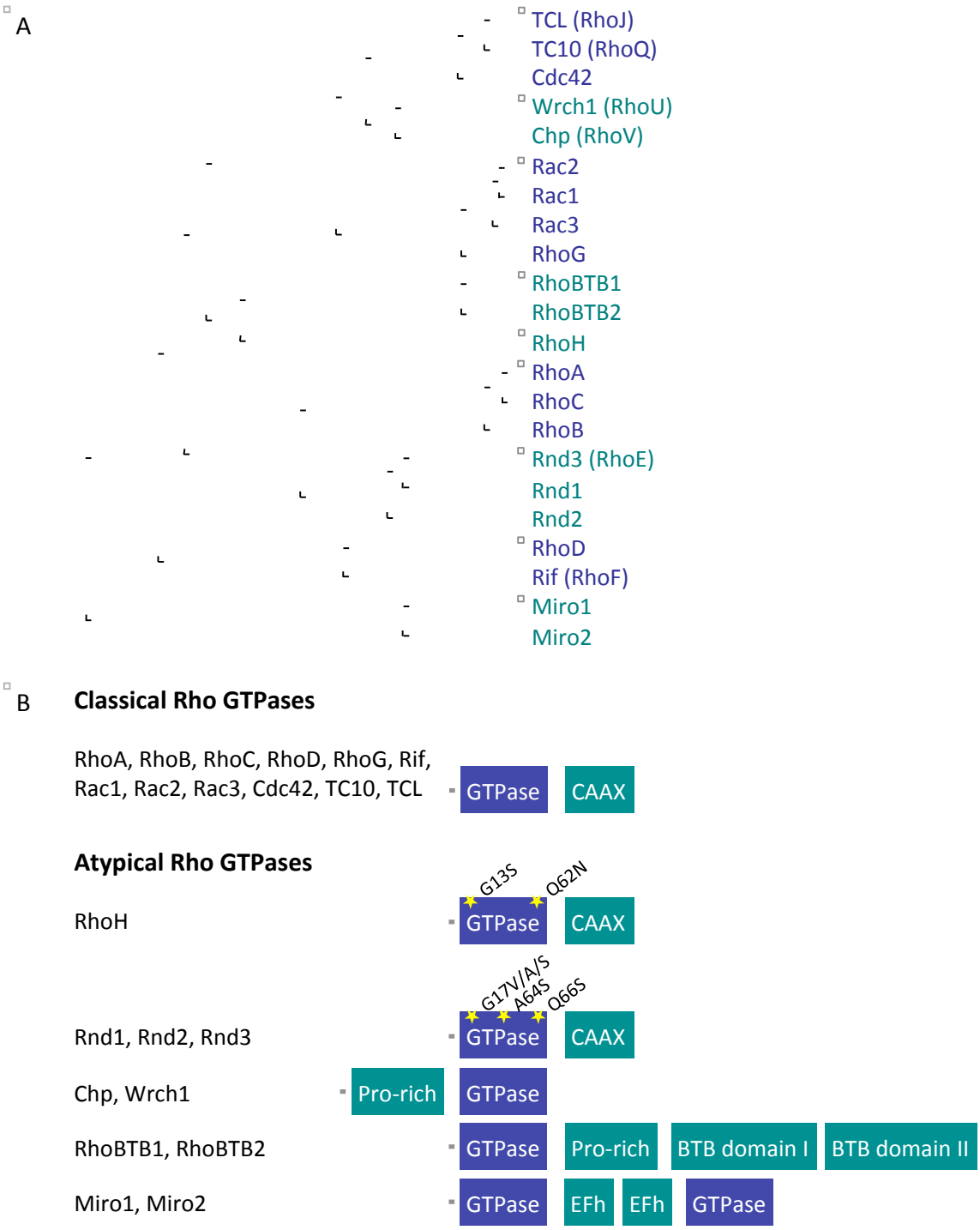

Figure 3
The subgroups and domain organisation of Rho GTPases.
(A) An unrooted phylogenetic tree of 22 Rho GTPases based on sequence similarities of the Rho GTPase domain using ClustlW algorithm (adapted from Aspenström *et al.*, 2004; Heasman and Ridley 2008). Rho GTPases of the same subfamily are grouped in boxes. Classical Rho GTPases are in blue and atypical Rho GTPases are in green. **(B)** A schematic representation of the structural organisation of motifs and conserved domains in Rho GTPases. Annotations in the GTPase domain show the substitution of conserved amino acid. BTB = Broad complex/Tramtrack/Bric-a-brac; CAAX = isoprenylation signal; EFh = calcium-binding EF hand; Pro-rich = proline-rich motif.

The CAAX motif is recognised for post-translational isoprenylation, the addition of a lipid moiety, which is required for localisation to membranes, where Rho GTPases can transduce signals to and from receptors of the ECM.

1.4.2 Rho and actomyosin contractility

Rho signalling can be activated *in vitro* by treating serum-starved fibroblasts with lysophosphatidic acid (LPA). This activation is characterised by rapid assembly of stress fibres and large focal adhesions, and cell contraction (Ridley and Hall, 1992, Kolodney and Elson, 1993). Rho-activated assembly of these stress fibres are mediated via Rho effectors, which include a formin called mammalian diaphanous 1 (mDia1), and Rho-associated kinase (ROCK; Watanabe *et al.*, 1997, Ishizaki *et al.*, 1997; see Fig. 4). Activation of mDia1 leads to the activation of profilin, a protein required for the polymerisation of actin into stress fibres (Watanabe *et al.*, 1997, Chang and Peter, 2002). The contraction of stress fibres is generated by the incorporation of activated, phosphorylated non-muscle myosin (Tan *et al.*, 1992). Activated ROCK positively regulates the assembly of contractile actin stress fibres by directly phosphorylating the myosin light chain (MLC), and also by inactivating MLC phosphatase (Noda *et al.*, 1995, Hirose *et al.*, 1998; see Fig. 4). ROCK also activates LIM domain-containing kinase (LIMK) via phosphorylation, which inactivates cofilin, the actin-severing protein (Maekawa *et al.*, 1999). Together, these pathways stabilise filamentous (F)-actin by inducing actin polymerisation for the assembly of contractile stress fibres. This pathway may also mediate fibripositor stabilisation or actomyosin-driven contraction observed in embryonic tendon cells.

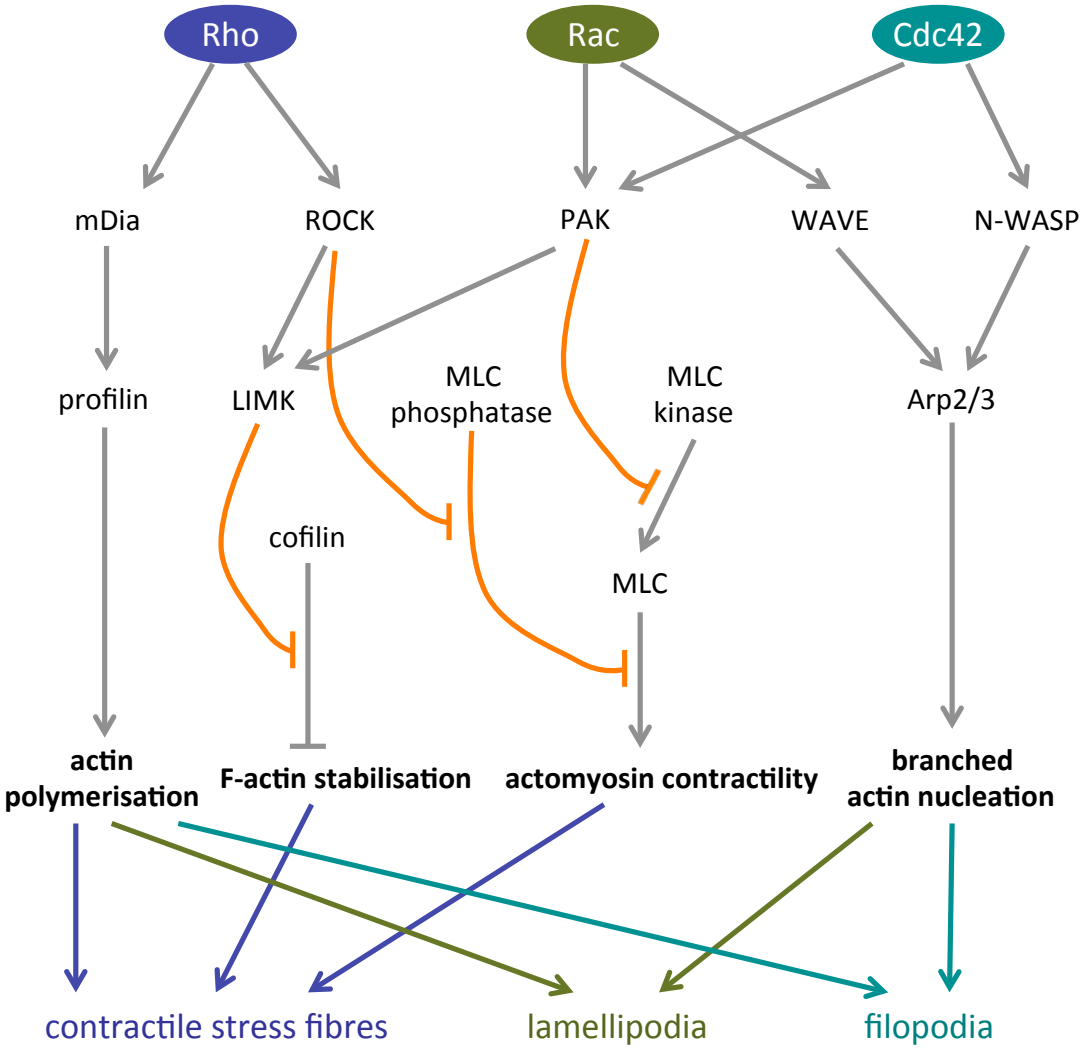

Figure 4
Rho GTPase signal transduction leads to actin reorganisation.
Activation of Rho, Rac and Cdc42 leads to the formation of contractile stress fibres, lamellipodia and filopodia, respectively. See text for details.

1.4.3 Rac and lamellipodia formation

Rac1 induces actin polymerisation into a meshwork at the leading edge of migratory cells, which produces membrane ruffles called lamellipodia. Effectors of Rac include WAVE (Wiskott-Aldrich syndrome protein verprolin homologous) and p21-activated kinase (PAK1; Miki *et al.*, 2000, Sells *et al.*, 1997, Knaus *et al.*, 1998; see Fig 4 for schematic). Rac activation of the WAVE leads to activation of the Arp2/3 complex, required for nucleation and polymerisation of branched actin filaments (Stradal *et al.*, 2004, Yamazaki *et al.*, 2007). PAK can phosphorylate LIMK and inhibit cofilin (Edwards *et al.*, 1999). PAK can also phosphorylate and inactivate MLC kinase, which decreases phosphorylated MLC, thereby reducing actomyosin contractility (Sanders *et al.*, 1999). In embryonic tendon, the cells form large lamellipodia-like plasma membrane protrusions that are stabilised by cadherin-11 (Richardson *et al.*, 2007). Interestingly, morpholino-knockdown of cadherin-11 disrupts lamellipodia formation in *Xenopus* cranial neural crest cells (Kashef *et al.*, 2009). In this system, cadherin-11 functions as an inhibitor of GEF activity towards Rac, RhoA and Cdc42, preventing their activity to be switched off (Kashef *et al.*, 2009). The formation of plasma membrane ECM channels in embryonic tendon cells might also be regulated by Rac.

1.4.4 Cdc42 and filopodia formation

Unlike lamellipodia, filopodia contain cross-linked parallel actin filaments. Cdc42 mediates the formation of filopodia (also known as microspikes), which are long thin, finger-like membrane protrusions at the leading edge of the cell, reminiscent of fibripositors. Cdc42 also activates PAK, which leads to actin polymerisation and stabilisation of F-actin in similar mechanisms described for Rac activation (Harden *et al.*, 1996, Sells *et al.*, 1997). In addition, Cdc42-GTP can bind directly to and activate

WASP (Wiskott–Aldrich syndrome protein) or the ubiquitously expressed N-WASP, which interacts with Arp2/3 complex and profilin and induces nucleation of branched actin (Symons *et al.*, 1996, Abdul-Manan *et al.*, 1999). The cross-linking of actin filaments in filopodia has also been shown to require the actin-bundling protein fascin (Adams and Schwartz, 2000, Vignjevic *et al.*, 2006).

1.5 Rho GTPase activating proteins

The intrinsic GTP hydrolytic activity of GTPases is very slow. Efficient hydrolysis of GTP requires a GAP, which accelerates the hydrolytic activity up to 10^5-fold by stabilising the bound Rho GTPase during GTP hydrolysis (Rittinger *et al.*, 1997b). GAPs were originally thought to be terminators of GTPase signalling, but it is now known that some GAPs have a primary role in regulating GTPase signalling whereas some are also signal effectors. There are over 70 genes encoding proteins that contain a RhoGAP domain (Tcherkezian and Lamarche-Vane, 2007). This multitude of Rho-specific GAPs, as well as GEFs, is thought to ensure signalling specificity, for example, via tissue-specific expression, specificity for a single GTPase or signalling pathway, or that some RhoGAPs act as scaffold proteins or effectors for crosstalk between Rho GTPases and other signalling pathways (reviewed by Tcherkezian and Lamarche-Vane, 2007).

The RhoGAP domain is made of nine alpha-helices, of which four form a shallow pocket of hydrophobic residues and conserved residues, including the highly conserved catalytic arginine residue, which is orientated to allow Rho GTPase-binding (Barrett *et al.*, 1997). The mechanistic principle of RhoGAPs is similar to how GTP hydrolysis occurs in Gα subunits during G protein-coupled receptor activation (Coleman *et al.*, 1994). Conserved residues in the shallow pocket of the RhoGAP

domain form salt-bridging and hydrogen bond interactions with conserved regions in the bound Rho GTPase called the P-loop, switch I and switch II regions, as shown in the Rho/RhoGAP interface in Fig. 5A and B (Rittinger *et al.*, 1997a, Rittinger *et al.*, 1997b). Binding of the GTPase causes a conformational change in the RhoGAP domain, enabling the catalytic arginine finger to be positioned directly into the active site of the Rho GTPase. This change enables the guanidinium group of arginine to interact with the main carbonyl group of the glutamine residue of the GTPase ($Gln63_{Rho}$ or $Gln61_{Cdc42}$) and stabilise the transfer of charge during GTP hydrolysis (Rittinger *et al.*, 1997b). Therefore the function of RhoGAPs is not only to supply an arginine residue to stabilise the developing negative charge on the oxygen atoms of γ-phosphate to enable GTP-hydrolysis, but also to stabilise the structure of the bound Rho GTPase, by interacting with the switch regions.

1.5.1 RhoGAPs and matrix assembly

The role of RhoGAPs in the deposition and organisation of ECM has not been well characterised. Most studies on RhoGAPs to date are concentrated on how RhoGAPs regulate cell adhesion to, migration on or invasion through the ECM (Furukawa *et al.*, 2001, I *et al.*, 2004, McHenry *et al.*, 2010, Doherty *et al.*, 2011). p190B-RhoGAP (Arhgap5) was one of the first RhoGAPs to be studied. P190B-RhoGAP negatively regulates Rho activity, where microinjection of p190RhoGAP into fibroblasts *in vitro* inhibited stress fibre formation but not membrane ruffling (Ridley *et al.*, 1993). p190RhoGAP mediates RhoA inactivation upon cell attachment to fibronectin, which is essential for cell spreading. Expression of a GAP-deficient p190RhoGAP can prevent this initial inactivation of RhoA (Arthur and Burridge, 2001). RhoGAP activity can be regulated by phosphorylation and protein-protein interactions. For example, in

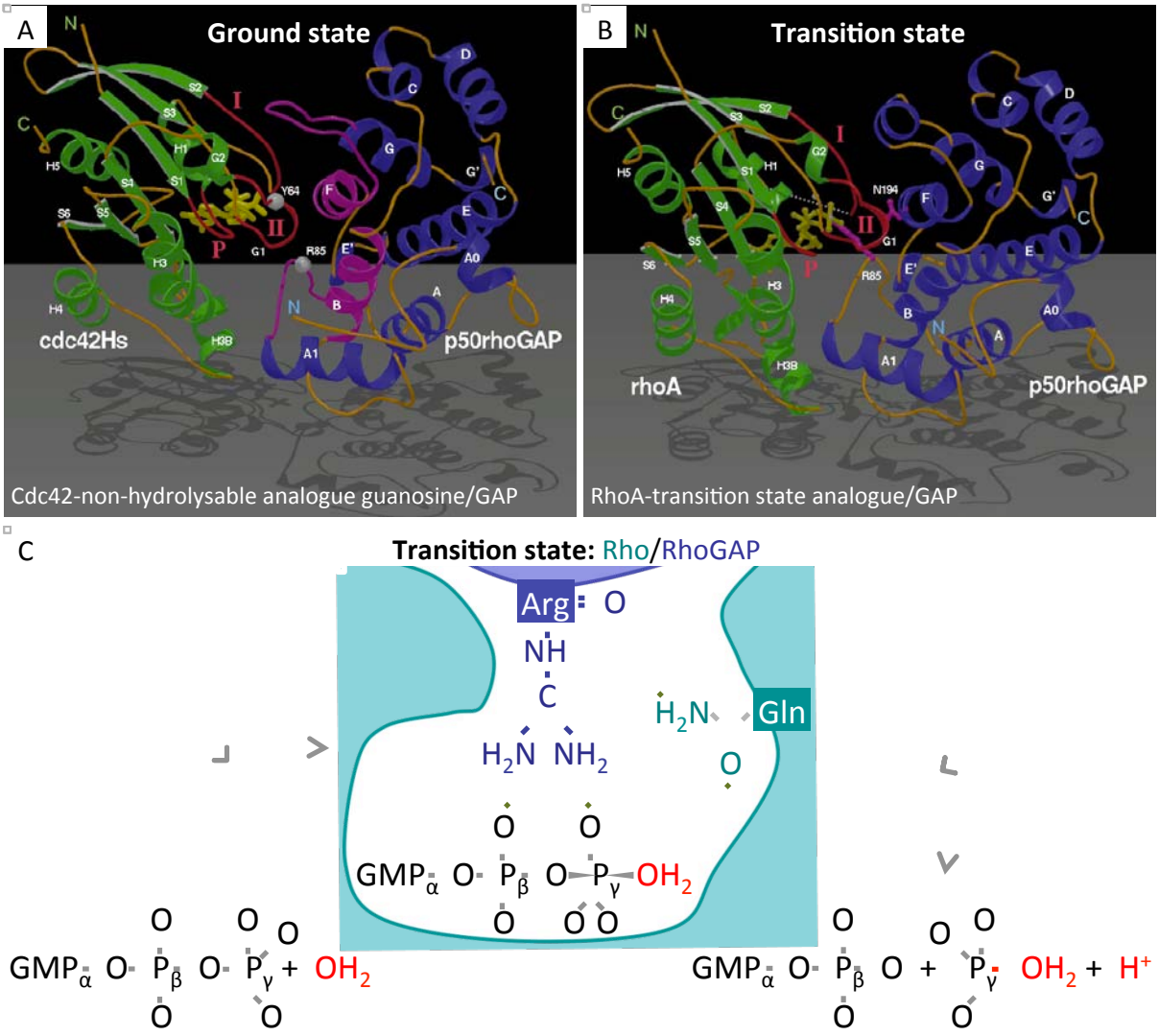

Figure 5

Mechanism of RhoGAP-induced GTP hydrolysis.

Conformational changes as a result of interaction between Rho and RhoGAP demonstrated by the following heterodimer complexes: **(A)** Cdc42-5'-[β,γ-imido]triphosphate (a non-hydrolysable analogue)/p50RhoGAP (ground state) and **(B)** RhoA-GDP-aluminium fluoride (which mimics the terminal phosphate of GTP, a transition-state analogue)/p50RhoGAP (transition state) complexes viewed along the heterodimer interface. The GTPases are shown in green the ball-and-stick representations of the respective analogues are shown in yellow. The RhoGAP is shown in blue. I, II and P refer to the switch I, switch II and P loop, respectively. **(C)** Schematic representation of GTP hydrolysis from the nucleotide in tri-phosphate form to the transition state of hydrolysis in a Rho-GTP/RhoGAP complex and the products of GTP hydrolysis. Adapted from Rittenger *et al.* (1997a, 1997b) and a review by Bos *et al.* (2007).

melanoma cells, activation of integrin β1 causes tyrosine phosphorylation of p190RhoGAP, which is localised to sites of fibronectin-collagen matrix degradation by invadapodia, which are actin-rich membrane protrusions seen invasive cells (Nakahara *et al.*, 1998). Tyrosine phosphorylation of p190RhoGAP by Src kinase enables it to associate with p120RasGAP *in vivo* (Roof *et al.*, 1998). Rnd proteins interact with p190RhoGAP to enhance their RhoGAP activity towards RhoA and cause disruption to stress fibre formation (Wennerberg *et al.*, 2003). In addition, p190B-RhoGAP can interact with Rac1 and this interaction is required for cell spreading on collagen or fibronectin matrices (Bustos *et al.*, 2008). There is very little evidence explaining how p190RhoGAP-mediated regulation of the actin cytoskeleton affects the ECM, however, there are some studies that link p190RhoGAP function with deposition and degradation of the ECM. For examples, overexpression of p190B-RhoGAP during mammary gland development in mice caused an increased in collagen deposition surrounding mammary ducts (Vargo-Gogola *et al.*, 2006), and targeting p190B-RhoGAP in endothelial cells for knockdown using siRNAs caused a reduction in expression of matrix metalloproteinase 2 (MMP2) and MMP14 (or MT1-MMP; Guegan *et al.*, 2008). Together these data show that p190RhoGAP can regulate actin cytoskeletal reorganisation and its expression affects ECM deposition. However, understanding how the two processes are connected requires further investigations.

Recently, a role for RhoGAP-regulated actin reorganisation in ECM organisation has been found for deleted in liver cancer 1 (DLC1). DLC1 is a RhoGAP that was first identified as a tumour suppressor in cancer (Ng *et al.*, 2000, Yuan *et al.*, 2003). Contraction of collagen gels is mediated via Rho-activated assembly of contractile stress fibres (Grinnell *et al.*, 2003). Overexpression of DLC1 can cause loss of stress

fibres but increase in membrane protrusions *in vitro* (Kim *et al.*, 2007), suggesting that DLC1 is a negative regulator of actin stress fibres (Wong *et al.*, 2008, Zhou *et al.*, 2008). Knockdown of the cell-matrix adhesion protein tensin 2, which links the actin cytoskeleton to adhesions (as discussed previously in section 1.3), was able to inhibit collagen gel contraction by human foreskin fibroblasts (Clark *et al.*, 2010). However, knockdown of DLC1 in cells with tensin 2 knockdown was able to rescue collagen gel contraction, which suggested that cell-matrix adhesions signals negatively regulate DLC1 to allow stress fibre assembly required for the remodelling of collagen matrices (Clark *et al.*, 2010). Intriguingly, cells isolated from DLC1-null mouse embryos have fewer actin stress fibres (Durkin *et al.*, 2005). This observation shows that although DLC1 negatively regulates stress fibres, it is also required for their formation and thus it is critical to regard these regulators, GAPs and GEFs, when studying Rho GTPase signalling.

1.6 Thesis aims

The regulators of actin reorganisation required for processes including cell elongation, fibripositor formation and actomyosin contractility during the assembly of a strong, collagen-rich matrix are unknown and Rho GTPase signalling is hypothesised to be involved. The aims of this thesis are:

i. **To identify a candidate regulator of actin reorganisation during the patterning of the tendon matrix.**

   The approach will be to use microarray comparison of gene expression of tendon tissues at different developmental stages: embryonic (E21), during which the patterning of the ECM is established and the organisation of the actin cytoskeleton has been linked to the organisation of collagen fibrils, and postnatal (3 weeks and 6

weeks old), when the cell shape changes and the tissue grows in size. From this analysis, a putative RhoGAP called Arhgap28 was identified as a candidate regulator of actin reorganisation during the formation of tendon tissue.

ii. **To examine the role of Rho signalling in tendon tissue formation and to determine the function of Arhgap28 in regulating the actin cytoskeleton.**

The approach will be qPCR analysis of gene expression during tendon tissue formation using a tractable tendon construct culture model, overexpression of Arhgap28 clone and treatment with small molecules to modulate Rho signalling in cells in culture.

iii. **To investigate the function of Arhgap28 in tissue formation *in vivo*.**

The approach will be to knockout Arhgap28 in mouse and study the effects on the tissue development and actin reorganisation in cells isolated from Arhgap28-null mice.

The experimental approaches described in this thesis are expected to provide new information on the role of actin reorganisation on the formation of a mechanically strong, collagen-rich tissue. The information is critical for the development of medical strategies needed to improve tendon healing, with broader applications in fibroses and disorders where collagen fibrils are disorganised.

CHAPTER 2

METHODS AND MATERIALS

2. Methods and Materials

2.1 Source of materials

All chemicals and sterilised culture reagents were obtained from Sigma-Aldrich (Dorset, UK); characterised human mesenchymal stem cells (hMSCs) and culture reagents for these cells were purchased from Lonza Biosciences (Verviers, Belgium); and cell culture materials were purchased from Corning and BD Falcon (supplied by Appleton Woods, Birmingham, UK) unless otherwise stated. Fertilised chicken eggs were supplied by Henry Stewart and Company (Lincolnshire, UK). Control IgGs were purchased from Santa Cruz Biotechnology (supplied by Insight Biotechnology, Middlesex, UK).

2.2 Cell culture

2.2.1 Human mesenchymal stem cells

Characterised hMSCs were thawed and cultured in MSC Growth Medium (supplemented with growth supplements, L-glutamine and penicillin and streptomycin) at 37°C, 5% CO_2 in a humidified environment, passaged 1 to 3 when subconfluent and used between passages 4 to 6.

2.2.2 Primary culture of embryonic chick tendon cells

Fertilised chicken eggs were incubated at 39°C in a humidified environment upon delivery (E0). Between E10 and E14, eggs were chilled for 30-60 minutes and embryos were decapitated. Metatarsal tendons were pulled and chick tendon cells were released by treatment with 1000 U/ml bacterial collagenase type 4 (Worthington Biochemical Corporation, supplied by Lorne Laboratories, Berkshire, UK) in 0.25% trypsin (Invitrogen, supplied by Life Technologies, Paisley, UK) for 60 to 90 minutes,

pipetting every 10 to 15 minutes. Cells were passed through a 70 µm cell strainer, centrifuged for 5 minutes at 400 x g and resuspended in Dulbecco's modified Eagle's medium containing 4.5 mg/l glucose, non-essential amino acids and 110 mg/l sodium pyruvate (DMEM), supplemented with 10% foetal calf serum (FCS), 2 mM L-glutamine, 10,000 units (U)/ml penicillin and 10 mg/ml streptomycin at 37°C, 5% CO_2 in a humidified environment, passaged 1 to 4 when subconfluent and used between passages 3 to 7.

2.2.3 NIH3T3 fibroblasts

Murine NIH3T3 fibroblasts were cultured in DMEM, supplemented with 10% FCS, 2 mM L-glutamine, 10 000 U/ml penicillin and 10 mg/ml streptomycin at 37°C, 5% CO_2 in a humidified environment, passaged 1 to 6 every 3 days and used between passages 35 and 40.

2.2.4 SaOS-2 cells

Human SaOS-2 osteosarcoma cells were cultured in RPIM-1630, supplemented with 10% FCS, 2 mM L-glutamine, 10 000 U/ml penicillin and 10 mg/ml streptomycin at 37°C, 5% CO_2 in a humidified environment, passaged 1 to 3 once a week and used between passages 12 and 18.

2.2.5 Three-dimensional fibrin gel culture system

For three-dimensional culture of cells to form tendon-like tissues, the method described in Kapacee *et al.* (2008) was used. In brief, 6-well culture plates were lined with Sylgard Silicone Elastomer (Dow Corning, supplied by World Precision Instruments, Hertfordshire, UK). Two ~8 mm lengths of Mersilk Suture 3-0 (Ethicon,

supplied by Bunzl Healthcare, Middlesex, UK) were placed 1 cm apart and pinned into the silicone with 0.1 mm stainless steel minutien pins (Fine Science Tools GmbH, Heidelberg, Germany). Plates were sterilised by incubation for 1 hour in 100% ethanol under ultraviolet light and washed with sterile phosphate-buffered saline (PBS) before cells were seeded. For each well, 7.5 x 10^5 cells in 500 µl fibrin gel solution (20 mg/ml fibrinogen cleaved with 200 U/ml thrombin) were seeded, then the plate was incubated for 5 minutes at 37°C. After, 5 ml of DMEM, supplemented with 10% FCS, 2 mM L-glutamine, 200 µM L-ascorbic acid 2-phosphate, 10,000 U/ml penicillin and 10 mg/ml streptomycin was added to each well. Plates were incubated at 37°C, 5% CO_2 in a humidified environment with fresh medium replaced every 2 to 3 days. During medium changes, fibrin gels were scored using a sterile pipette tip to detach the edges of fibrin gels and allow them to contract and form a tendon-like tissue construct between the two sutures. Point of full contraction is termed T0, and subsequent culture of 3, 7 or 14 days is referred to as T3, T7 or T14, respectively.

2.2.6 Transient transfections

DNA was transfected using Lipofectamine 2000 (Invitrogen) according to manufacturer's protocol for 12-well plate and 6-well plate format. 24 hours after transfection, cells were either analysed by indirect immunofluorescence, active GTPase pull-down assays or western blotting.

2.2.7 Collagen gel contraction assay

Collagen gels were prepared using type I collagen from rat tail tendon (Invitrogen) adjusted to a final concentration of 1.25 mg/ml with ice-cold serum-free medium. 1 ml was aliquoted into each well of a 12-well plate and incubated for 45 minutes at 37°C in

5% CO_2 in a humidified environment, followed by incubation with serum-containing medium for 1 hour, with 2 changes of medium. When cells were confluent, cells were treated as described in section 2.2.8 below. Then edges of the gels were scored with a sterile pipette tip to detached the gel from the plate. Photographs were taken with a digital SLR over 4 days. The area of each gel was measured using ImageJ software (Abramoff *et al.*, 2004). The area was converted to a percentage of the original, and the means for each treatment group was calculated. Two-way ANOVA followed by a Bonferroni test was used to determine significance differences compared to the control sample.

2.2.8 Modulating Rho signalling in cells and tendon constructs

To modulate Rho signalling cells, collagen gels or tendon constructs were washed with PBS three times and then equilibrated for 30 minutes with serum-free medium and then treated for 30 minutes with final concentration of 5 μM lysophosphatidic acid (LPA; Sigma) in 0.1% DMSO or 10 μM Y27632 (ROCK inhibitor; Sigma) in 0.1% DMSO, diluted in serum-free medium, all at 37°C, 5% CO_2 in a humidified environment. Treated tendon constructs were incubated at room temperature. The cells were then analysed by indirect immunofluorescence, active GTPase pull-down assays or in collagen gel contraction assays. Tendon constructs were analysed using a recoil assay (see below).

2.2.9 Tissue recoil assay

Each tendon-like tissue was cut at one suture end to allow it to contract, and imaged using a digital SLR at a fixed focal point over an hour with 10-second intervals. The length of the constructs in each image was measured using ImageJ software. The

length was converted to a percentage of the original and the means for each experimental group were calculated. The mean values were then fitted to a 3-parameter exponential decay function using SigmaPlot (Systat Software Inc.). One-way ANOVA and a Dunnett's test was used to determine significance differences between the derived $T_{1/2}$ and recoil baseline values compared to control constructs incubated in 0.1% DMSO.

2.3 RNA methods

2.3.1 RNA isolation and DNase treatment

For the isolation of RNA from cells in monolayer, cells were washed with ice-cold PBS three times and lysed with TRIzol reagent (Invitrogen) according to manufacturer's protocol. For the isolation of RNA from 3D tissue constructs, dissected tendons or animal tissues, samples were washed with ice-cold PBS 3 times and snap frozen in liquid nitrogen with 500 µl TRIzol. Frozen tissues were homogenised using a Mikro-Dismembrator U (B. Braun Biotech International, Germany) at 2000 Hz for 90 seconds two times. The volumes of dismembrated samples were made up to 1 ml with TRIzol before continuing with the manufacturer's instructions. Isolated RNA was treated with 5 U RQ1 DNase (Promega, Hampshire, UK) in 50 µl reactions, following the manufacturer's protocol for RNA precipitation and resuspended in DEPC water. Integrity of DNase-treated RNA samples were analysed by gel electrophoresis in 1% agarose gels in Tris-borate-EDTA buffer (Applied Biosystems). RNA concentrations were determined using a NanoDrop ND-1000 (Thermo Fisher Scientific, Basingstoke, UK).

2.3.2 Reverse transcription

A 40 µl master mix consisting of 1 x reverse transcriptase (RT) reaction buffer, 5 mM $MgCl_2$, 1.88 µM oligo $d(T)_{16}$ primers or random hexamer primers, 40 U RNase inhibitor, 1.25 mM of each dNTP and 50 U Multiscribe reverse transcriptase (all from TaqMan Reverse Transcriptase reagents, Applied Biosystems, supplied by Life Technologies, Paisley, UK) was used to synthesise cDNA from 0.5 to 2.0 µg DNase-treated RNA using the following thermal cycler parameters: 25°C for 10 minutes, 48°C for 30 minutes and 95°C for 5 minutes.

2.3.3 Primer design

All primers used in this study were designed using Primer3 version 0.4.0 (Rozen and Skaletsky, 2000). Primers used for qPCR and RT-PCR were designed across exons or in distinct exons to amplify non-genomic DNA. Primers were purchased as HSPF-purified DNA oligos from Eurofins MWG Operons, Ebersberg, Germany).

2.3.4 Polymerase chain reaction (PCR)

A 25 µl master mix consisting of 1 x BioMix Red buffer (containing final concentration of 2 mM $MgCl_2$ and dNTP; Bioline, London, UK) and 10 pmoles of each forward and reverse primers (see Tables 1 and 2) was used to amplify PCR products from 1-2 µl cDNA. The conditions for the amplification were as follows: 95°C for 3 minutes followed by 30 cycles of 95°C for 30 seconds, 60°C for 30 seconds, 72°C for the appropriate time to extend the product and a final extension at 72°C for 5-10 minutes. PCR products were analysed by gel electrophoresis in 2% agarose gels and purified for sequencing using QIAquick PCR Purification kit reagents (Qiagen, Sussex, UK).

2.3.5 Sequencing reaction

All PCR products produced from primers were validated and confirmed by DNA sequencing. A 15 µl reaction consisting of 1x BigDye Terminator v3.1 sequencing reaction buffer, 1 µl BigDye Terminator v3.1 (Applied Biosystems) and 3 pmoles of either the forward or reverse primer (listed in Tables 1-3) was used for sequencing purified templates. The conditions for the amplification were as follows: 96°C for 1 minute followed by 25 cycles of 96°C for 10 seconds, 50°C for 5 seconds, 60°C for 4 seconds. PCR products were precipitated and subsequently sequenced by the DNA Sequencing Facility, University of Manchester. Sequences were analysed using the BLAST software against the NCBI nucleotide database and aligned with the expected sequence.

2.3.6 Quantitative PCR (qPCR)

Triplicates of 10 µl reactions consisting of 1x reaction buffer containing 3 mM MgCl2, hot-start DNA polymerase, dNTPs (SensiMix SYBR no-ROX kit, Bioline), 2.5 pmoles of each forward and reverse primers (listed in Table 1) was used to amplify PCR products from 1 µl cDNA. The conditions for the amplification were as follows: 95°C for 10 minutes, followed by 40-50 cycles of 95°C for 15 seconds, 60°C for 15 seconds, 72°C for 15 seconds. The $2^{-\Delta\Delta Ct}$ method (Livak and Schmittgen, 2001) was used to analyse relative fold changes in gene expression compared to the experimental control group. A two-sample t-test, or one-way ANOVA followed by a Dunnett's test was performed to determine significance differences compared to the control sample. Regression analysis was performed in the correlation of mouse age and Arhgap28 expression.

Species	Gene	Forward primer 5'-3'	Reverse primer 5'-3'	Product size
rat	Arhgap28	CGTGAAAGTTCCCCTTGTGT	GAGAGGTGGGCAGTTCTCTG	224 bp
rat	GAPDH	ATGGGAAGCTGGTCATCAAC	GTGGTTCACACCCATCACAA	221 bp
human	Arhgap28	TGGCACCAAACCTTTTCTTC	TTGGGAGCTGCTTCTTCAAT	192 bp
human	GAPDH	GAGTCAACGGATTTGGTCGT	GACAAGCTTCCCGTTCTCAG	186 bp
chicken	Arhgap6	ACGATCTTTGGCCCTAACCTGT	ACAACATCTGGGTCGGTCTCTA	206 bp
chicken	Arhgap18	GGCTTATGATCGGGAAAAGCAC	GCAGCGTTCCCCAATATTTCCT	247 bp
chicken	Arhgap28	TGGACAAAGAGCCAGAGGTT	GTTTTCTCGTCTCCGCACTC	216 bp
chicken	DLC1	CCTGCGGGTCAGGAAAATCTAA	TTGCTGAGGTCTGGAGTGTG	216 bp
chicken	Racgap1	TGGAGTACTGGAGCCAGCTT	GGGGTCATGCTGAAGGTAGA	211 bp
chicken	GAPDH	CCTCTCTGGCAAAGTCCAAG	CATCTGCCCATTTGATGTTG	200 bp
chicken	COL1A1	CTGAAGAAGGCTCTGCTGCT	AGGAGCCAAGTCAATGATGG	183 bp
chicken	FN1 fibronectin	GATCACCGCAGACAAAAGGT	GACCACTGCCAAAGCCTAAG	207 bp
chicken	ITGB1 integrin β1	AATGTGGTGCATGCAGATGT	TTGATCGATCGCAGTTGAAG	220 bp
chicken	ITGA11 integrin α11	ATGACAGCCTTCGTCTGCTT	GTCAGCTGTGTCCAGCACAT	219 bp
chicken	ACTN1 α-actinin	TCACAGACATCGTCCAGAGC	CTCCTGAGAAGGCGTGGTAG	206 bp
chicken	TNS1 tensin	ACAACGTCTGCCACCTCTTT	CCCCAAATTCACTTCCCTCT	206 bp
chicken	VCL vinculin	GGTCGTCGTCTAGCCAATGT	CAGACACCTCCTGGGTCATT	214 bp
chicken	RhoA	CCCAACGTGCCTATCATCTT	GCAGCTCTAGTGGCCATTTC	212 bp
chicken	Rac1	GCCATGGCAAAAGAGATAGG	TTGGCATTGAATGTGATGCT	220 bp
chicken	Cdc42	CTGGTGGTGCATCTCCCTAT	AAAGGTCCTGCACACAATCC	213 bp
chicken	RhoQ	CGTGATGACCCCAAAACTCT	TCACCGTGTGTTTCTTTGGA	196 bp
mouse	Arhgap6	GCTGCTGTCAACATCTGGAA	TCAGGCTCCAACAGGAGAGT	247 bp
mouse	Arhgap18	GCCCAGACACTCAAGAAAGG	TGTCGTCTACACTGGCTTGG	153 bp
mouse	Arhgap28	GCCATTCAGCTCAACAGTCA	TAGGGCTTGATGACCCATTC	212 bp
mouse	Arhgap28 (Exon6-11)	TGCTGTTCACACCAATGGAT	AACATGACCGCAGCTTCTCT	624 or 388 bp
mouse	Arhgap28-V5-His	CAAAGATGTCCTGGCGAAAT	AACTAGAAGGCACAGTCGAGG	233 bp
mouse	DLC1	TGTGCTGAGAGAACGTCACC	ACTCCACAGACAGGGACACC	200 bp
mouse	Racgap1	CACAGACAATTTGGGCACAC	GCATGCCCTCTCCAATCTTA	239 bp
mouse	GAPDH	AACTTTGGCATTGTGGAAGG	ACACATTGGGGGTAGGAACA	223 bp
mouse	COL1A1	GCCTGCTTCGTGTAAACTCC	TTGGTTTTTGGTCACGTTCA	224 bp
mouse	RhoA	GTGGATGGGAAGCAGGTAGA	TTGTTCCCAACCAGGATGAT	212 bp
mouse	Rac1	CTGAAGTGCGACACCACTGT	CTTGAGTCCTCGCTGTGTGA	203 bp
mouse	Cdc42	CTGTTTCCGAAATGCAGACA	AATCCTCTTGCCCTGCAGTA	201 bp
mouse	RhoQ	CTCATGAGCTATGCCAACGA	GGATTTACCACGGAGAAGCA	203 bp

Table 1
Primers for RT-PCR and qPCR.
List of primers used to detect expression of rat, human, chicken and mouse genes.

2.4 Comparative gene expression microarrays

2.4.1 Sample preparation

For the comparison of tendon tissues at different developmental stages, tail tendons were dissected from Sprague Dawley rats of triplicate litters at three developmental stages: E21, 3 weeks and 6 weeks postnatal. For the comparison of bone tissues between *Arhgap28*$^{+/+}$ and *Arhgap28*$^{del/del}$ mice (see section 2.9), tibia and fibula were dissected from three P0 neonatal litters each from defined *Arhgap28*$^{+/+}$ or *Arhgap28*$^{del/del}$ breeding. Bones were incubated in 1000 U/ml bacterial collagenase type 4 (Worthington Biochemical Corporation) in 0.25% trypsin (Invitrogen) for 25 minutes at 37°C with agitation every 10 minutes. The bones were then removed of any excess muscle and cartilage tissues and washed in PBS. RNA was isolated using a dismembrator and treated with DNase as described previously in section 2.3.1. RNA integrity was confirmed by gel electrophoresis. Integrity and measurement of total RNA was further performed using Agilent 2100 Bioanalyzer (Agilent Technologies, Stockport, UK). RNA was amplified by two-cycle cDNA synthesis, then labelled cRNA was synthesised and hybridised to Rat Genome 230 2.0 or Mouse Genome 430 2.0 GeneChip arrays (Affymetrix, High Wycombe, UK).

2.4.2 Microarray analyses

All statistical analyses were performed by Dr Leo Zeef (University of Manchester); Microarray data sets were analysed by dChip (DNA-Chip) Analyzer to normalise the array readouts (Li and Wong, 2001). Normalised readouts were analysed using the Robust Multichip Average method as described by Irizarry *et al.* (2003). Principal component analysis (PCA) was employed to confirm that different variables were present as a quality control for the arrays. *p* values for each probe set were generated

by Limma t-test and variant pooling with the respective controls either the (E21 or *Arhgap28*$^{+/+}$) and *q* values were subsequently generated by applying false discovery rate correction. Gene ontology analysis was performed on probe sets that have detected fold changes greater than 2 using Database for Annotation, Visualisation and Integrated Discovery (DAVID) online tool (Huang da *et al.*, 2009).

2.5 V5-His-tagged mouse Arhgap28 overexpression clone

2.5.1 Sequencing endogenous Arhgap28 transcript in mouse

Primers designed to amplify overlapping segments (of ~900 bp) was used to analyse of mouse Arhgap28 mRNA (see Table 2). The cDNA template used in these reactions was generated using random hexamer primers (as described in sections 2.3.1-5). A cDNA clone of the short isoform of *Mus musculus* Arhgap28 (BC066788.1; Source BioScience Geneservice, Cambridge, UK) was used as control template in these reactions.

2.5.2 Cloning into pcDNA6/V5-His C

Please see Appendix 1 for breakdown of the cloning procedure. For the generation of a C-terminus V5-His-fusion Arhgap28 clone, the sequence encoding V5-His (GKPIPNPLLGLDST-$(His)_6$) was introduced immediately 5' of the stop codon of the endogenous, larger Arhgap28 isoform cDNA. The cDNA clone of the short Arhgap28 isoform was digested with EcoRI and BsmBI (New England Biolabs, Hertfordshire, UK) following the manufacturer's instructions to produce a 1123 bp fragment of the 5' portion of the Arhgap28 clone. For the preparation of the 3' portion of endogenous Arhgap28 transcript, a 1209 bp fragment was amplified from mouse tendon cDNA made with random hexamers (generated as described in sections 2.3.1-2) using a forward primer that covered a unique endogenous BsmBI restriction recognition site

Reaction #	Forward primer 5'-3'	Reverse primer 5'-3'	Larger isoform	Smaller isoform
1	CGTTGGTCTCGGTCTTTGTT	CTCTGTAGGGCCACAAAACC	780 bp	780 bp
2	CCTGCGGGAAATTGAGAGTA	GTGGCGGATTTTCTTCATGT	808 bp	808 bp
3	GAAGAACGTTCCAGCAGAGG	GTTCATGCGGTTCTTGGATT	766 bp	766 bp
4	AGAGAAGCTGCGGTCATGTT	TAGGGCTTGATGACCCATTC	821 bp	-
5	AGAGAAGCTGCGGTCATGTT	CAGGGATACCTGCCTGTGAT	-	821 bp
6	GCCATTCAGCTCAACAGTCA	AGGAGAAACGGAAGACACCA	800 bp	-
7	CATGGTGTGAGGGAGCTTTC	GGCTCCACAGGTAAGGAACA	759 bp	-
8	CAAAGATGTCCTGGCGAAAT	TCTCTTTTGTGGGCAAATCC	-	813 bp
9	GCTTGTGGAAGCTGGAGACT	CAGGGATACCTGCCTGTGAT	767 bp	-
10	GGGTTTCTGTGTGTCCCTGT	TCTCTTTTGTGGGCAAATCC	752 bp	-
11	TCGGCTATGCCTTTTTGTTC	AAATCCATGGAGAGCAGTGG	826 bp	826 bp
12	TGCCGTTAGCTTTCAGTGTG	GGAAAATAGTTGAAAATGCCTGTC	443 bp	400 bp
			Wild type	**Del7-9**
13	TGCTGTTCACACCAATGGAT	AACATGACCGCAGCTTCTCT	624 bp	388 bp
14	GAAGAACGTTCCAGCAGAGG	GTTCATGCGGTTCTTGGATT	766 bp	-

Table 2
Primers for sequencing murine Arhgap28 mRNA transcripts.
List of primers used to perform overlapping RT-PCRs.

Purpose	Forward primer 5'-3'	Reverse primer(s) 5'-3'	Product size
3' portion of endogenous Arhgap28 for cloning	Internal BsmBI site AAGATTTGGGTTGACCGAGACG	New BstBI site AATTCGAAGGGCTTGATGACCC	1209 bp
Sequencing from T7 primer site	TAATACGACTCACTATAGGG		NA
Sequencing from BGH primer site	AACTAGAAGGCACAGTCGAGG		NA
Genotyping *Arhgap28* wild type, *Arhgap28*^{gt} and or *Arhgap28*^{del} alleles	CCCGAATACCTAGCAGTGGA	Wild type allele TACCGAGATCTGGGGAACAG	493 bp
		Mutant allele CAACGGGTTCTTCTGTTAGTCC	354 bp
Genotyping *Arhgap28 del7-9* (*Arhgap28*^{del}) allele	CCCCCTGAACCTGAAACATA	GAGGCAGGAGGATCTCTGTG	400 bp
Genotyping *Cre* transgene	TTCAATTTACTGAACGTACA	AAACAGCATTGCTGTCACTT	350 bp

Table 3
Primers for cloning full length murine Arhgap28-V5-His and genotyping.
List of primers used to generate cDNA for cloning, sequencing and genotyping.

and a reverse primer that created a new BstBI site immediately before the stop codon. iProof High-Fidelity DNA Polymerase (Bio Rad Laboratories, London, UK) was used following the manufacturer's protocol (see Table 3 for primer sequences). Conditions for the amplification were as follows: 98°C for 3 minutes followed by 30 cycles of 98°C for 30 seconds, 60°C for 30 seconds, 72°C for 30 seconds and a final extension at 72^{o}C for 10 minutes. The PCR fragment was sequenced and cut with BsmBI and BstBI restriction enzymes (New England Biolabs). pcDNA6/V5-His C vector was prepared by digestion with EcoRI and BstBI restriction enzymes (New England Biolabs). The three cut fragments were purified using QIAquick Gel Extraction kit (Qiagen) and ligated using T4 DNA Ligase (New England Biolabs) in a 20 µl reaction incubated overnight at 4°C. 10 µl of the reaction was used for transforming competent cells.

2.5.3 Transformation

One Shot Stbl3 Chemically Competent Cells (Invitrogen) were transformed with 10 µl of the ligation mixture following the manufacturer's instructions. The transformation mixture (100 µl) was plated onto Lysogeny broth (LB) agar plates containing 50 µg/ml amplicillin and incubated overnight at 37°C. Single colonies were amplified in 2 ml LB containing 50 µg/ml ampicillin for 6 hours, with shaking at 225 rpm at 37°C. Glycerol stock was made from 100 µl of the culture once the sequence was confirmed. DNA was purified from each culture using QIAprep Spin Miniprep kit (Qiagen) following the manufacturer's protocol.

2.6 Protein methods

2.6.1 Protein isolation

Cells in monolayer were washed with ice-cold PBS three times and incubated with ~10 µl/cm^2 of ice-cold cell lysis buffer (20 mM Tris/HCl pH 7.6, 150 mM NaCl, 1 mM ethylene diamine tetra-acetic acid (EDTA), 1% Igepal CA-630, 50 mM sodium fluoride) containing complete, mini EDTA-free protease inhibitor cocktail (Roche, Sussex, UK) and phosphatase inhibitors (1 mM sodium orthovanadate and 1 mM sodium pyrophosphate) on ice for 10 minutes. Cell lysates were scraped into an eppendorf and passed through a 27 G syringe 3 times and then centrifuged for 10 minutes at 10 000 x g, at 4^{o}C to pellet cell debris. Concentration of the protein in the supernatant was then determined using BCA protein assay (Pierce, supplied by Thermo Fisher Scientific), following the manufacturer's protocol.

2.6.2 Active GTPase pull-down assays

Activity of RhoA was measured using Active Rho Pull-Down Assay (Pierce) according to manufacturer's protocol. In brief, cells were plated at a density of 3 x 10^4 cells/cm^2 and cultured to 80-90% confluence. Cells in each 15 cm dish were washed with ice-cold Tris-buffered saline three times and then lysed with 700 µl Lysis/Binding/Wash Buffer. Cell lysates were scraped into an eppendorf, vortexed briefly and incubated on ice for 5 minutes. The lysates were centrifuged for 15 minute at 16 000 x g, at 4°C. 700 µl of the cell lysate was incubated with 400 µg of glutathione S-transferase (GST)-rhotekin-receptor binding domain and 100 µl 50% agarose resin slurry for 1 hour at 4°C on a vertical rotator, at 5 rpm. The excess supernatant was saved for analysis of total RhoA. The incubations were centrifuged for 30 seconds at 6000 x g, at 4°C to remove the unbound lysate and washed with 400 µl Lysis/Binding/Wash Buffer 3 times. The beads

were then resuspended in 50 µl of 2 x SDS Sample Buffer and boiled at 98°C for 5 minutes for analysis of RhoA by western blotting.

2.6.3 SDS-PAGE and western blotting

NuPAGE Novex 10 % polyacrylamide Bis-Tris gels (Invitrogen) were run in MOPS buffer (50 mM 3-(N-morpholino) propane sulfonic acid, 50 mM Tris base, 0.1% SDS, 1 mM EDTA, pH 7.7) or in MES buffer (50 mM 2-(N-morpholino) ethanesulfonic acid, 50 mM Tris base, 0.01% SDS, 1 mM EDTA, pH 7.3) at 200 V to resolve extracted protein. Resolved proteins were transferred onto Hybond-P PVDF membranes (GE Healthcare, Hatfield, UK). Membranes were blocked for 1 hour with 5% Marvel in PBS containing 0.2% Tween 20. Blots were then incubated at 4°C overnight with primary antibodies, rabbit monoclonal anti-RhoA (#2117 from Cell Signaling Technology, Hertfordshire, UK; diluted 1:2000) or mouse monoclonal anti-V5 epitope (MCA1360 from AbD Serotec, Oxford, UK; diluted 1:1000), diluted in the blocking buffer. Blots were washed with PBS containing 0.2% Tween 20 for 10 minutes three times before they were incubated for 1 hour at room temperature with the appropriate HRP-conjugated secondary antibodies (Pierce) diluted (1:1000) in the blocking buffer. Signals were detected with SuperSignal West Dura Substrate (Pierce) and Hyperfilm ECL (GE Healthcare).

2.7 Immunofluorescence

Cells or tendon constructs were washed with ice-cold PBS 3 times and fixed with ice-cold 4% paraformaldehyde in PBS for 20 minutes at RT. Fixed cells were washed with PBS containing 0.1% Tween 20 three times and blocked with 1% bovine serum albumin, 0.1% Triton X-100 in PBS containing 0.1% Tween 20 for 1 hour. Cells were incubated with primary antibodies, mouse monoclonal anti-V5 epitope (diluted 1:500),

mouse monoclonal anti-vinculin (V9131 from Sigma; diluted 1:500), or the appropriate control IgGs, diluted in the blocking buffer overnight at 4°C. Cells were washed with PBS containing 0.1% Tween 20 for 10 minutes three times and incubated with Alexa Fluor 594-conjugated antibodies (1:200; Invitrogen) and/or Atto 488-conjugated phalloidin (1:500; Sigma) diluted with the blocking buffer for 1 hour at room temperature, protected from light. Stained cells were washed with PBS containing 0.1% Tween 20 for 10 minutes three times and mounted using Vector Shield containing DAPI (Vector Laboratories, Northamptonshire, UK). Fixed 3D tissue constructs were snap frozen in cryo embedding medium and 7 µm longitudinal sections were cut and mounted onto SuperFrost slides (Menzel-Gläser GmbH, supplied by Thermo Fisher Scientific). Slides then stained with Atto 488-conjugated phalloidin diluted in the blocking buffer. Fluorescent images were taken using a digital camera attached to an Olympus BX51 (Middlesex, UK) and captured using MetaVue imaging software (Molecular Devices, CA, USA).

2.8 Transmission electron microscopy

Tissues were fixed for 30 minutes with 2% glutaraldehyde in 100 mM phosphate buffer pH 7. Tissues were cut into smaller (~1 mm^2) specimens and fixed overnight at 4°C in fresh fixative. Fixed tissues were washed with 100 mM phosphate buffer pH 7 and post-fixed for 50 minutes in 2% glutaraldehyde, 1% osmium tetraoxide in 100 mM phosphate buffer pH 6.2 and washed extensively with distilled water. Specimens were *en bloc* overnight at 4°C with 1% aqueous uranyl acetate. After, specimens were dehydrated through a graded series of acetone (30, 50, 70 and 90%) for 10 minutes each, and in 100% acetone for 10 minutes four times. Specimens were incubated for 10 minutes in propylene oxide and infiltrated with increasing concentrations of Agar

Low Viscosity Resin (Agar Scientific, Essex, UK) according to manufacturer's protocol and embedded in fresh 100% resin and cured for 24 hours at 60°C. 70 nm sections were cut, stained with 1% lead citrate and examined by Tecnai 12 Biotwin TEM (FEI Electron Optics, Netherlands). Triplicate samples were used in this experiment. For each sample, at least 13 images of TEM sections were taken and examined by counting. The number of fibripositors and fibricarriers were divided by the number of nuclei present in the same image (whole nuclei were counted as 1 and nuclei at the edge on the image were counted as 0.5). Two-sample T tests were used to determine a significance difference between the means of experimental groups.

2.9 Animals

2.9.1 Arhgap28 mice

Experiments were performed in compliance with the UK Home Office and Institutional regulations governing animal breeding and handling. Using homologous recombination in agouti C57BL/6N embryonic stem (ES) cell, the L1L2_Bact_P targeting gene trap cassette (including the genes encoding β-galactosidase and neomycin) was introduced into intron 6 of the Arhgap28 gene by the NIH Knockout Mouse Project (KOMP; CA, USA). In addition, exons 7-9 are flanked by *loxP* sites. ES cells containing the Arhgap28 gene trap allele (*Arhgap28*^{gt}) were injected into C57BL/6J blastocysts to produce germ line-transmitting chimeras (prepared at the University of Oulu, Finland). Chimeric males were assessed on coat colour and mated with wild type C57BL/6J females to produce heterozygous progeny, which were then mated to obtain mice homozygous for the Arhgap28 gene trap allele (*Arhgap28*$^{gt/gt}$). For the generation of Arhgap28 deleted exons 7-9 (*Arhgap28*^{del}) mutant males heterozygous for the Arhgap28 gene trap allele were mated with females from a line of *Cre* transgenic mice (a kind gift from

M. Briggs, University of Manchester, UK) to delete the *loxP*-flanked exons 7-9 by DNA recombination. Heterozygous F1 offspring were then mated to generate *Arhgap28*$^{del/del}$ mice.

2.9.2 Genotyping

Mice were genotyped using genomic DNA extracted from ear punches of adult mice or amniotic sacs of embryos using 200 µg/ml Proteinase K (Invitrogen) in buffer containing 17.6 mM N-lauroyl sarcosine, 100 mM NaCl and 5% Chelex 100 resin (Bio Rad Laboratories) incubated at 55°C for 2 hours, mixed occasionally by vigorous vortexing. The resulting DNA supernatant was purified by precipitation with phenol:chloroform:isoamyl alcohol and resuspended in 50-100 µl DEPC water. Genotypes were determined using specific primer pairs (see Table 3) from 1 µl genomic DNA using BioMix Red PCR reagents (Bioline). Genotyping PCRs were performed as described in section 2.3.4. The annealing temperature for the wild type/mutant allele PCR was 53°C. The annealing temperature for the *Arhgap28*^{del} allele was touch-down from 70-60°C for 10 cycles followed by 20 cycles at 60°C. The annealing temperature for the *Cre* transgene was 50°C.

2.9.3 Whole mount X-gal stain

For detection of beta-galactosidase expression, E10.5-E15.5 embryos were fixed for 1 hour in 3.7% PFA in PBS pH 8 at room temperature. For older embryos the skin was removed before being fixed for 1 hour in 3.7% PFA in PBS pH 7.4 at room temperature. Embryos were then washed with PBS containing 0.1% Triton X-100 for 15 minutes twice. Each embryos was then stained with 20 ml of freshly prepared X-gal staining solution (1 mM X-gal (Qiagen), 5 mM potassium ferricyanide ($K_3Fe(CN)_6$), 5 mM

potassium ferrocyanide ($K_4Fe(CN)_6$), 1 mM $MgCl_2$ in PBS containing 0.1% Triton X-100) for 24 hours at 37°C. After staining, the embryos were rinsed with PBS and post-fixed in 4% PFA in PBS overnight at 4°C. After post-fix, the embryos were either processed for paraffin embedding or dehydrated in 70% ethanol for 6 hours and cleared with glycerol (10 ml of each 30, 50 and 80% glycerol in 1% potassium hydroxide and then 100% glycerol), incubating at 37°C for 2-3 days each.

2.9.4 Histology

Embryos were fixed overnight in either 4% PFA in PBS. They were then processed and embedded in paraffin wax. 6 µm sagittal sections were cut and mounted onto SuperFrost slides. For haematoxylin and eosin staining, slides were de-paraffinised and stained using an automated stainer and cleared into Histo-Clear (Thermo Fisher Scientific). For Alizarin red S staining, sections were deparaffinised with xylene and rehydrated through a graded ethanol series. Sections were then washed with distilled water and stained with 2% Alizarin red S pH 4.2 for 10 minutes, washed with distilled water and dehydrated. Images were captured using a Carl Zeiss Axiocam Colour CCD camera with associated AxioVision software.

2.9.5 Mechanical testing

Elastic modulus of tendons was measured as described in Kalson *et al.*, (2010). In brief, tendons were pulled from P14 mouse tails and mounted onto a sandpaper (grade 100) frame, with a 1 cm length window, using superglue. The sandpaper frame was clamped in an Instron 4301 mechanical testing machine fitted with a 100 N load cell (Instron Inc, High Wycombe, UK). Only samples that failed in the mid portion of the tendon were included. Tendons were tested to failure with a strain rate of 5 mm per

minute. The length and width of the samples tested were measured from a digital photograph using ImageJ, which were used to derive corrected elastic modulus values. One-way ANOVA followed by a Dunnett's test was performed to determine significance differences compared to wild type.

2.9.6 Bone length measurements

X-rays of mice were produced using a Flaxitron x-ray specimen radiograph system (Flaxitron Bioptics, Berkshire, UK) and x-ray film (GE Healthcare). Bone measurements were taken from scanned radiographic images using ImageJ software. One-way ANOVA followed by a Dunnett's test to determine significance differences compared to wild type.

CHAPTER 3

IDENTIFICATION OF A CANDIDATE REGULATOR OF ACTIN REORGANISATION DURING TENDON TISSUE FORMATION

3. Identification of a Candidate Regulator of Actin Reorganisation During Tendon Tissue Formation

3.1 Chapter introduction

The second half of rodent embryonic development (E13.5 up to E21) is a critical stage in the growth of tendons, when the ECM becomes populated with bundles of parallel collagen fibrils. The appearance of fibrils is associated with the appearance of tension-sensitive, actin-stabilised fibripositors at the plasma membrane of embryonic tendon cells, which contain newly synthesised, narrow-diameter collagen fibrils (described in the Introduction). Disruption to the actin cytoskeletal network in embryonic tendon tissue leads to the disorganisation of collagen fibrils in the ECM (Canty *et al.*, 2006). The mechanism of actin reorganisation required for the specialised shape of embryonic tendon cells and the architectural organisation of the tendon ECM is unknown. Fibripositors are abundant in late embryonic fibroblasts but absent from postnatal fibroblasts; the fibripositors disappear abruptly a few days after birth in mouse and rat. The disappearance of fibripositors shortly after birth offered the opportunity to identify genes responsible for the formation of fibripositors and the assembly of a collagen fibril matrix. The Rho GTPases (e.g. Rho, Rac and Cdc42) are major regulators of actin reorganisation and are fundamental for filopodia and lamellipodia formation, retraction of plasma membranes, cell spreading and mechanotransduction. Their activity is regulated in specific tissues by RhoGAPs. Chapter 3 describes the results of a gene array comparison of embryonic and postnatal tendon, which shed light on the differences in gene expression during the development of tendon, and the discovery of Arhgap28, a putative RhoGAP and regulator of actin reorganisation in embryonic tendon fibroblasts.

3.2 Results

3.2.1 Cell shape changes during tendon tissue assembly

Samples of embryonic day 21 (E21), 3 weeks and 6 weeks postnatal rat tail tendons were fixed and examined by TEM. The results show that the ultrastructures of embryonic and postnatal rat tail tendon are similar to that previously described for chick and mouse tendons (see Fig. 6A; Parry *et al.*, 1978, Canty *et al.*, 2004, Ansorge *et al.*, 2011). Transverse sections of E21 rat tail tendon analysed by TEM show evenly-shaped, narrow-diameter fibrils in ECM channels formed by the plasma membrane of the cells (Fig. 6A). In contrast, tendons at 3 weeks and 6 weeks postnatal contain densely packed fibrils of varying diameters in the ECM. In sections of E21 tendon, fibripositors and internal fibril-containing compartments called fibricarriers are present (see Fig. 6A, inset). In comparison, fibripositors and fibricarriers are much reduced in number at 3 weeks postnatal and by 6 weeks are virtually absent. Fibripositors and fibricarriers were quantitated from electron micrographs using the method described by Canty and co-workers (2006). This method provides a value of 'fibripositors (or fibricarriers) per nucleus', as an indication of the number of these structures in a randomly selected 70 nm-thick section of a cell. On average there were 3 fibripositors per nucleus and 3 fibricarriers per nucleus in embryonic tendon cells, significantly more than those found in the postnatal tendon cells ($p < 0.001$; see Fig. 6B). 3D reconstructions of tendon cells in embryonic and postnatal tendon from serial scanning electron microscope sections show the stark differences in cell shape (see Fig. 6C). These data are consistent with extensive cytoskeletal reorganisation from embryonic to postnatal development.

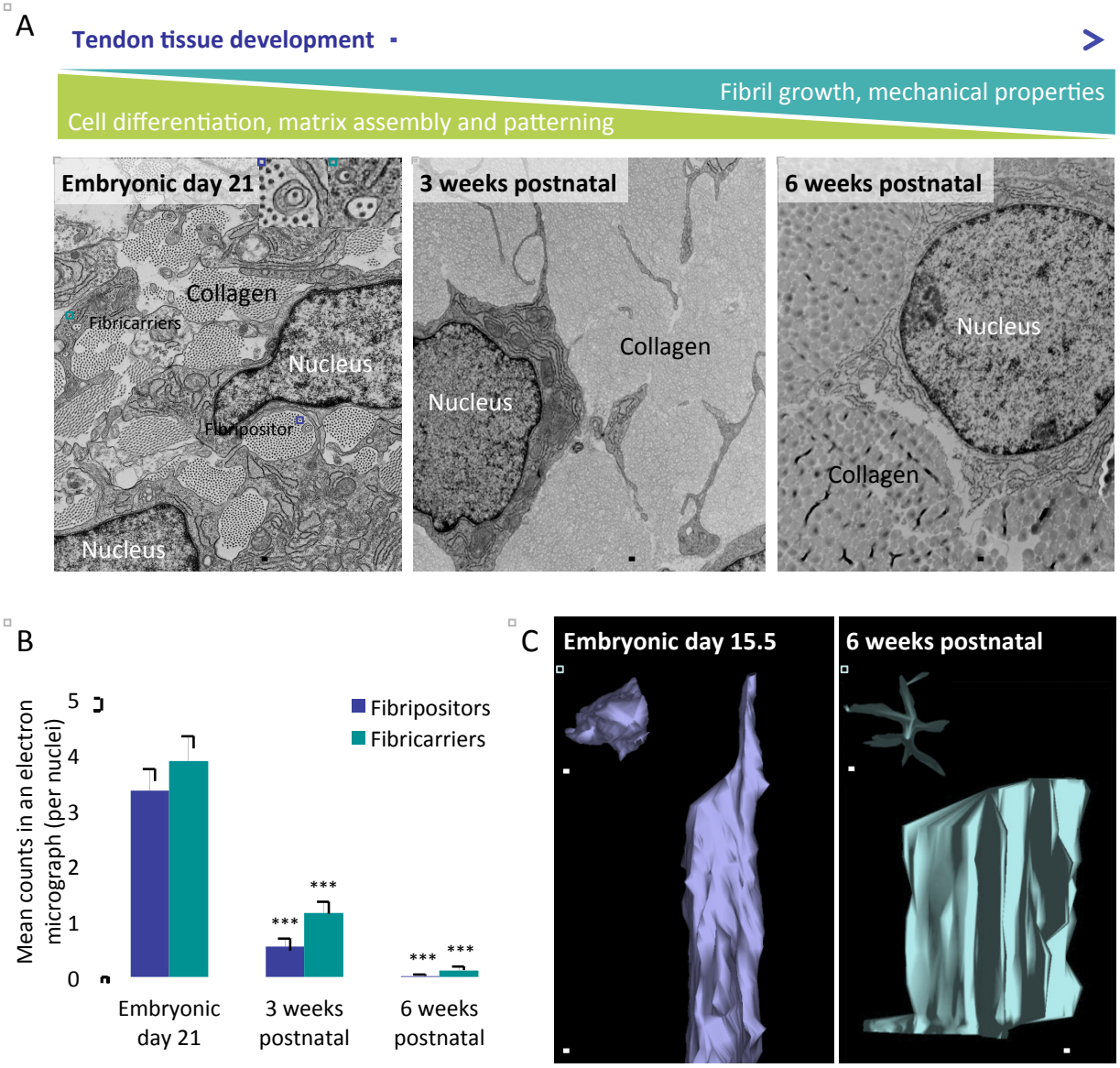

Figure 6

Ultrastructure and cell shape of embryonic and postnatal tendon cells.

(A) Transverse sections of rat tail tendon were examined by TEM. Representative micrograph of embryonic day 21, 3 weeks and 6 weeks postnatal samples showing the ultrastructure of the tissue. Bars = 500 nm. **(B)** Number of specialised membrane protrusions, fibripositors and collagen-containing vesicles, fibricarriers per nucleus in an electron micrograph (micrographs from 3 biological replicates counted = 46, 39, 40). Bars show SEM. *** indicate significant differences found when compared to E21, $p < 0.001$. **(C)** 3D reconstructions of tendon cells from embryonic and postnatal tendon tissues shown along and (inset) across the tendon axis. Bars = 5 µm. Reconstructions were made by Nick Kalson and Diana Golijani.

3.2.2 Comparative microarray analysis

Rat tail was chosen for this analysis because it was possible to dissect tendon tissues cleanly from the embryo for RNA isolation. RNA was isolated from tail tendon tissues of E21, 3 week- and 6 week-old rats and prepared for cDNA microarray analysis. As part of RNA quality control, the integrity of the RNA samples was analysed by gel electrophoresis (Fig. 7A). The microarray readouts were normalised using dChip analysis and then analysed by principal component analysis (PCA). PCA uses a mathematical algorithm to assess similarities and differences between the expression profiles of the samples, and provides a visual representation of the two largest, uncorrelated variables, the principal components (PC #1 and PC #2), calculated (Ringnér, 2008). The first principal component (PC #1) accounted for 61% of the total variability between the samples and clearly separated the samples from the three developmental stages (Fig. 7B). The second principal component (PC #2), which is unrelated to PC #1, accounted for almost 20% of the remainder variability between the samples, clearly showing that triplicates from each time point could be grouped (Fig. 7B). Table 4 shows the data from the dChip analysis, which indicated that the microarray readouts were reliable. The median intensities of the arrays were between 93 and 158 (arbitrary units; see Table 4). The present call percentage (P call %) indicates the percentage of total probe sets on the arrays that were hybridised to the cRNA. In each array, hybridisation to 60-70% of the probe sets was detected. Percentage of array and single outliers showed no anomalies in the readouts of individual probe sets and probes (see Table 4). Further, comparison of microarray readouts for control genes (listed in Table 5) show expected expression patterns for tendon tissue. Together, these analyses confirm that the microarray readouts pass quality control and are reliable.

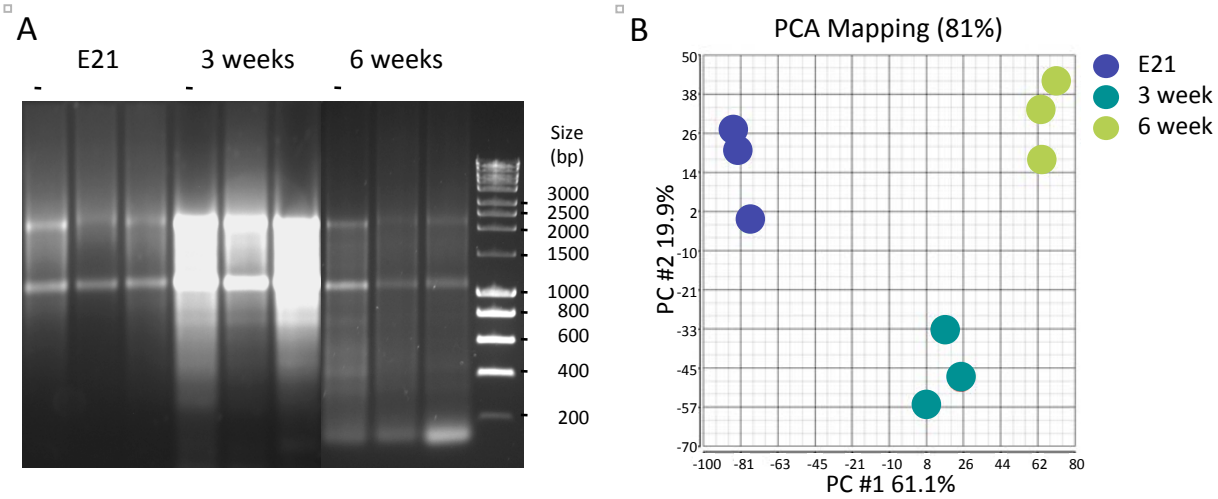

Figure 7
RNA isolated from embryonic and postnatal rat tail tendon for microarray.
(A) Agarose gel showing total RNA isolated from triplicate samples of embryonic and postnatal rat tail tendons. **(B)** PCA mapping of variability between the array samples.

Array[A]	Median Intensity[B]	P call %[C]	% Array outlier[D]	% Single outlier[E]
E21_1	119	65.9	0.293	0.046
E21_2	139	63.4	1.794*	0.229
E21_3	137	67.8	0.354	0.048
3 week_1	131	63.3	0.096	0.053
3 week_2	158	62.9	0.148	0.087
3 week_3	145	64.1	0.161	0.081
6 week_1	100	58.8	0.457	0.137
6 week_2	102	60.9	0.338	0.100
6 week_3	93	58.9	0.498	0.104

Table 4
dChip analysis of microarray data sets.
(A) Triplicate samples of E21, 3 weeks and 6 weeks postnatal rat tail tendons indicated by the number at the end of each array name. **(B)** Median intensity of microarray chip for each triplicate of each experimental group. **(C)** Present (P) call percentage indicates the percentage of total probe sets detected. **(D)** Array outlier percentage indicates the percentage of probe sets that have outliers in the average readout profile of each probe within a probe set. **(E)** Percentage single outlier indicates the percentage of probes that do not have the same intensity pattern of other probes within the same probe set. *Value still below warning level of 5%.

Gene	Gene symbol	E21	3 weeks	6 weeks
tendon matrix genes				
collagen, type 1, alpha 1	COL1A1	19455.5 3066.9	20960.7 3124.3	17602.5 4447.1
collagen, type 1, alpha 2	COL1A2	23885.3 19431.5	24292.3 20889.4	20965.5 16695.1
collagen, type 2, alpha 1	COL2A1	8283.6 543.8 548.0	3372.2 58.6 468.5	1077.5 27.9 300.6
fibronectin	FN1	2940.1	2374.3	2258.8
integrin alpha 5	ITGA5	49.7	47.8	36.5
integrin beta 1	ITGB1	3237.2 332.6	2637.2 256.9	1744.8 176.6
scleraxis	SCX	2215.5	1548.0	1305.7
fibromodulin	FMOD	16609.6	17861.4	13478.5
biglycan	BGN	1338.6	360.6	314.5
tenascin C	TNC	841.8	1433.4	1887.2
tenomodulin	TNMD	14425.7	12097.0	10522.6
actin genes				
alpha-skeletal-actin	ACTA1	279.8	776.5	315.1
alpha-cardiac actin	ACTC1	123.8 17.4 27.1 11.8 20.4	44.2 13.1 23.4 11.9 24.8	42.1 13.2 23.1 12.2 19.1
beta-cytoskeletal actin	ACTB	1255.6 6118.1	1099.5 5532.2	745.0 3584.9
gamma-cytoskeletal actin	ACTG1	6724.5 38.5	5612.3 40.8	5210.2 51.5
alpha-smooh muscle actin	ACTA2	59.4	82.5	66.5
gamma-smooth muscle actin	ACTG2	14.5	62.0	20.3
house-keeping genes				
ribosomal protein S18	18s	8748.3	12808.3	7986.7
glyceraldehyde 3 phosphate dehydrogenase	GAPDH	3917.1	4619.8	2390.0
hypoxanthine guanine phosphoribosyl transferase	HPRT	425.8	933.2	869.5
ubiquitin	UBB	5113.7 6345.2	5244.4 6606.0	4772.7 5600.1

Table 5
Expression of control genes in embryonic and postnatal rat tail tendon.
Mean intensities from hybridisation of triplicate samples to probe set(s) for the genes listed.

3.2.3 Gene ontology analysis

The microarray data showing the changes in expression detected by 31,042 probe sets is visually represented in a heat map shown in Appendix 2. The heat map is generated from hierarchical clustering of genes (or probe sets), which is based on similarities in the expression level and the expression profile. Expression profiles detected by each probe set (some genes have more than one probe set) in the microarray can fit into one of eight major profiles (see Fig. 8). In the interest of selecting a target gene to investigate tendon tissue formation, only genes that were highly expressed at E21 and then significantly downregulated ≥ 2-fold at 3 weeks postnatal were included ($q < 0.01$; see section 2.4.2 on derivation of q values). From the readouts, 1632 probe sets fitted this criterion, and of these probe sets, the gene IDs of 1070 were recognised by the Database for Annotation, Visualisation and Integrated Discovery (DAVID) online tool (Huang da *et al.*, 2009). DAVID was used to identify enriched gene ontology categories, in which genes are placed into functional groups according to their cellular component, molecular function or biological process. DAVID functional annotation clustering produced 243 clusters. The cluster with the highest enrichment score of 13.36 contained four gene ontology components in which genes of the cytoskeleton were over-represented (listed in Appendix 3). This result further suggests that major cytoskeletal reorganisation occurs between embryonic and postnatal tendon development.

3.2.4 Arhgap28 as a candidate regulator of actin reorganisation in tendon formation

Rho GTPase signalling is the major regulatory pathway for actin reorganisation. Seven genes from the GTPase signalling family fitted the exclusion criteria (see Fig. 8). There

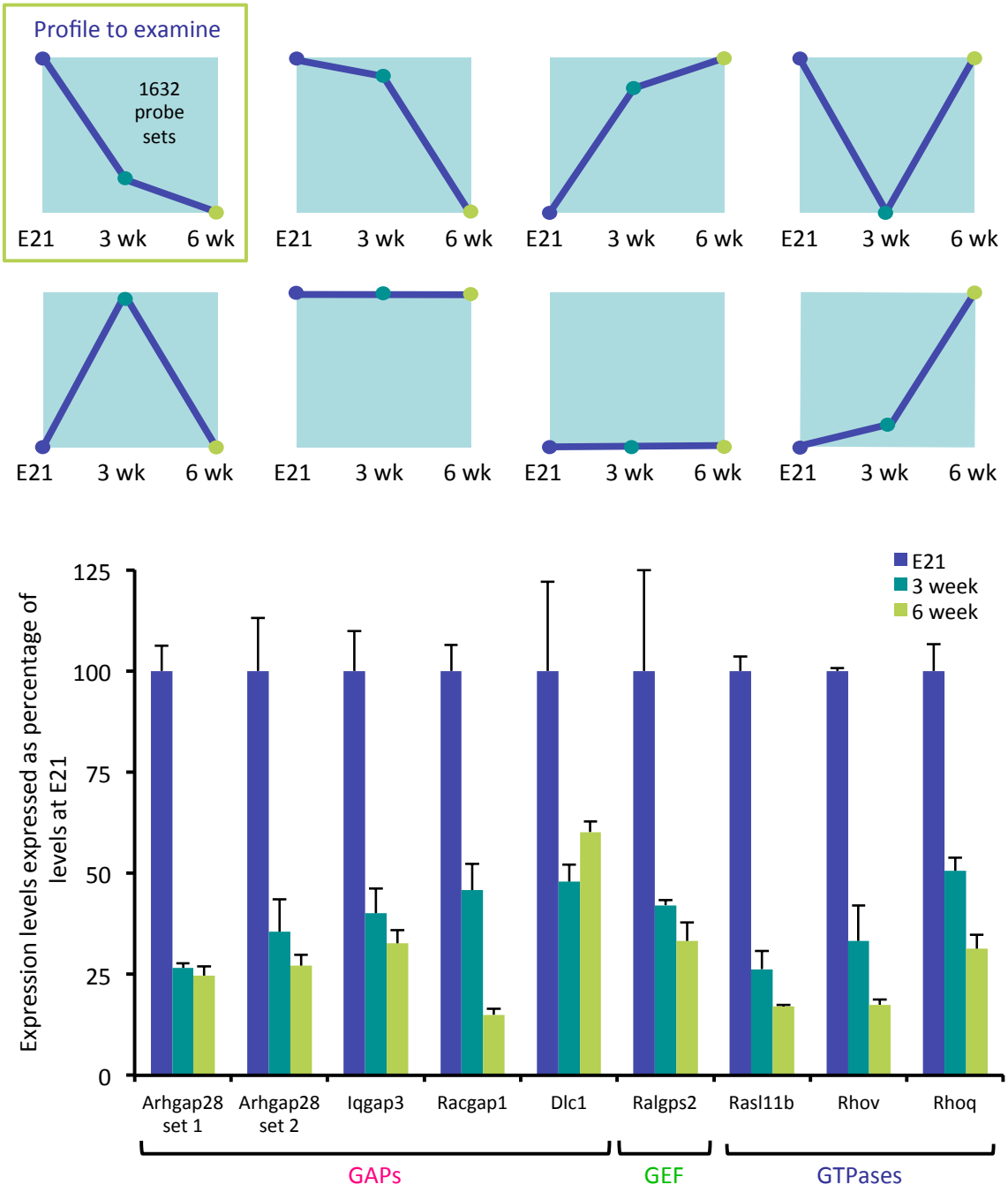

Figure 8

Candidate regulators of actin reorganisation from the GTPase signalling family.

Readouts from each microarray probe set can be divided into 8 major expression cluster profiles. Genes of the GTPase signalling family (GAPs, GEFs and GTPases) that are upregulated at least 2-folds in embryonic rat tail tendon tissues and significantly downregulated postnatal ($q < 0.001$). Gene expression levels of postnatal rat tail tendon is expressed as a percentage of the level of E21 rat tail tendon. Bars show SEM.

were five genes encoding GAPs: Arhgap28, Arap2, Iqgap3, Racgap1 and DLC1; one gene encoding a GEF: Ralgps2; and three genes encoding GTPases: Rasl11b, RhoV and RhoQ. The expression of Arhgap28, detected by two probe sets, showed the most significant reduction from embryonic to postnatal tendon development (see Fig. 8), suggesting that Arhgap28 is a good candidate regulator of Rho signalling in embryonic tendon.

3.3 Discussion

The chapter identifies a novel RhoGAP, Arhgap28, as a candidate regulator of actin reorganisation during the patterning of tendon tissue. Data from this study show that embryonic (E21) rat tail tendon tissue had significantly more fibripositors and fibricarriers than postnatal (3 week- and 6 week-old) tail tendon tissue, which is in line with data derived from mouse tail tendons (Canty *et al.*, 2004, Humphries *et al.*, 2008). Comparison of cell shape and data from a comparative gene expression microarray study between embryonic and postnatal tendon tissue indicate that there are major cytoskeletal changes during tendon development. Analysis of molecules involved in GTPase signalling that were differentially upregulated in embryonic tendon identified Arhgap28 as a RhoGAP that might regulate actin reorganisation during the assembly of an orgnaised collagen-rich ECM.

Rat tail tendon tissues were used as it is possible to isolate them from both embryonic and postnatal stages. Data from quality control analyses suggested that the microarray readouts were significant and PCA analysis was able to group the triplicate samples of E21, 3 week- and 6 week-old tendon tissues. Over 1500 probe sets identified genes that were highly expressed in E21 rat tail tendon and downregulated in 3 weeks

postnatal rat tail tendon. However, no changes were observed in the expression levels of integrins and actin adapter molecules between embryonic and postnatal tendon tissues, which suggest that these molecules are not regulated transcriptionally.

It is thought that GAPs can regulate GTPases in a tissue-specific manner where as GTPases are more ubiquitously expressed (Tcherkezian and Lamarche-Vane, 2007). Arhgap28, a putative GAP for Rho-like small GTPases, such as RhoA, Rac1 and Cdc42, was found to be expressed in E21 rat tail tendon and downregulated in postnatal tail tendon tissue. Rho GTPases mediate a variety of cellular processes, including actin cytoskeleton remodelling, membrane ruffling (lamellipodia) and protrusions (filopodia), and cell contractility (reviewed by Kaibuchi *et al.*, 1999). Many similar processes are also present in embryonic tendon cell (discussed in the Introduction). RhoGAPs stimulate the intrinsic hydrolytic activity of Rho GTPases. Therefore, Arhgap28 could, potentially, be an important regulator of actin reorganisation during tendon tissue assembly.

To date, there are no published data on the physiological functions of Arhgap28. Based on sequence similarities Arhgap28 is closely related to Arhgap6, Arhgap11a, Arhgap11b, Arhgap18, Arhgap40, DLC1 (Arhgap7), DLC2 (Arhgap27) and DLC3 (Arhgap38; see Fig. 9). Some of these RhoGAPs have been characterised to regulate actin reorganisation. Proteins of the DLC family are tumour suppressor genes (Ng *et al.*, 2000, Ching *et al.*, 2003, Durkin *et al.*, 2007). Knockout of DLC1 is embryonic lethal at E10.5 and examination of mouse embryonic fibroblasts isolated from E9.5 embryos revealed disrupted stress fibres and focal adhesions (Durkin *et al.*, 2005). DLC2 and DLC3 have been shown to have GAP activity for RhoA and Cdc42 (Ching *et al.*, 2003,

Figure 9 (overleaf)
Unrooted phylogenetic tree of human RhoGAP proteins.
Based on alignment of the GAP domain using ClustlW algorithm (adapted from Peck 2002). * denotes the human genes that have orthologous *Drosophila* genes. Names in green denote additional RhoGAP domain-containing proteins listed by the HUGO gene nomenclature committee and these are mapped onto the phylogenetic tree (in green lines) according to the homology of RhoGAP domains as recognised by the Conserved Domain Database (Marchler-Bauer 2011).

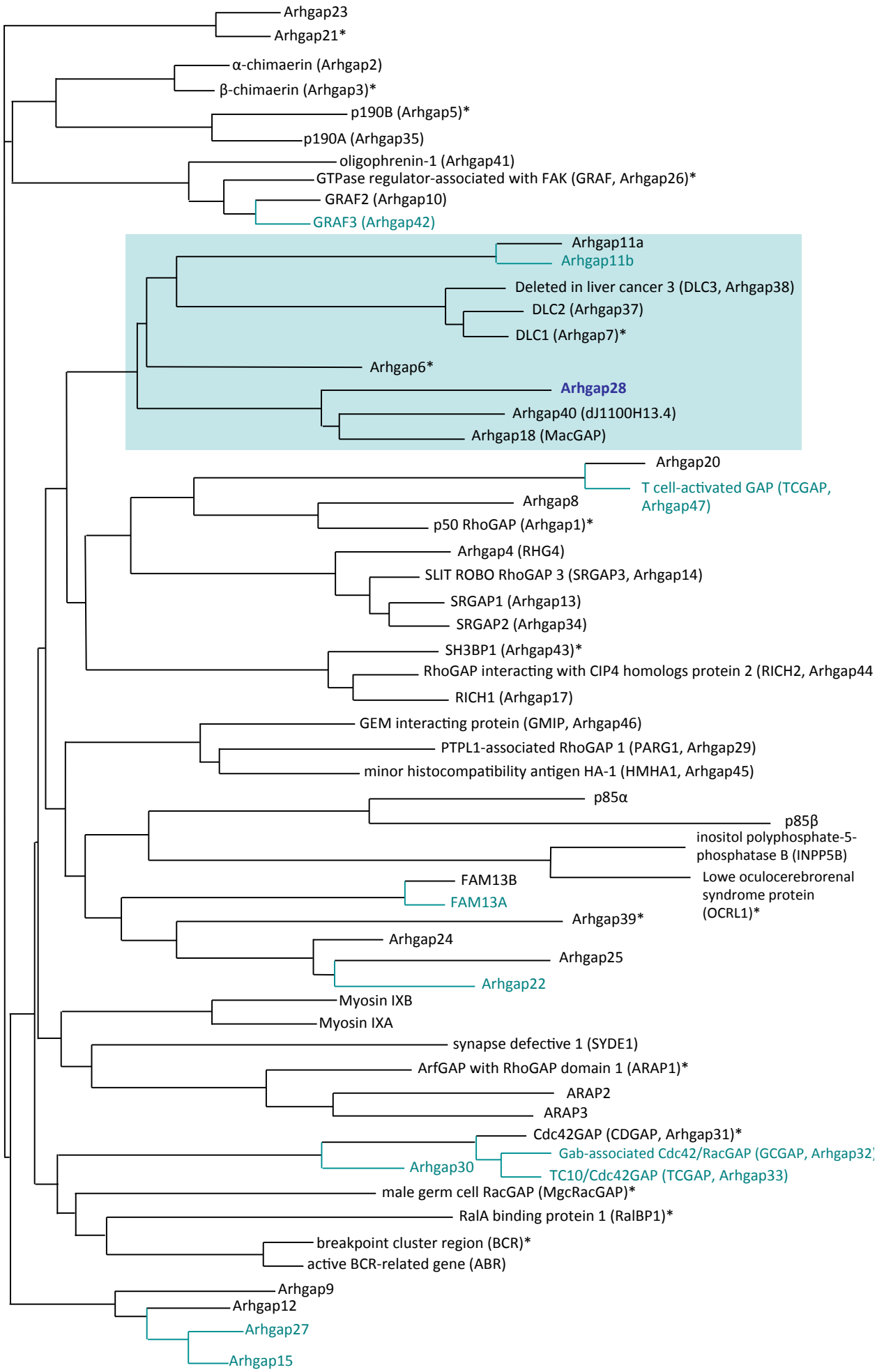
Arhgap23
Arhgap21*
α-chimaerin (Arhgap2)
β-chimaerin (Arhgap3)*
p190B (Arhgap5)*
p190A (Arhgap35)
oligophrenin-1 (Arhgap41)
GTPase regulator-associated with FAK (GRAF, Arhgap26)*
GRAF2 (Arhgap10)
GRAF3 (Arhgap42)
Arhgap11a
Arhgap11b
Deleted in liver cancer 3 (DLC3, Arhgap38)
DLC2 (Arhgap37)
DLC1 (Arhgap7)*
Arhgap6*
Arhgap28
Arhgap40 (dJ1100H13.4)
Arhgap18 (MacGAP)
Arhgap20
T cell-activated GAP (TCGAP, Arhgap47)
Arhgap8
p50 RhoGAP (Arhgap1)*
Arhgap4 (RHG4)
SLIT ROBO RhoGAP 3 (SRGAP3, Arhgap14)
SRGAP1 (Arhgap13)
SRGAP2 (Arhgap34)
SH3BP1 (Arhgap43)*
RhoGAP interacting with CIP4 homologs protein 2 (RICH2, Arhgap44
RICH1 (Arhgap17)
GEM interacting protein (GMIP, Arhgap46)
PTPL1-associated RhoGAP 1 (PARG1, Arhgap29)
minor histocompatibility antigen HA-1 (HMHA1, Arhgap45)
p85α
p85β
inositol polyphosphate-5-phosphatase B (INPP5B)
Lowe oculocerebrorenal syndrome protein (OCRL1)*
FAM13B
FAM13A
Arhgap39*
Arhgap24
Arhgap25
Arhgap22
Myosin IXB
Myosin IXA
synapse defective 1 (SYDE1)
ArfGAP with RhoGAP domain 1 (ARAP1)*
ARAP2
ARAP3
Cdc42GAP (CDGAP, Arhgap31)*
Gab-associated Cdc42/RacGAP (GCGAP, Arhgap32)
Arhgap30
TC10/Cdc42GAP (TCGAP, Arhgap33)
male germ cell RacGAP (MgcRacGAP)*
RalA binding protein 1 (RalBP1)*
breakpoint cluster region (BCR)*
active BCR-related gene (ABR)
Arhgap9
Arhgap12
Arhgap27
Arhgap15

Kawai *et al.*, 2007). Mice lacking functional Arhgap6 protein are phenotypically normal, despite the fact that Arhgap6 is a GAP for RhoA and causes the loss of actin stress fibres in cultured cells (Prakash *et al.*, 2000). Arhgap18 also has specificity for RhoA and disrupts actin stress fibres, where knockdown of Arhgap18 can enhance stress fibre formation (Maeda *et al.*, 2011). It is likely that Arhgap28 similarly regulates actin stress fibre assembly. Although the functions of Arhgap28 have not been reported, its differential expression has been listed in a variety of cDNA microarray studies, as summarised in Table 6. These data suggest that Arhgap28 is likely to have RhoGAP function and thus is expected to be an excellent candidate to investigate for this thesis.

In summary, the results in this chapter have identified Arhgap28, a putative RhoGAP that is differentially upregulated during the establishment of the tendon ECM. Arhgap28 is related to RhoGAPs that regulate RhoA and stress fibre formation. It will be interesting to determine if Arhgap28 has similar functions, and to examine the role of Rho signalling in the formation of a functional tendon tissue.

Reference	Tissue (and organism if not human)	Analysis and observations
Zhao *et al.*, 2007	stromal cell cultured from prostate tissue	cDNA microarray; Arhgap28 was upregulated in stromal cell cultures derived from benign prostatic hyperplasia compared to cells derived from cancerous prostate tissue
Anraku *et al.*, 2008	lung tissue used for transplantation prior implantation	cDNA microarray; Arhgap28 was upregulated in tissues from patients who died as a consequence of primary graft dysfunction compared to lung tissues from case-matched patients who had excellent outcomes
Schilling *et al.*, 2008	osteoblasts and adipocytes derived from the differentiated hMSC (bone marrow)	cDNA microarray; Arhgap28 was upregulated 24 hours after initiating the trans-differentiation of adipocytes into osteoblasts and 24 hours after initiating the trans-differentiation of osteoblasts into adipocytes
Fèvre-Montagne *et al.*, 2009	meningioma tissue	cDNA microarray; Arhgap28 was upregulated in atypical meningiomas and anaplastic meingiomas compared to low-grade meningiomas
Floyd *et al.*, 2009	atherosclerotic plaque tissue from aorta of *ApoE*$^{-/-}$ mice	cDNA microarray; Arhgap28 was upregulated in plaques of mice exposed to concentrated ambient air pariticles compared to mice exposed to filtered air
Wetmore *et al.*, 2010	serum mRNAs from rat liver	cDNA microarray; Arhgap28 was upregulated in serum after treatment with hepatotoxins, acetaminophen but not after treatment with D-(+)-galactos-amine
Hashimoto *et al.*, 2011	prefrontal cortex of mice	cDNA microarray; Arhgap28 was upregulated in male withdrawal seizure-resistant mice compared to female mice and to male and female withdrawal seizure-prone mice
Lippi *et al.*, 2011	primary culture of murine hippocampal neurons	siRNA transfection; knockdown of Arhgap28 mRNA did not significantly alter spine morphology (filopodia or neuronal spines)
Wansbury *et al.*, 2011	mammary primordium of E12.5 mouse embryos	cDNA microarray; Arhgap28 was upregulated in the mammary mesenchyme compared to the mammary primordial bud epithelium
Chan *et al.*, 2012	spermatozoa of rat model for human testicular cancer treatment	DNA methylation analysis; Arhgap28 gene was hyper-methylated in spermatozoa of rats after treatment with bleomycin, etoposide and *cis*-platinum
Gewurz *et al.*, 2012	HEK cells containing GFP reporter for NFκB activation	siRNA screen; knockdown of Arhgap28 reduced Epstein Barr virus latent membrane protein mutant- and interleukin-1β-stimulated but not TNFα-stimulated, NFκB activation
Hadj-Hamou *et al.*, 2012	breast tissue angiosarcomas	cDNA microarray; Arhgap28 was downregulated in radiation-induced tumours compared to primary tumours
Paramanik and Thakur, 2012	mitochondrial extract of mouse brain tissue	pull-down assay and motif scanning; Arhgap28 was found to interact with ligand-binding domain of oestrogen receptorβ and seven consensus motif for casein kinase 2 phosphorylation sites
Pradat *et al.*, 2012	deltoid muscle	cDNA microarray; Arhgap28 was upregulated in patients with advanced amyotrophic lateral sclerosis compared to controls and patients with early state of amyotrophic lateral sclerosis
Yang *et al.*, 2012	CD133^{+} cells cultured from glioblastoma multiforme (brain tumour)	cDNA microarray; Arhgap28 was upregulated in these radio-resistant tumour initiating (CD133^{+}) cells after being cultured with cancer-preventative polyphenol resveratrol
Zhu *et al.*, 2012	embryonic palatal mesenchyme cells	cDNA microarray; Arhgap28 was downregulated in cells treated with TGFβ

Table 6
Summary of studies in which Arhgap28 is identified as a candidate of interest.

CHAPTER 4

ARHGAP28-RHO SIGNALLING EFFECTS ON TENDON MATRIX ORGANISATION

4. Arhgap28-Rho Signalling Effects on Tendon Matrix Organisation

4.1 Chapter introduction

During the establishment of an organised ECM, tendon cells undergo dynamic actin reorganisation (Canty *et al.*, 2006; discussed previously in the Introduction). The development of mechanical strength and stiffness of this ECM requires actomyosin-generated cellular tension (Kalson *et al.*, 2010). The RhoGAP Arhgap28 was identified previously in Chapter 3 and is predicted to regulate the dynamic remodelling of the actin cytoskeleton in embryonic tendon cells. The function of Arhgap28 is hypothesised to be the same as the closely related RhoGAPs, Arhgap6 and Arhgap18, which regulate RhoA activity and stress fibre formation (discussed in Chapter 3). It is not known if RhoA-regulated actin stress fibre formation is important for cells in tendon tissues. Chapter 4 describes the results obtained from studies of Arhgap28 and Rho GTPases expression in embryonic chick tendon cells cultured in the 3D tendon construct culture system. Overexpression of an Arhgap28 cDNA clone and small molecules to alter Rho signalling were used to determine the effects of Arhgap28 overexpression and modulated RhoA signalling on actin reorganisation and collagen fibril remodelling. The experimental findings showed that Arhgap28 negatively regulates RhoA-activated assembly of stress fibres, which are required for the generation of cellular tension to organise collagen-rich ECM.

4.2 Results

4.2.1 Arhgap28 expression in tendon tissues *in vivo*

Arhgap28 expression in rat tail tendon tissues previously determined by the microarray analysis in Chapter 3 was validated by qPCR (see Fig. 10). Arhgap28 expression was significantly reduced from E21 to 3 weeks postnatal by 7-fold, and by

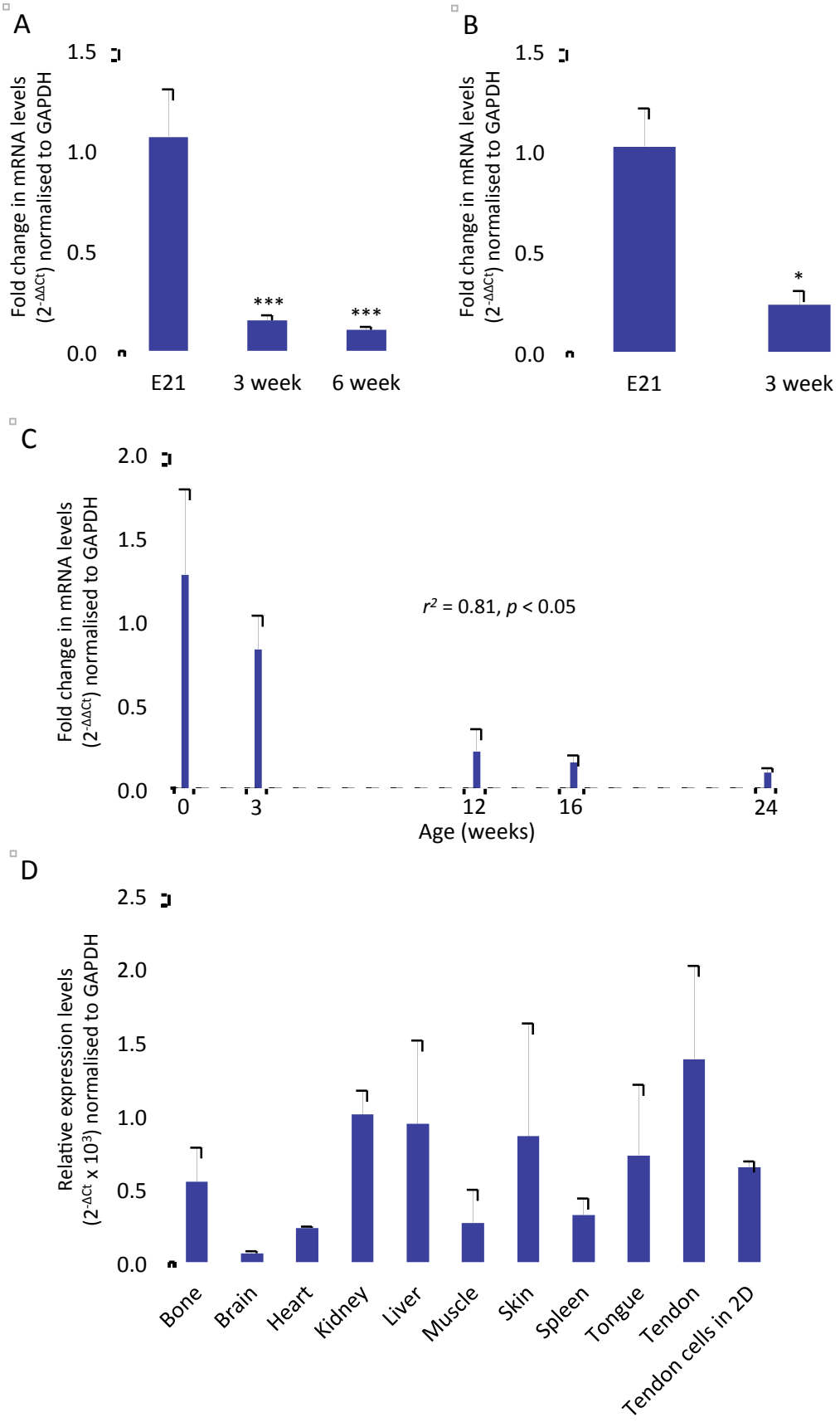

Figure 10

Arhgap28 expression in tendons *in vivo*.

(A) The expression of Arhgap28 by embryonic and postnatal rat tail (n = 3) and **(B)** flexor tendons (n = 3), *** and * indicate significant differences found when compared to E21, $p < 0.001$ and $p < 0.05$, respectively. **(C)** mouse tail tendons from birth to 24 weeks (n = 3; $r^2 = 0.81$, $p < 0.05$) and **(D)** neonatal mouse tissues (n = 1). Fold changes in arhgap28 gene expression normalised to GAPDH ($2^{-\Delta\Delta Ct}$ values). Bars show SEM.

10-fold from E21 to 6 weeks postnatal ($p < 0.001$; Fig. 10A). To determine if another type of tendon tissue exhibits this trend, Arhgap28 expression was examined in load-bearing flexor tendons. The results showed that Arhgap28 expression was significantly reduced by 3-fold in flexor tendons isolated from 3-week old rats compared to E21 rat embryos ($p < 0.05$; Fig. 10B). Arhgap28 expression was also examined in different developmental stages of murine tendon tissues. Mouse tendons are difficult to isolate from embryos. Therefore, the earliest time point at which tendon were dissected from mouse-tail (the most accessable location) was from newborn (P0) mice. Nonetheless, P0 tendons retain embryonic characteristics, which include narrow-diameter collagen fibrils, fibripositors, fibricarriers and ECM channels (see Appendix 4). qPCR was performed on mouse tendon tissues from different ages. As the age of the mice increased from 0 to 24 weeks, the expression of Arhgap28 decreased ($r^2 = 0.81$, $p < 0.05$; Fig. 10C). These data show that Arhgap28 is downregulated as tendons proceed from embryonic to postnatal development.

To determine the tissue-specific expression of Arhgap28, qPCR was performed on a number of tissues from P0 mice, including those in which collagen matrices can be found (bone and skin) and where type I collagen is not expressed (brain; see Fig. 10D). Arhgap28 was expressed in bone, kidney, liver, skin, tongue and tendon tissues. The expression levels were lower in brain, heart, skeletal muscle and spleen. This finding shows that Arhgap28 has a restricted, but not exclusive, tissue expression. The expression of Arhgap28 in tissues as diverse in function as tendon, bone, liver and tongue, might suggest a function involved in non cell-specific actin reorganisation.

4.2.2 Arhgap28 is upregulated in tendon constructs

In further attempts to identify the functions of Arhgap28, its expression was studied in tendon cells, which express Arhgap28 (see Fig. 10D) cultured on 2D tissue culture plastic and in 3D tendon-like constructs. Plastic has a stiffness of 4 x 10^4 kPa compared to 4 kPa of the tendon constructs (Kalson *et al.*, 2010). Therefore, measurement of Arhgap28 levels cultured on plastic and in tendon-like constructs would be expected to provide information on the role of Arhgap28 in responding to or sensing cell-matrix stiffness.

To minimise cell- and species-specific effects, the study was broadened to include human mesenchymal stem cells (hMSCs), which have been shown to be able to generate tendon-like constructs (Kapacee *et al.*, 2010). Thus, hMSCs and embryonic chicken tendon cells were seeded into a fibrin gel, which contracted during culture to form a linear tendon construct (see Fig. 11A). hMSCs take ~14 days to reach T0 (a nomenclature used to describe the time point at which tendon constructs are fully formed). hMSCs in T0 constructs had a significant, 7-fold upregulation of Arhgap28 expression compared to cells cultured in a 2D plastic monolayer for the same length of time ($p < 0.001$; Fig. 11B). The mechanical strength and stiffness of tendon constructs can continue to increase in culture after T0 (Kalson *et al.*, 2010). Arhgap28 expression was examined in tendon constructs formed by human mesenchymal stem cells at T7 and T14 (7 and 14 days after T0, respectively) and compared to cells that have been cultured in monolayer for the same length of time. Arhgap28 expression continued to increase with time in culture, both in cells in monolayer and in tendon constructs, although expression in tendon constructs remained greater than in monolayer at all time points examined (Fig. 11B).

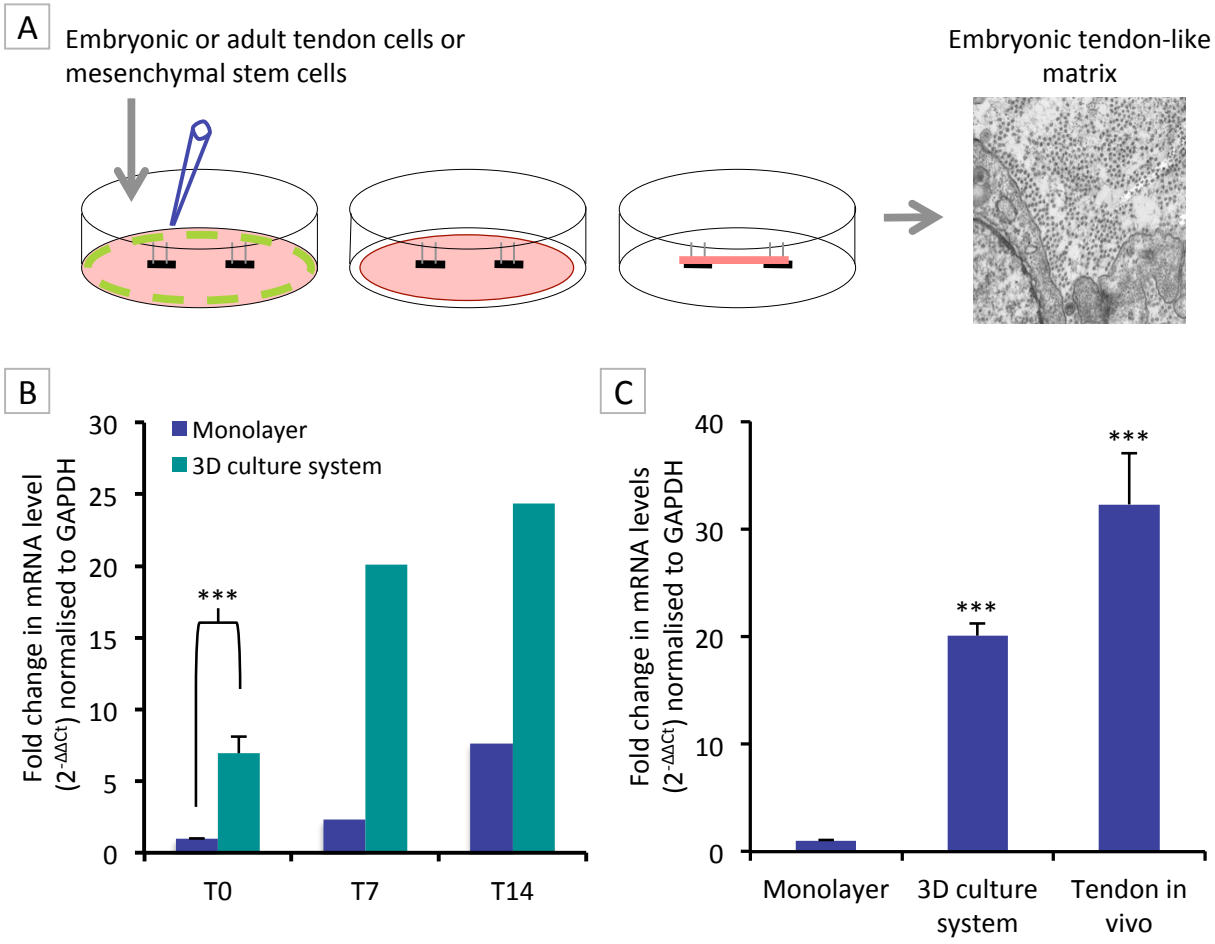

Figure 11

Arhgap28 expression in embryonic tendon-like tissue constructs formed by *in vitro*.

(A) Schematic to show the 3D culture system used to form embryonic tendon-like tissues *in vitro* as described in section 2.2.5. **(B)** The expression of Arhgap28 by human mesenchymal stem cells (hMSCs) cultured in monolayer and in the 3D tendon culture system at matched time points (T0: n = 6, T7, T14: n = 1). **(C)** The expression of Arhgap28 by embryonic chick tendon cells cultured in monolayer, in the 3D tendon culture system and from tendons *in vivo* (n = 3). Fold changes in arhgap28 gene expression normalised to GAPDH ($2^{-\Delta\Delta Ct}$ values). Bars show SEM. *** indicate significant differences found when compared to monolayer, $p < 0.001$.

To determine if the level of Arhgap28 expression in tendon constructs is comparable to embryonic tendon, embryonic chick tendon and the isolated cells were examined. Similar to the results observed in hMSCs, Arhgap28 expression in embryonic chick tendon cells was significantly upregulated by 20-fold in tendon constructs compared to culture in monolayer ($p < 0.001$; see Fig. 11C). Arhgap28 expression in embryonic chick tendon tissue was even more upregulated compared to cells in monolayer, by 30-fold ($p < 0.001$; Fig. 11C). These findings suggest that the tendon construct is a good culture model for studying the role of Arhgap28 in tendon tissue formation *in vitro*.

4.2.3 Tendon matrix gene expression during formation of tendon constructs

Cells cultured in the 3D tendon construct culture system experience a host of changes, which include 2D to 3D environment, cell shape, disorganised matrix to alignment collagen-rich matrix, and high levels of 2D, multi-directional tension to uniaxial tension. To explore the possible factors that may explain the differences in Arhgap28 expression in cells cultured on 2D plastic or in a 3D matrix, the expression of matrix molecules, adhesion molecules, RhoGAP and Rho GTPase genes were examined throughout the formation of tendon constructs. The formation of tendon constructs by embryonic chick tendon cells took 9 days in the experiments described in this section. RNA was isolated from cells cultured in 2D day 0 (d0), in the fibrin gel in 3D (d0, d3, d6), in fully formed tendon constructs (T0) and during the improvement of mechanical properties (T3, T7, T14; see Fig. 12-13).

As described previously in the Introduction, collagen fibrillogenesis is dependent upon fibronectin fibrillogenesis and integrins. COL1A1 expression was readily detectable in 2D and significantly increased by 6-fold at T0 ($p < 0.001$; see Fig. 12A). However, after

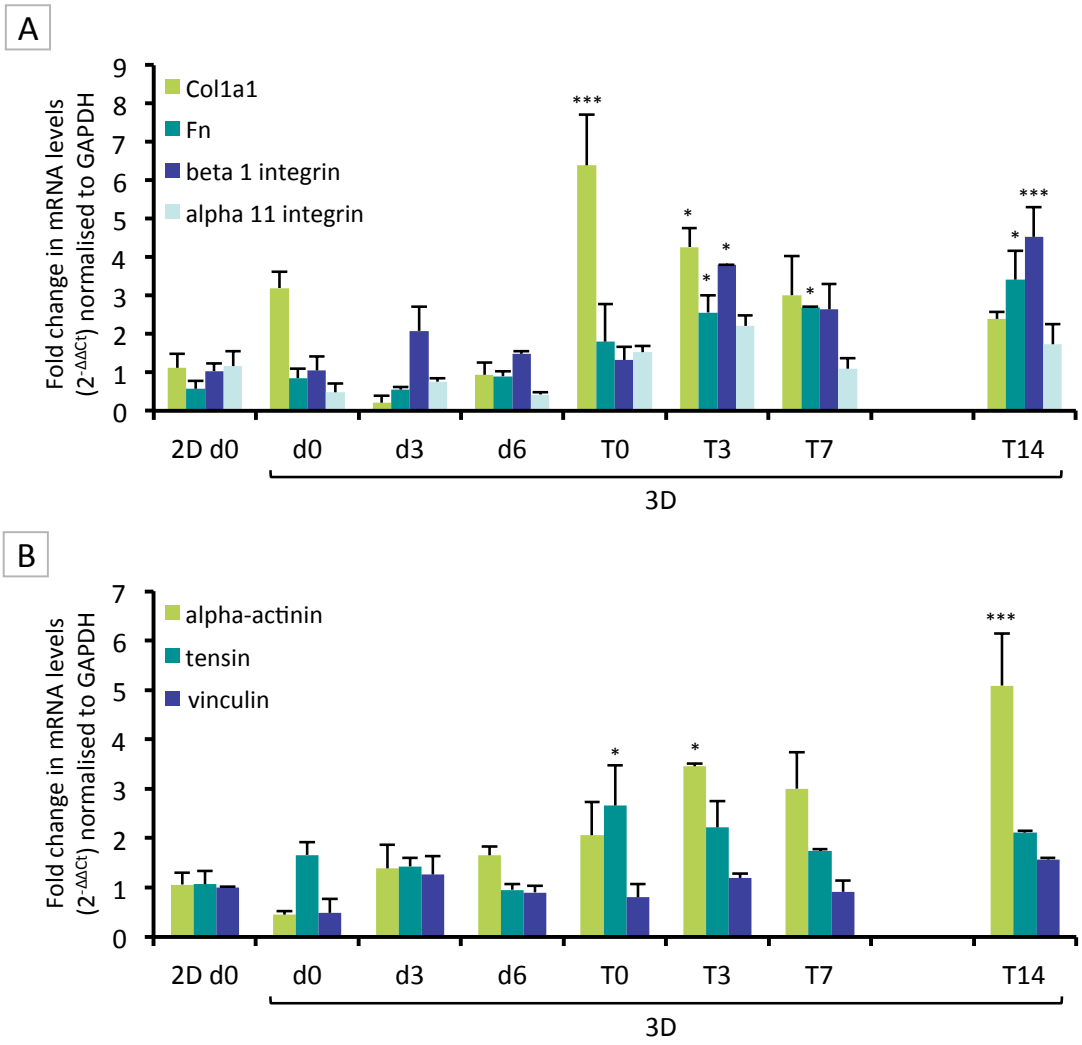

Figure 12

Expression of ECM and adhesion genes during tendon construct formation.

Primary embryonic chick tendon cells were seeded into fibrin gels for the formation of tendon constructs. **(A)** The expression of Col1a1, fibronectin, β1 integrin and α5 integrin genes and **(B)** genes encoding adhesion proteins α-actinin, tensin and vinculin was quantified by qPCR (n = 3). Fold changes in gene expression normalised to GAPDH ($2^{-\Delta\Delta Ct}$ values). Bars show SEM. *** and * indicate significant differences found when compared to monolayer (2D at day 0), $p < 0.001$ and $p < 0.05$, respectively.

T7, COL1A1 expression was no longer significantly different to cells in 2D. Fibronectin (FN1) expression was upregulated during the formation of tendon constructs, and at T14, reached 6-fold higher than expression in 2D at d0 ($p < 0.05$; Fig. 12A). The expression of collagen-binding integrins, integrin β1 (ITGB1) and α11 (ITGA11), that are involved in collagen assembly were also detected (Fig. 12A; Velling *et al.*, 2002). At T14, ITGB1 expression was 4-fold greater than 2D at T0 ($p < 0.001$). However, no significant increase in ITGA11 expression was observed (Fig. 12A). Collectively, these expression data suggest that assembly of ECM in tendon constructs occurred most prominently once uniaxial tension is established (T0 onwards).

As part of the characterisation of tendon construct formation by embryonic chick tendon cells, expression of adhesion proteins involved in signal transduction from cell-matrix adhesions to the assembly of contractile stress fibres was examined (see Fig. 12B). The expression of α-actinin (ACTN1) increased as tendon constructs formed and reached a significant 5-fold increase at T14 compared to expression in 2D at d0 ($p < 0.001$, Fig. 12B). Tensin (TNS1) expression was significant upregulated by 2-fold at T0 ($p < 0.05$; Fig. 12B). No significant change in vinculin (VCL) expression was observed (Fig. 12B). These data are suggestive of signal transduction form cell-matrix adhesions in tendon constructs.

4.2.4 RhoGAP and Rho GTPase expression during formation of tendon construct

Arhgap6 and Arhgap18 are RhoGAPs closely related to Arhgap28 that have recently been demonstrated to have RhoGAP activity specific for RhoA (Prakash *et al.*, 2000, Maeda *et al.*, 2011). Both RhoGAPs were upregulated during the development of

tendon constructs. Arhgap6 was significantly upregulated by 3-fold at T0 ($p < 0.05$), and reached 6-fold higher at T14 compared to expression in 2D at d0 ($p < 0.001$; Fig. 13A). At T14, Arhgap18 upregulation was 7-fold greater than in 2D at d0 ($p < 0.001$; Fig. 13A). Upregulation in Arhgap6 and Arhgap18 during the deposition of a collagen matrix suggests that regulation of Rho signalling and stress fibres by these RhoGAPs plays an important role. As expected, Arhgap28 expression was significantly upregulated in tendon constructs, from 14-fold at T3 to 35-fold at T14, compared to expression in 2D at T0 ($p < 0.05$, $p < 0.001$, respectively; Fig. 12A), confirming that Arhgap28 is important during the process of tendon construct formation *in vitro*. The further upregulation in Arhgap28 expression after T0 indicates that Arhgap28 is involved in the development of mechanical properties of tendon constructs.

Two other RhoGAPs, DLC1 and Racgap1 were identified in the microarray as differentially upregulated in embryonic tendon (see Chapter 3). The expression of DLC1 was significantly upregulated by 5-fold at T14 whereas Racgap1 was only significantly upregulated, by 4-fold, after 3 days in fibrin ($p < 0.001$; Fig. 13B). Due to the time point at which these RhoGAPs are upregulated, these data suggest that they are not likely to be involved in the assembly of the tendon matrix. Rho GTPases were also examined. The expression of RhoA, Rac1, Cdc42 and RhoQ (one of the candidates identified in the microarray) were all significantly upregulated at T14 (Fig. 13C). These data suggest that Rho signalling might not be regulated transcriptionally during tendon construct formation but once the mechanical properties of the tissues are fully developed (at T14), Rho signalling is upregulated.

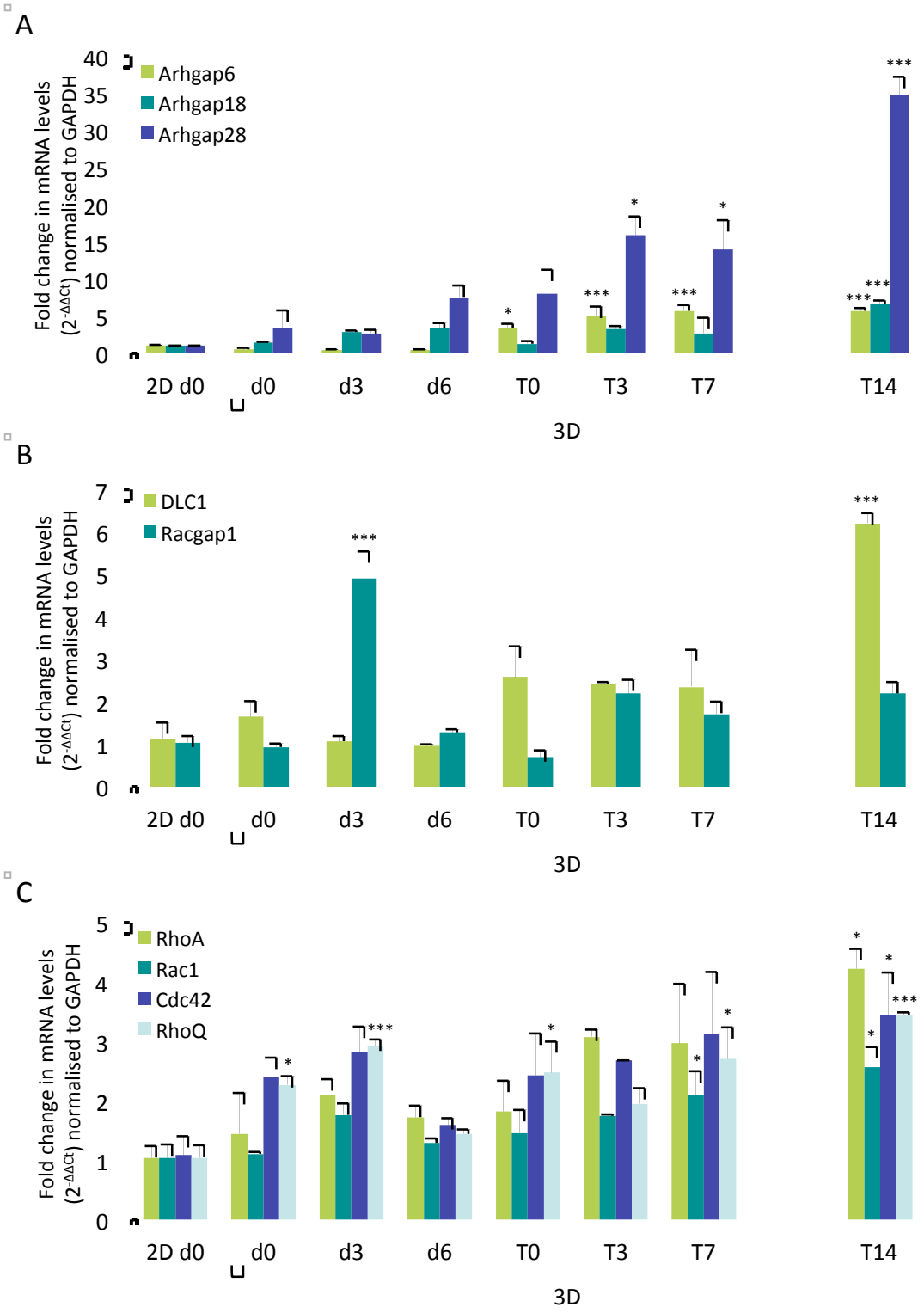

Figure 13

Expression of RhoGAPs and Rho GTPases during tendon construct formation.

Primary embryonic chick tendon cells were seeded into fibrin gels for the formation of tendon constructs. **(A)** The expression of genes encoding Arhgap28 and related RhoGAPs, Arhgap6 and Arhgap18; **(B)** candidate RhoGAPs, DLC1 and Racgap1; and **(C)** Rho GTPases, RhoA, Rac1, Cdc42 and RhoQ was quantified by qPCR (n = 3). Fold changes in gene expression normalised to GAPDH ($2^{-\Delta\Delta Ct}$ values). Bars show SEM. *** and * indicate significant differences found when compared to monolayer (2D at day 0), $p < 0.001$ and $p < 0.05$, respectively.

4.2.5 Gene expression changes during tendon tissue recoil

Tendon tissue develops under tension *in vivo* and this is reproduced in the 3D culture system for tendon constructs from T0 onwards (Kapacee *et al.*, 2008, Kalson *et al.*, 2010). To inspect if tensile forces affect the expression of Arhgap28 and other Rho GTPase signalling, fully formed tendon constructs at T0 were untensioned and gene expression was analysed after 1, 6 and 24 hours (Fig. 14). Of all the RhoGAPs examined, only Arhga6 and Arhgap28 were significantly downregulated ($p < 0.05$; see Fig. 14A and B). No significant changes were found in the expression of Rho GTPases, RhoA, Rac1, Cdc42 and RhoQ, when tendon constructs were not under tension (Fig. 14C). Interestingly, expression of α-actinin, tensin and vinculin were significantly downregulated 24 hours after constructs were not under tension (Fig. 14D), which is indicative of the downregulation of contractile stress fibres.

4.2.6 Arhgap28 is predicted to function similarly to Arhgap6 and Arhgap18

Induction of Arhgap28 expression during tendon construct formation was mirrored by the expression of Arhgap6 and Arhgap18, which suggests that they are part of the same actin reorganisation mechanism. In addition, Arhgap6 and Arhgap28 were significantly downregulated when the tension in tendon constructs was lost. RhoGAP function is mediated via the RhoGAP domain (represented schematically in Fig. 15A), which enhances hydrolysis of GTP bound by the target Rho GTPase. Alignment of the RhoGAP domains of murine Arhgap6, Arhgap18 and Arhgap28 show high homology and confirms the presence of a putative catalytic arginine residue in Arhgap28 (Fig. 15B).

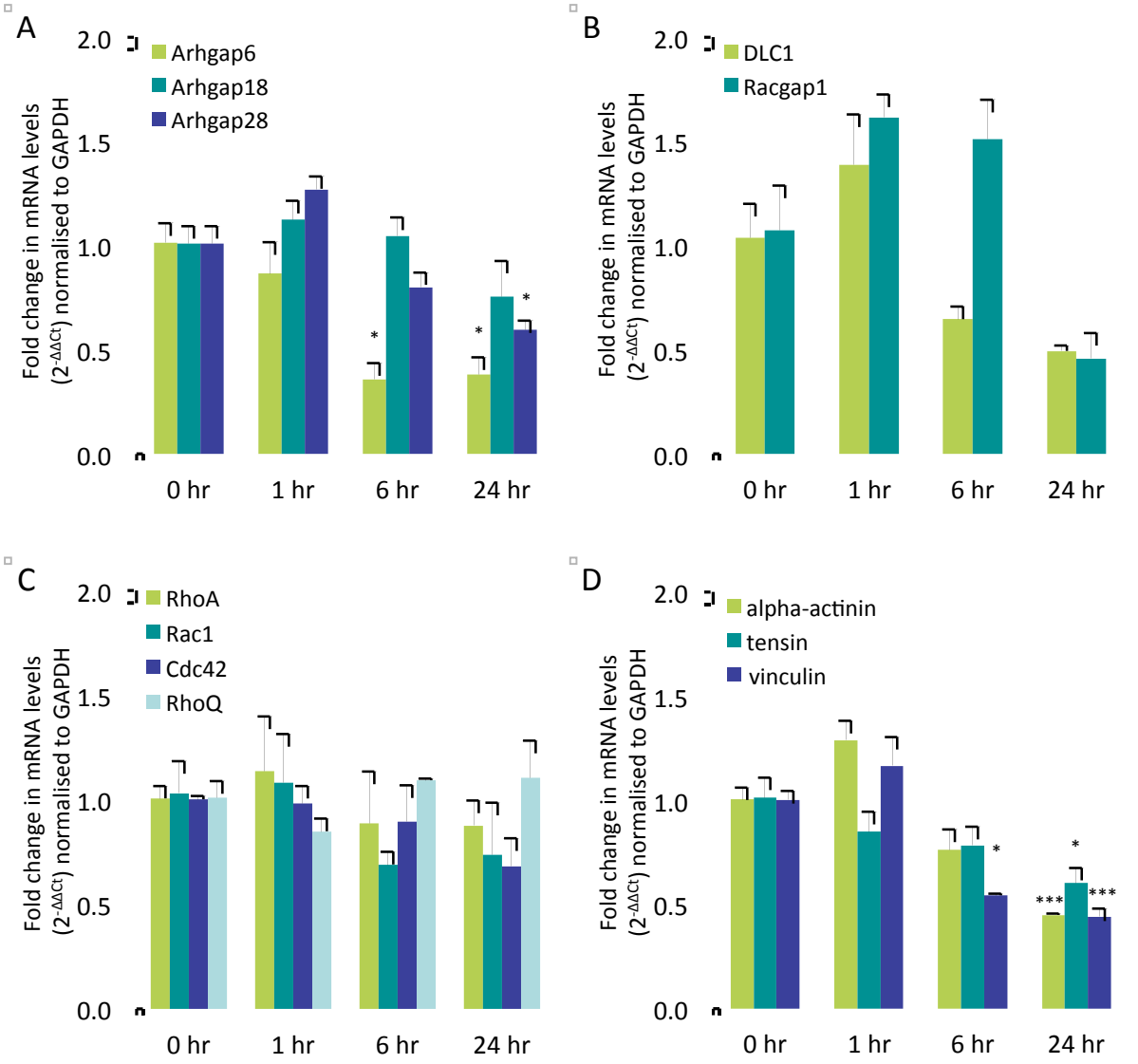

Figure 14

Gene expression by untensioned tendon constructs during recoil.

Tendon constructs formed by primary embryonic chick tendon cells were untensioned. **(A)** The expression of genes encoding Arhgap28 and related RhoGAPs, Arhgap6 and Arhgap18; **(B)** candidate RhoGAPs, DLC1 and Racgap1; **(C)** Rho GTPases, RhoA, Rac1, Cdc42 and RhoQ; and **(D)** adhesion proteins, α-actinin, tensin and vinculin was quantified by qPCR (n = 3). Fold changes in gene expression normalised to GAPDH ($2^{-\Delta\Delta Ct}$ values). Bars show SEM. *** and * indicate significant differences found when compared to 0 hr, $p < 0.001$ and $p < 0.05$, respectively.

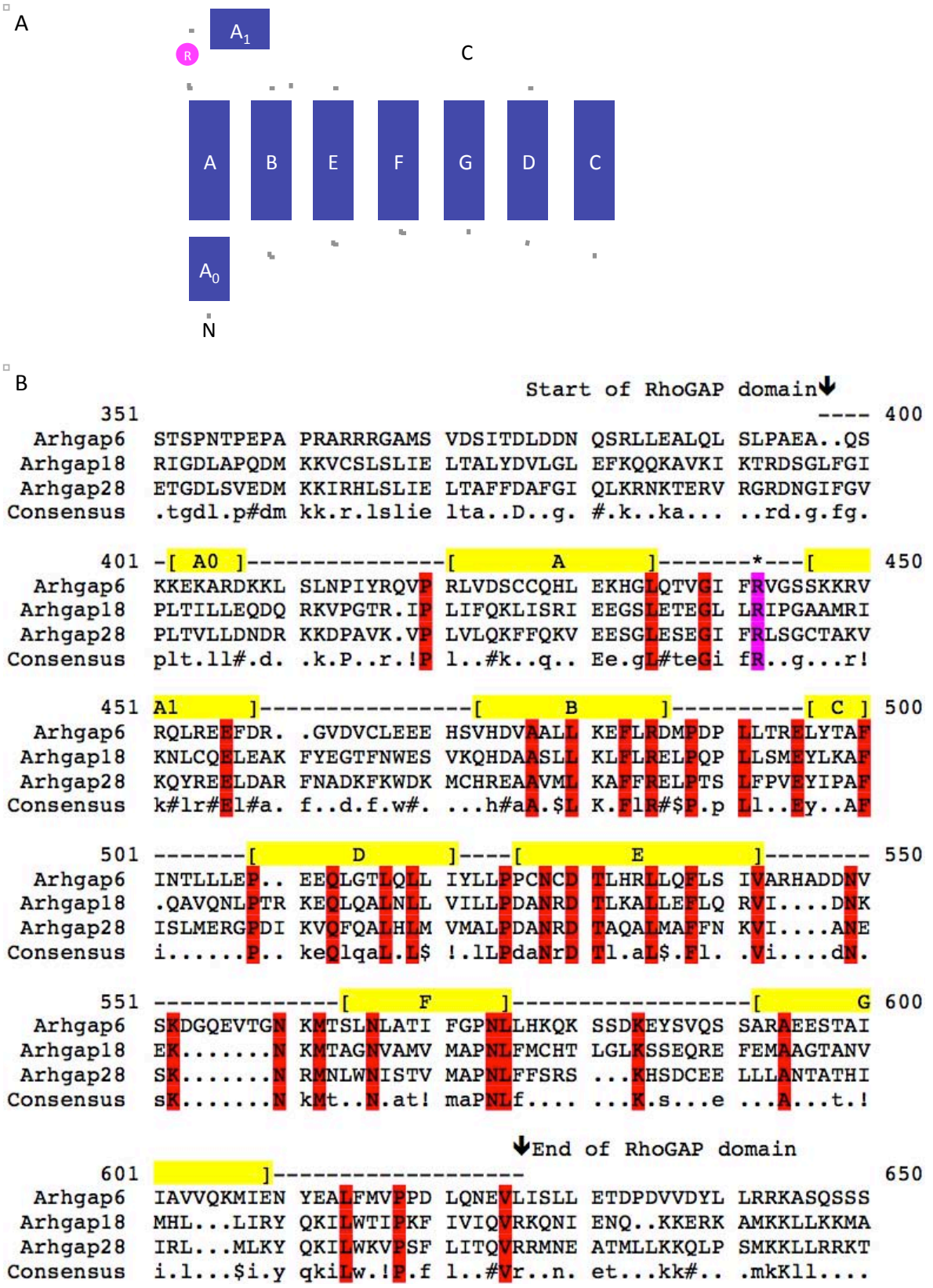

Figure 15

Sequence alignment of the RhoGAP domain of Arhgap28-related RhoGAPs.

(A) The helical segments and loops in RhoGAP domain. **(B)** The sequences of Arhgap6, Arhgap18 and Arhgap28 were aligned and the sequences of RhoGAP domain is shown. The helical segments (A0, A, A1, B, C, D, E, F and G) are shown in yellow. Residues conserved in all three RhoGAPs are highlighted in red. The catalytic arginine residue is highlighted in pink.

4.2.7 Validation of C-terminal V5-His fusion murine Arhgap28 cDNA clone

An overexpression strategy was taken to study Arhgap28 *in vitro*. First, it was noted that two major isoforms of murine Arhgap28 exists – Pubmed IDs: NM_172964.4 and BC066788.1, which encode products of 729 and 708 amino acid residues (aa), respectively, differing only in the C-terminus (see Fig. 16A). Using an overlapping PCR approach, the transcript expressed in tendon was determined to be the larger isoform (Fig. 16A and B). A cDNA clone of the smaller isoform was used as a control template for generating PCR fragments by primers specific for the smaller isoform (Fig. 16B). The products of the reactions were sequenced, and confirmed that the transcript expressed in Arhgap28 would putatively translate into the 729 aa protein. This full-length cDNA was cloned into a pcDNA6/V5-His C vector for the overexpression of a C-terminal V5-His fusion protein (see Fig. 17A; section 2.5.2 and Appendix 1 for cloning method).

The clone was tested in the readily transfectable murine NIH3T3 fibroblast cell line. RNA was isolated from NIH3T3 cells transiently transfected with the Lipofectamine transfection reagent only (L), empty vector (E) or Arhgap28-V5 clone (replicates #6 and #8) for RT-PCR. As expected, the expression of Arhgap28-V5 transcript was only detected in the replicates (Fig. 17B). “No RT controls” were included to demonstrate that contaminating plasmid DNA had been eliminated in DNase treatment (Fig. 17B). The predicted molecular weight of the fusion protein is 85 kDa. Proteins isolated from transfected NIH3T3 cells were analysed by western blotting using an antibody specific for the V5 epitope (see Fig. 17C). A band that migrated at the predicted molecular weight was observed in the replicates transfected with the Arhgap28-V5 clone but not in cells were transfected with empty vector. Validated V5-tagged proteins were also

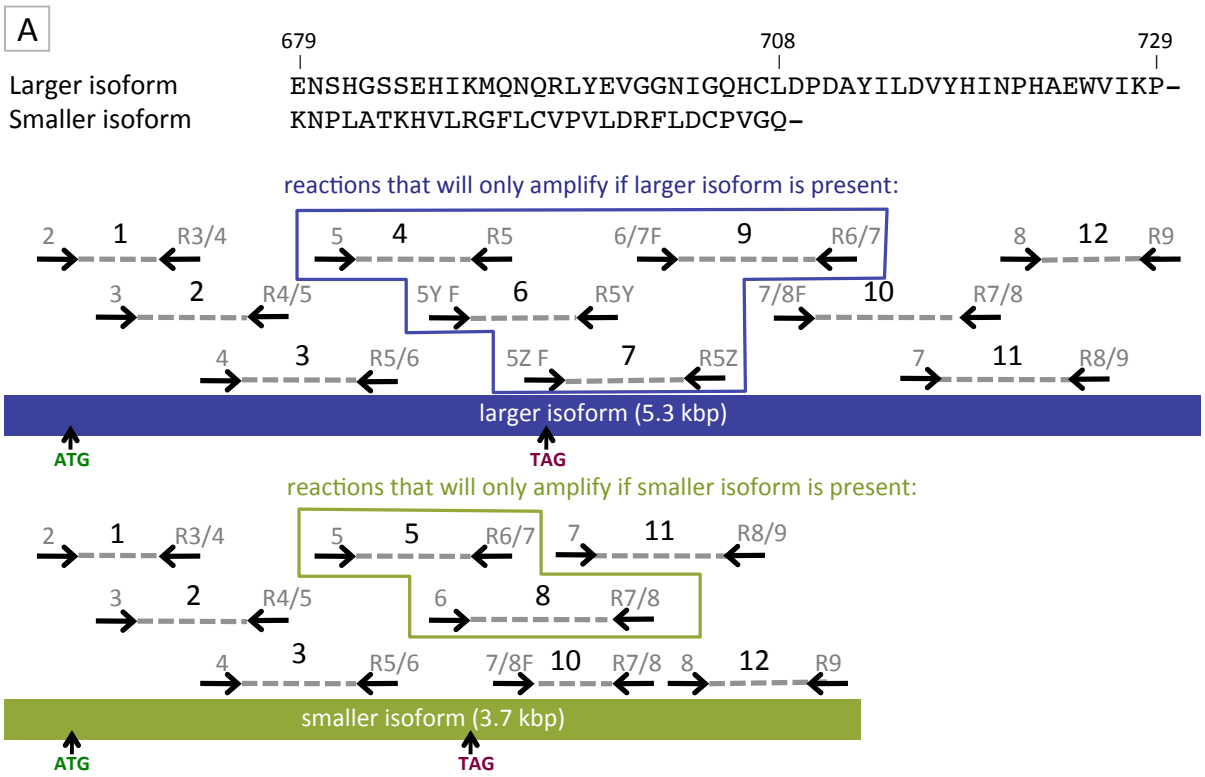

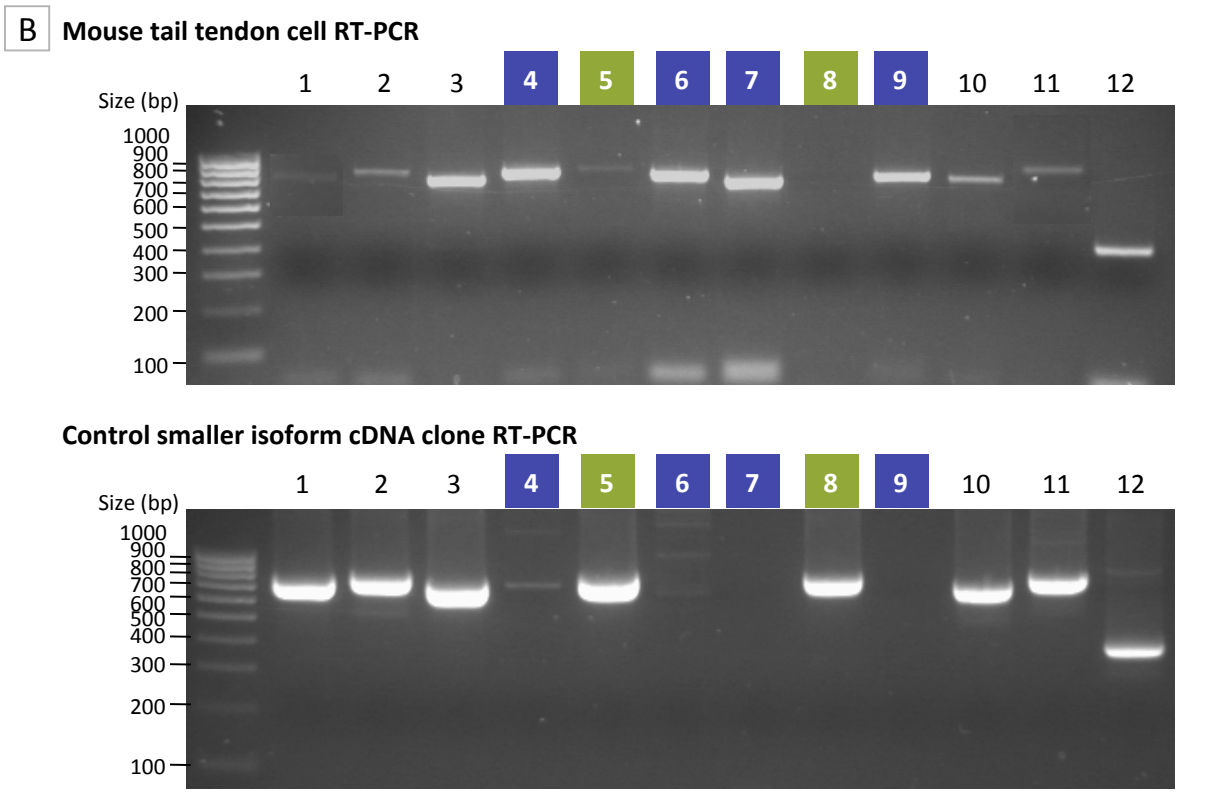

Figure 16

Sequencing of the endogenous Arhgap28 transcript expressed in mouse tendon.

(A) Difference in C-terminus of the two major Arhgap28 isoforms from amino acid residue 679. PCR strategy to determine the sequence of endogenous Arhgap28 transcript expressed in tendon. Overlapping products of PCR reactions 1 to 12 by specific primers (numbers in grey) are sequenced. Reactions in the boxes are unique to either the larger or the smaller isoform. ATG and TAG indicates the start and stop codons, respectively. Diagram not drawn to scale. **(B)** RNA was isolated from mouse tail tendon cells and the 12 overlapping RT-PCRs were performed and visualised by gel electrophoresis. Products were subsequently purified and confirmed by DNA sequencing. A cDNA clone of the smaller Arhgap28 isoform was used as control template.

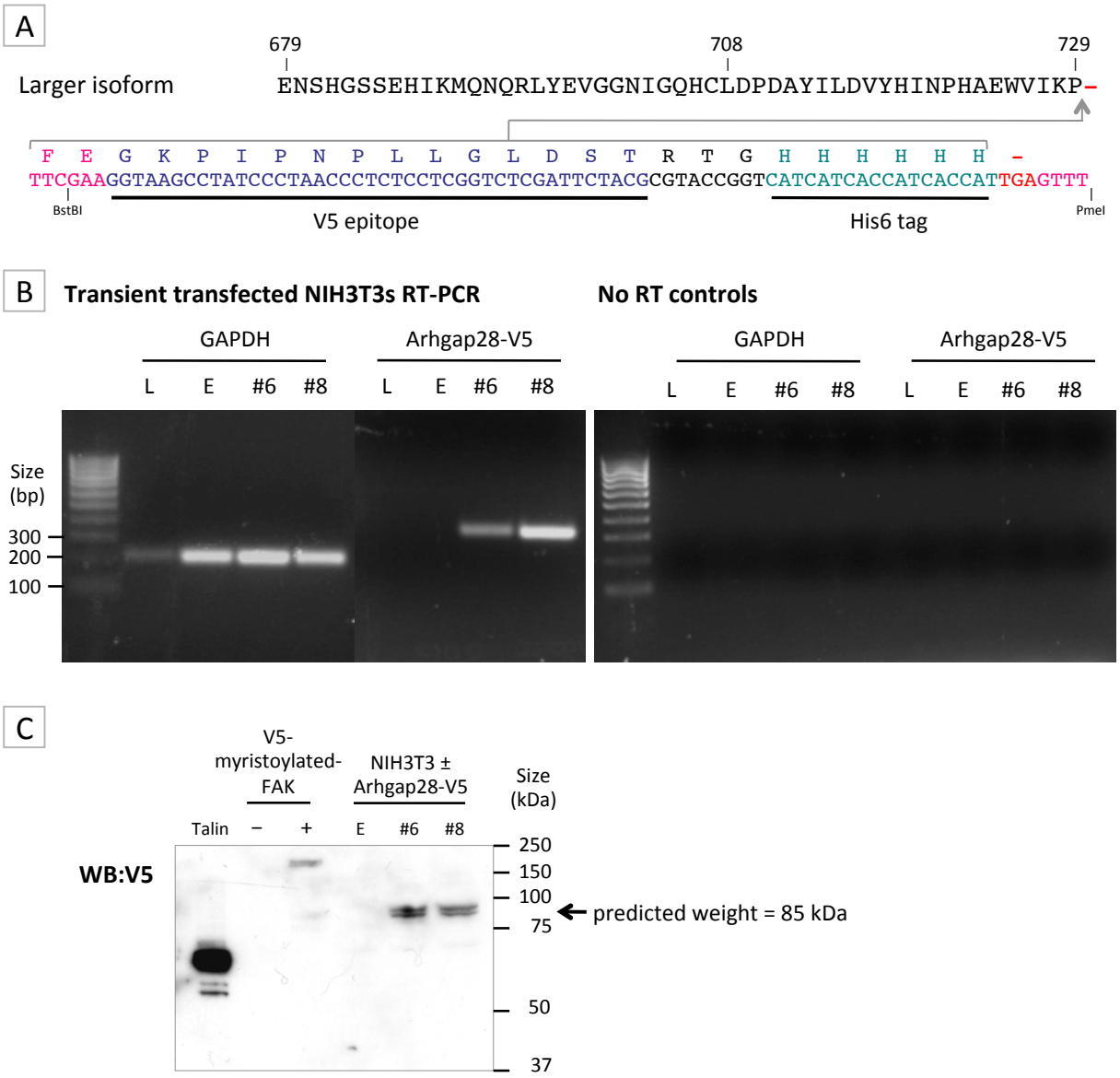

Figure 17

Expression of V5-tagged Arhgap28 in NIH3T3 fibroblasts.

(A) Arhgap28 was cloned into a pcDNA6 vector where a V5-His6 tag was introduced into the Arhgap28 sequence immediately 5' of the stop codon. **(B)** RNA was isolated from NIH3T3 fibroblasts transiently transfected with Lipofectamine only (L), the empty vector (E) or the Arhgap28-V5 clones (#6 or #8). RT-PCRs were performed to detect the expression of house-keeping gene, GAPDH (221 bp) or Arhgap28-V5 using specific primers (329 bp). No RT controls confirmed the absence of genomic contamination. **(C)** Protein was isolated for western blotting to detect V5-tagged protein expression. A positive signal was detected at ~90 kDa. The predicted molecular weight of Arhgap28-V5 is 85 kDa. Control lysates were included – Talin-V5 (60 kDa), mock transfection (–), myristoylated-FAK-V5 (+; 175 kDa).

included as positive controls for the antibody (see Fig. 17C). It is important to note here that custom-made and commercial antibodies specific for Arhgap28 were also tested but none detected a band corresponding to the one detected by the V5 antibody (see Appendix 5). These data confirm that this Arhgap28-V5 fusion protein could be used in overexpression studies *in vitro*.

4.2.8 Arhgap28 negatively regulates RhoA signalling and stress fibre assembly

To examine if Arhgap28 has the same negative regulatory effects on RhoA signalling and actin stress fibres as Arhgap6 and Arhgap18, SaOS-2 cells were selected for study because they form prominent stress fibres in 2D culture (cells adhered to tissue culture plastics or glass). Overexpression of Arhgap28-V5 was confirmed in transiently transfected cells by western blotting using the anti-V5 antibody (Fig. 18A). Active RhoA was examined by a rhotekin-GST pull-down assay to precipitate GTP-bound Rho. Total lysate and bound fractions were analysed by western blotting using an antibody specific for RhoA. Overexpression of Arhgap28-V5 caused a reduction in active RhoA compared to cells transfected with the transfection reagent or the empty vector only (Fig. 18B). Actin stress fibres were examined in transfected cells by phalloidin staining and immunofluorescence using the V5 antibody. SaOS-2 cells without staining for V5 exhibit prominent stress fibres (Fig. 18C). Cells expressing Arhgap28-V5, as identified by staining with V5 antibodies, have disrupted actin stress fibres (Fig. 18C). Multiple actin microspikes and membrane ruffles were also observed on the edge of these cells (see Fig. 18C, arrows). These overexpression studies suggest that Arhgap28 expression negatively regulates RhoA signalling.

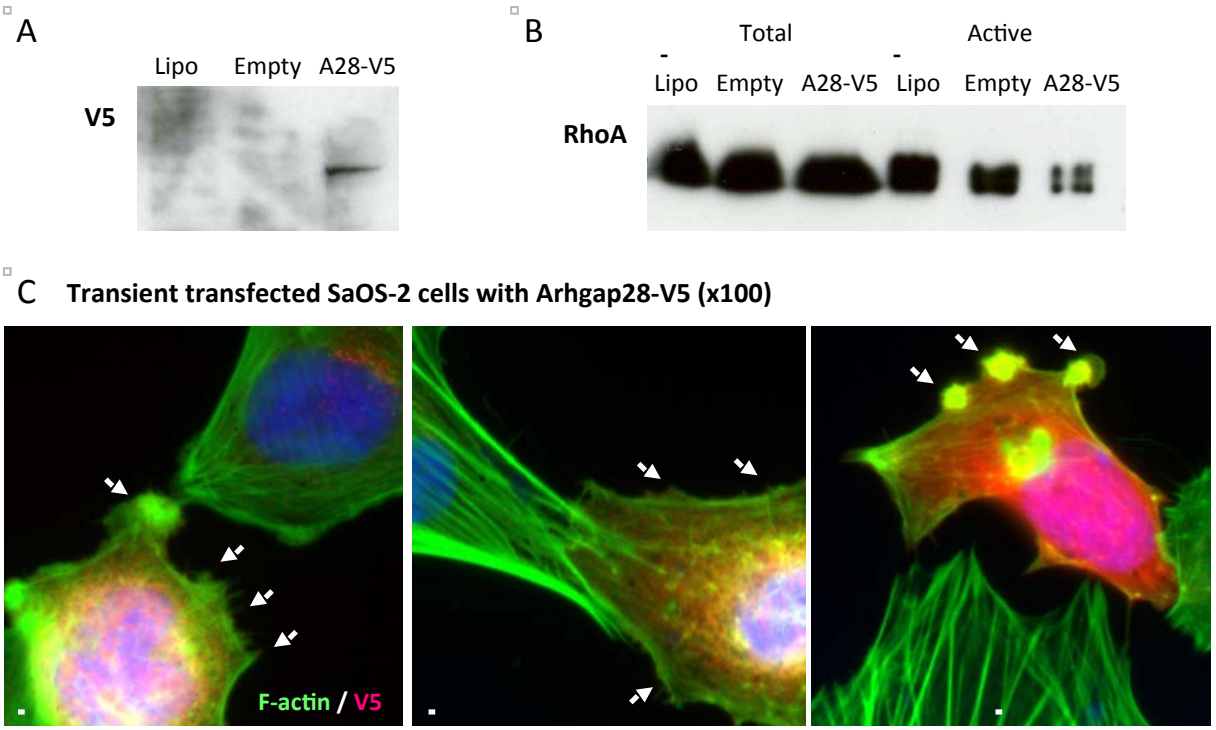

Figure 18

Arhgap28-V5 inhibits RhoA activation and stress fibre formation in SaOS-2 cells.

SaOS-2 cells were transfected with empty vector or Arhgap28-V5 cDNA. **(A)** The expression of Arhgap28-V5 was confirmed by western blotting suing an antibody to V5. **(B)** Active RhoA was measured by western blotting. A representative image of a western blot is shown (n = 2). **(C)** F-actin in cells expressing Arhgap28-V5 were visualised under high magnification (x100) using anti-V5 antibodies and phalloidin (n = 3). Arrows point to membrane ruffling and F-actin protrusions. Bars = 25 µm.

To examine if Arhgap28-V5 expression has the same effect in tendon cells, primary embryonic chick tendon cells were transiently transfected with the Arhgap28-V5 clone. These cells, like SaOS-2 cells, have prominent actin stress fibres *in vitro* (see Fig. 19). Expression of the V5-fusion protein in chick tendon cells was confirmed by staining with the V5 antibody (Fig. 19). However, due to the low transfection efficiency of primary cells (see Fig. 19A), the level of active RhoA would not be evident in a pull-down assay. Under higher magnification, embryonic tendon cells stained positive for V5 contained disrupted actin stress fibres compared to cells that have were not stained positive with the V5 antibody (Fig. 19B). Similar to SaOS-2 cells overexpressing Arhgap28-V5, tendon cells expressing the fusion protein displayed multiple actin microspikes and membrane ruffles (see Fig. 19B arrows). Taken together with the findings observed in SaOS-2 cells, these data indicate that Arhgap28 negatively regulates RhoA-mediated actin stress fibre assembly.

4.2.9 Modulating RhoA signalling affects tendon matrix remodelling

Arhgap28 is upregulated during tendon tissue formation and downregulated when tension is lost, therefore, it was hypothesised that Arhgap28 regulates RhoA-mediated cell contractility during collagen matrix assembly and organisation. To examine the effects of RhoA signalling on remodelling of collagen ECM, LPA was used to induce RhoA activation. SaOS-2 cells were treated with 5 µM LPA for 30 minutes in serum-free conditions and an increase in active RhoA was detected, compared to basal levels in controls (Fig. 20A). Assembly of actin stress fibres and focal adhesions were examined using phalloidin and vinculin antibody staining. SaOS-2 cells have prominent stress fibres and large vinculin focal adhesions in the cell periphery even in serum-free and 0.1% DMSO controls (Fig. 20B). Cells treated with LPA appeared to have more stress

A

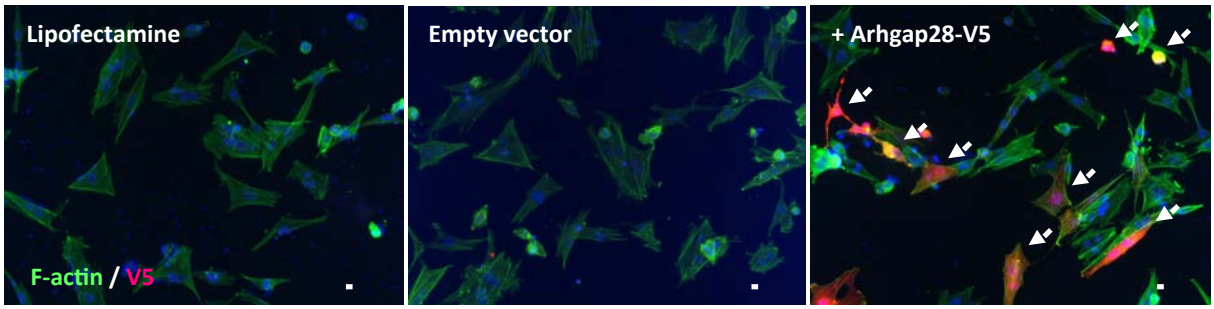

B **Transient transfected embryonic chick tendon cells with Arhgap28-V5 (x100)**

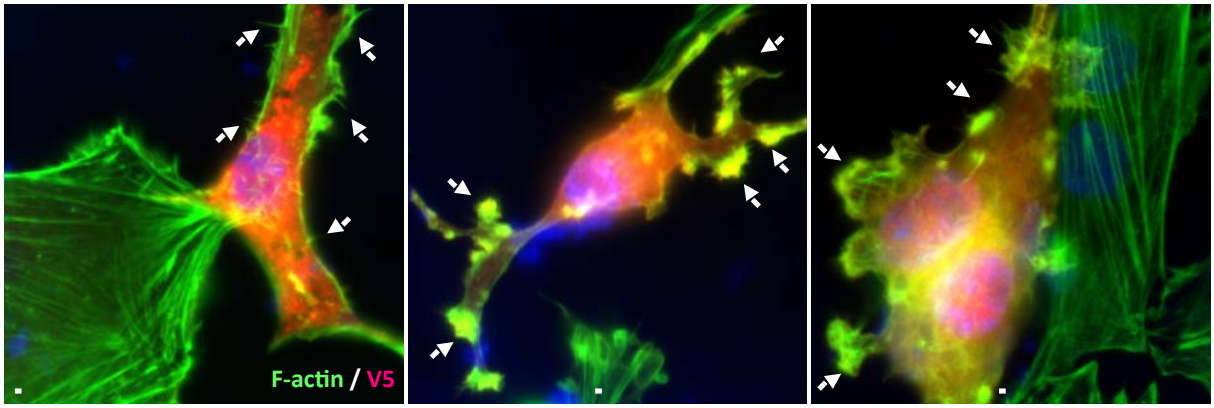

Figure 19
Overexpression of Arhgap28-V5 inhibits stress fibre formation in embryonic tendon cells.
(A) Primary embryonic chick tendon cells were transfected with empty vector or Arhgap28-V5 cDNA (n = 3). Bars = 50 µm. Arrows point to cells stained by V5 antibodies. **(B)** F-actin in cells overexpressing Arhgap28-V5 were visualised under high magnification (x100) using anti-V5 antibodies and phalloidin. Arrows point to membrane ruffling and F-actin protrusions. Bars = 25 µm.

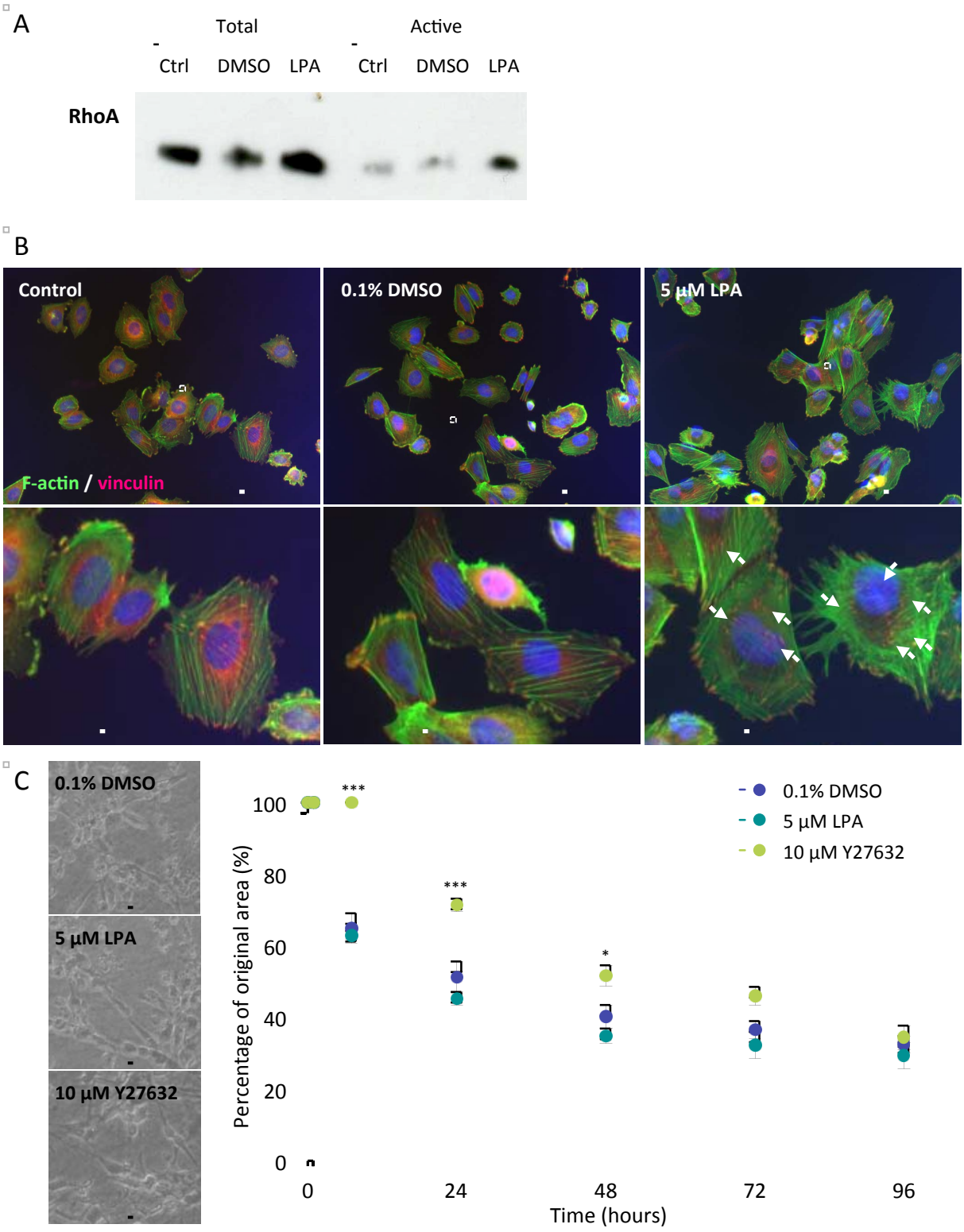

Figure 20

Modulating Rho signalling in SaOS-2 cells affects collagen gel contraction.

SaOS-2 cells were treated with and without 5 µM LPA in serum-free medium for 30 minutes. Serum-free and 0.1% DMSO controls were included. **(A)** RhoA in total lysates and Rhotekin-GST-bound fractions were measured by western blotting followed by densitometry. A representative image of a western blot is shown. **(B)** Focal adhesions and actin stress fibres were visualised by immunofluorescence using anti-vinculin antibodies and phalloidin. Bars = 100 µm. Arrows point to perinuclear focal adhesions. **(C)** Collagen gel contraction assay was performed in the presence of serum. The area of collagen gel was measured over 4 days. Bars show SEM. *** and * indicate significant differences found when compared to 0.1% DMSO control, $p < 0.001$ and $p < 0.05$, respectively.

fibres, and more vinculin-stained focal adhesions located in the cell periphery and close to the ventral side of nucleus (Fig. 20B, arrows).

Collagen gel contraction assay was performed to assess if modulating RhoA signalling affects collagen remodelling. SaOS-2 cells were plated onto collagen gels and treated with 5 µM LPA or 10 µM of the ROCK inhibitor Y27632 (to inhibit the downstream effector of RhoA activation), and the areas of the gels were measured over 4 days. Due to the length of time in culture, this experiment was performed in the presence of serum. In all conditions, cells appeared healthy and the collagen gels contracted down to ~40% of the original area (Fig. 20C). No significant differences were observed in LPA-treated collagen gels compared to 0.1% DMSO controls at any of the time points (Fig. 20C). This lack of difference could be due to the presence of growth factors in the serum in the 0.1% DMSO controls. However, treatment with Y27632 significantly inhibited the initial stages of gel contraction at 6, 24 and 48 hours (Fig. 20C), suggesting that Rho signalling is required for collagen gel remodelling.

To examine if modulating RhoA signalling also affects tendon cells, embryonic chick tendon cells were treated with 5 µM of LPA in serum-free conditions. LPA treatment increased basal level of active RhoA compared to 0.1% DMSO control (Fig. 21A). LPA also induced the assembly of more actin stress fibres and large vinculin focal adhesions in these cells (Fig. 21B). These data confirms that LPA induces RhoA activation in tendon cells. To determine if LPA treatment affects RhoA activation in tendon constructs, they were treated at T0 for 24 hours with 5 µM LPA in serum-free conditions. Due to the interference by the large amounts of collagen in tendon constructs, active RhoA assays could not be performed (Clark *et al.*, 2010). However,

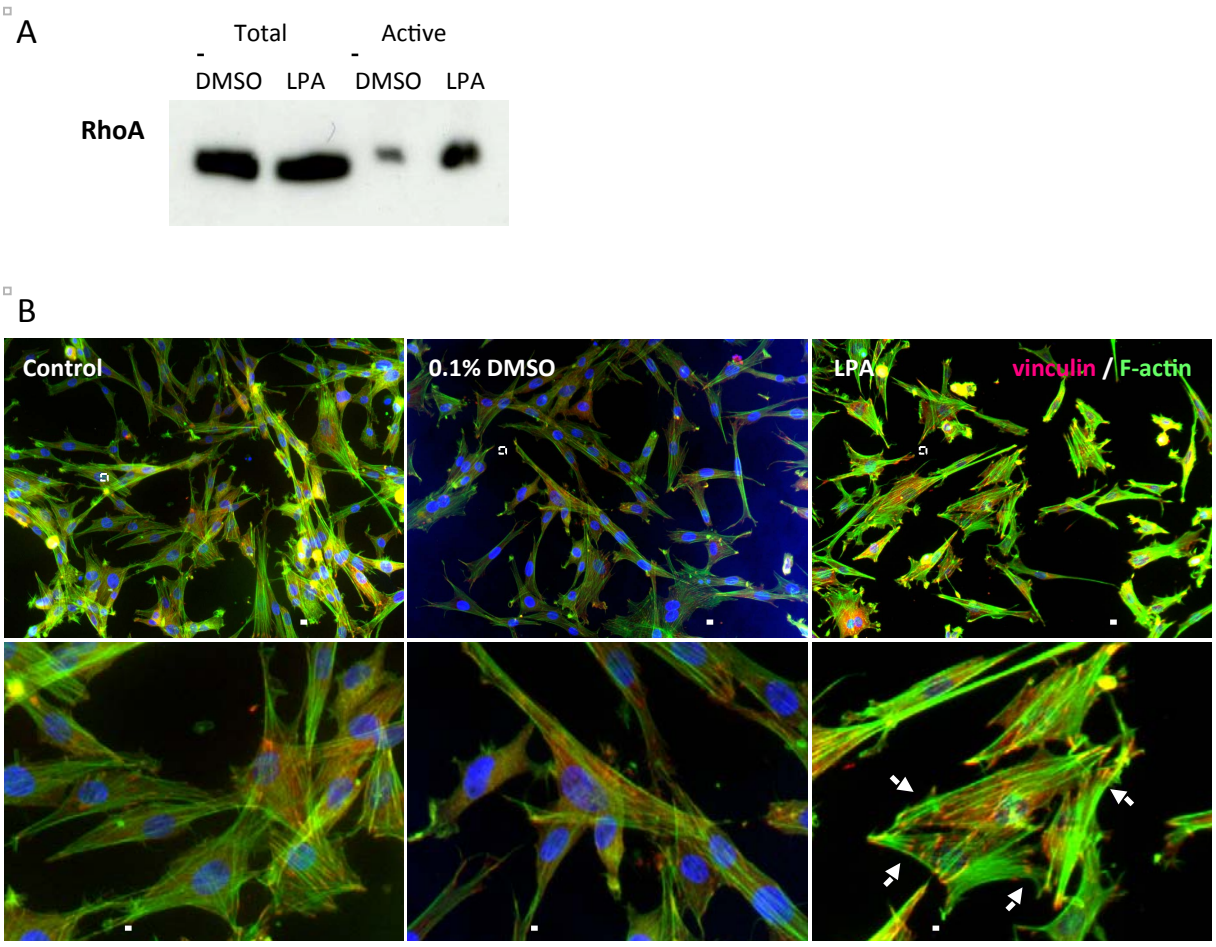

Figure 21
LPA stimulates RhoA activation and stress fibre formation in tendon cells.
Primary embryonic chick tendon cells were treated with and without 5 µM LPA in serum-free medium for 30 minutes. **(A)** RhoA in total lysates and Rhotekin-GST-bound fractions were measured by western blotting (n = 3). A representative image of a western blot is shown. **(B)** Focal adhesions and actin stress fibres were visualised by immunofluorescence using anti-vinculin antibodies and phalloidin (n = 3). Bars = 100 µm.

phalloidin staining of longitudinal sections confirmed that LPA could induce actin stress fibre assembly in tendon constructs (see Fig. 22A), so a similar induction of contractile actin stress fibres assembly via RhoA activation, observed in tendon cells in monolayer, was predicted in tendon constructs.

To determine if modulating RhoA signalling affects remodelling of the tendon matrix, fully formed tendon constructs were treated with LPA or Y27632 for two hours in serum-free conditions. Then the tension was released and the rate of recoil was measured at 10-second intervals over 30 minutes (Fig. 22B). A single exponential, 3-parameter fit of the mean length of tendon constructs was calculated. The recoil baseline deduced from this fit showed that tendon constructs treated with 0.1% DMSO recoiled to 60% of their original length (Fig. 22C). LPA treatment significantly increased recoil to 53% of the original length and tendon constructs treated with Y27632 could only recoil to 71% of their original length ($p < 0.001$; Fig. 22C). The rate of contraction was also deduced as a measure of $t_{1/2}$, which is the time taken for the tendon constructs to achieve half of their recoil baseline. Control tendon constructs took 7.4 ± 0.3 minutes, LPA treatment significantly reduced this to 5.4 ± 0.1 minutes and tendon constructs treated with Y27632 took significantly longer (11.2 ± 0.1 minutes) to contract to half its recoil baseline ($p < 0.001$; Fig. 22D). These data suggest that contraction of the tendon matrix is mediated by Rho signalling that is tightly regulated.

4.2.10 siRNA-mediated knockdown of Arhgap28 in tendon constructs

The tendon construct recoil experiment provides an assay to test if Arhgap28 is involved in regulating actin stress fibres and cellular contractility in combination with use of RNA interference. If the hypothesis that Arhgap28 negatively regulates RhoA

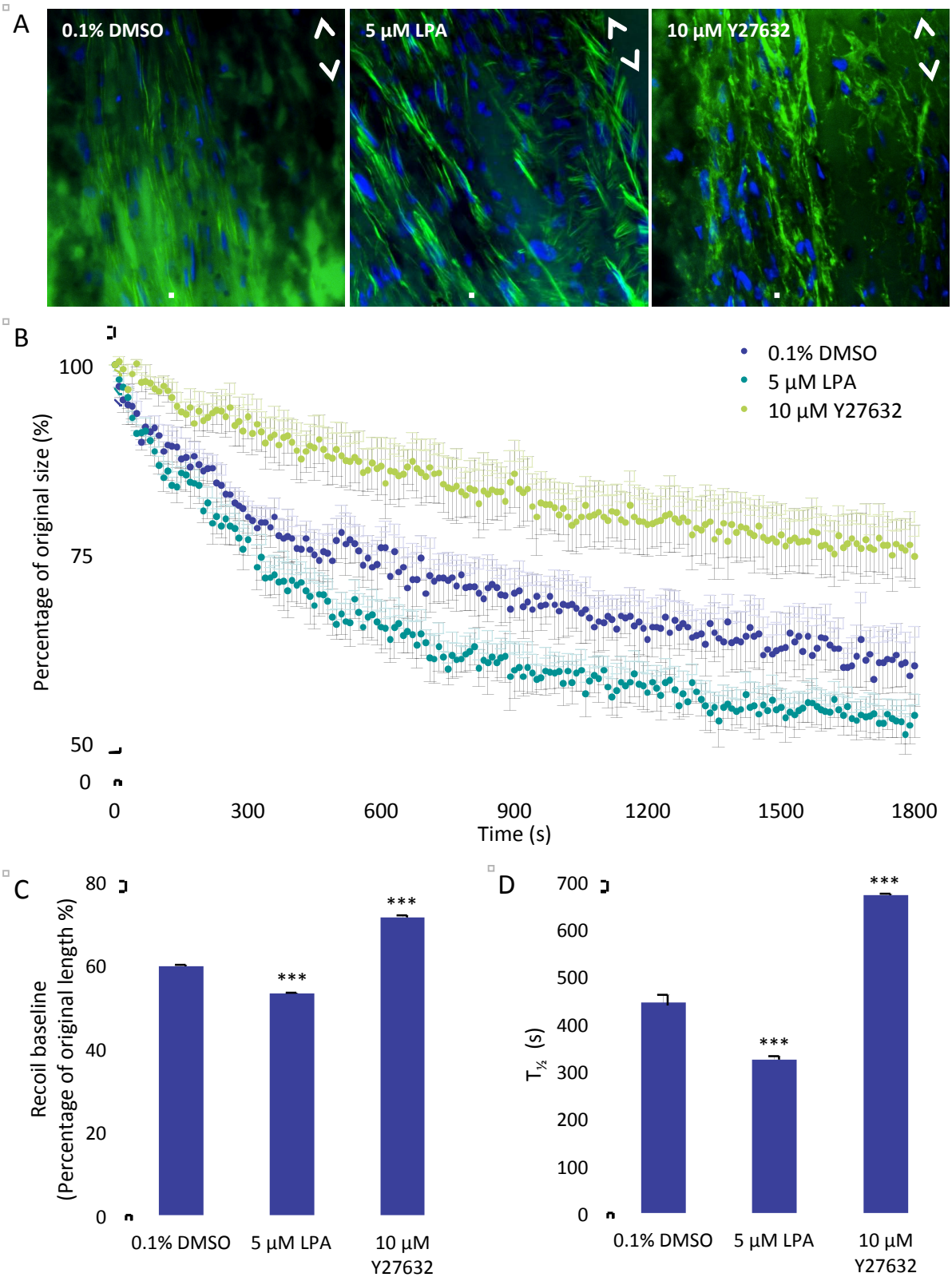

Figure 22

Modulating Rho signalling in tendon constructs affects tissue recoil.

Tendon constructs formed by primary embryonic chick tendon cells were treated with 5 µM LPA or 10 µM Y27632 for 2 hours in serum-free conditions. **(A)** Changes to actin stress fibres were observed in longitudinal sections with phalloidin staining. Bar = 50 µm. **(B)** After 2 hours, the constructs were un-tensioned and the recoil length was measured at 10 second-intervals for 30 minutes. A single exponential, 3-parameter fit was used to fit the mean values. Bars show SEM. **(C)** The recoil baseline, which is the calculated length of the construct at the end of the exponential fit**. (D)** The half-time, which is the time required to achieve half of the recoil baseline. *** indicates significant differences found when compared to 0.1% DMSO, $p < 0.001$.

and stress fibres is true, then knocking down Arhgap28 would lead to increased rate of tendon construct tissue recoil. However, compensation from Arhgap6 and Arhgap18 might be expected. During this PhD, siRNAs targeting the chick Arhgap28 transcript were tested (see Fig. 23). Due to low transfection efficiency of primary chick tendon cells using Lipofectamine, the Amaxa electroporation system was tested as described previously (Richardson *et al.*, 2007). Electroporation of cells produced ~50% knockdown in Arhgap28 mRNA levels (see Fig. 23A). However, the formation of tendon constructs by these cells takes up to 9 days raised concerns regarding if siRNA knockdown would persist. Therefore fully formed tendon constructs were removed from culture and electroporated as described for embryonic chick tendons (Richardson *et al.* 2007). However, consistency with knockdown data obtained from cells was not achieved (see Fig. 23A) and that tendon constructs were no longer under tension made this method undesirable. An alternative method of electroporation was tested; a Grass Instruments SD9 Stimulator that is often used to deliver molecules including siRNAs to *Xenopus* embryos via electroporation (described by Bonev *et al.*, 2011; see Fig. 23B). The method was optimised using labelled oligos and propidium iodide staining for cell death (see Fig. 23C). However, due to the limited penetration of the siRNAs into the tissue, a notable knockdown in Arhgap28 mRNA level was not detected (see Fig. 23D). For further investigating of the function of Arhgap28, a suitable method for knocking down is required.

4.3 Discussion

This chapter described a possible new function for the novel RhoGAP, Arhgap28, in the regulation of RhoA activation and actin stress fibre formation. Arhgap28 was upregulated during the formation of an organised embryonic tendon matrix *in vivo* and

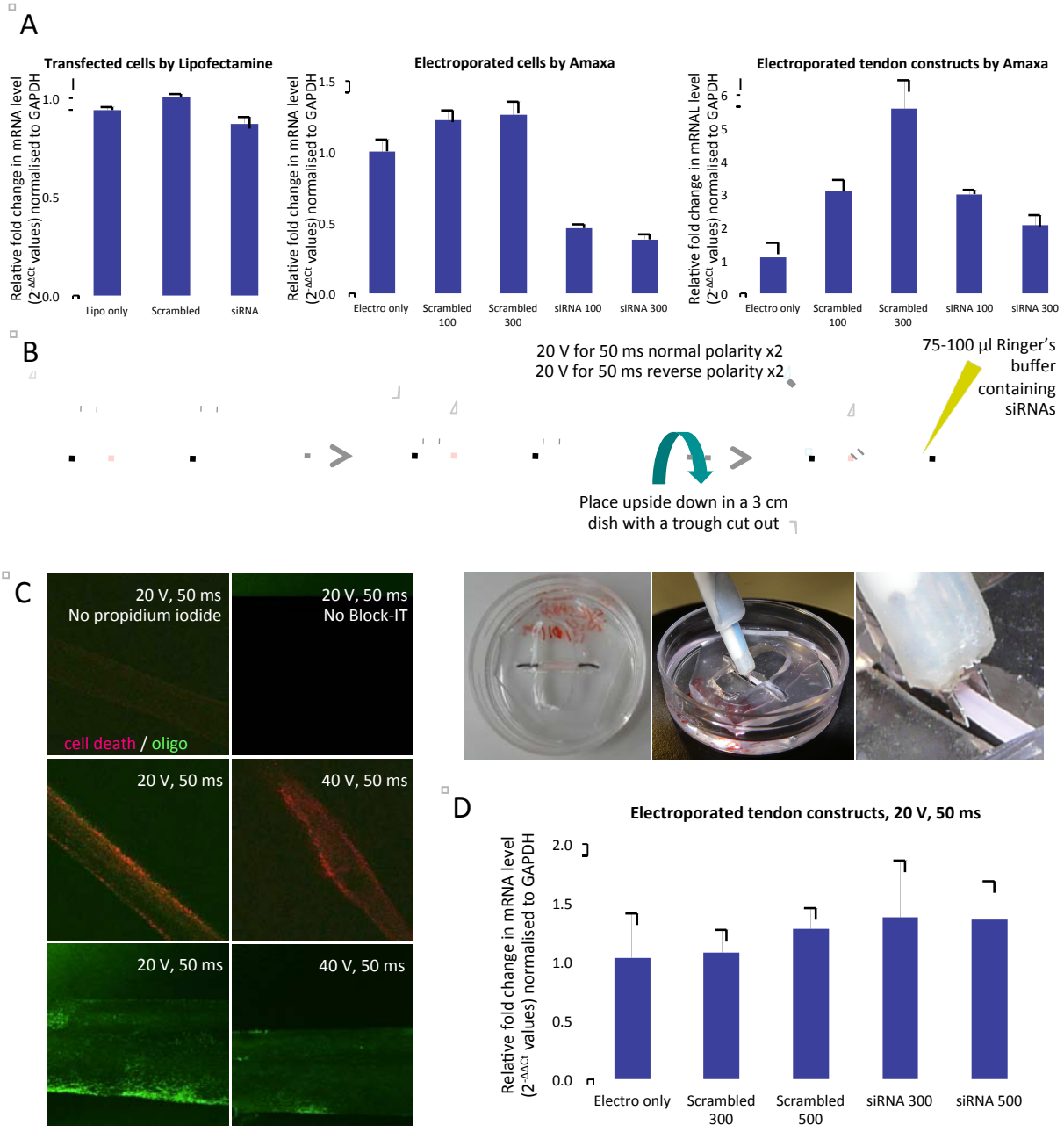

Figure 23

Strategies used to knockdown Arhgap28.

(A) Arhgap28 was targeted for knockdown using siRNAs (100 or 300 pmol) in primary embryonic chick cells using Lipofectamine and Amaxa electroporator, and in in tendon constructs using the Amaxa. Arhgap28 mRNA levels were measure by qPCR (n = 2). **(B)** Fully formed tendon constructs made with embryonic chick tendon cells on Sylgard were cut away from the well. Excess Sylgard was cut away from the edges, a hole in the Sylgard was cut from underneath the construct with disturbing the tissue and the minutien pins were trimmed down. The tendon construct attached to the Sylgard was then inverted into a 35 mm dish containing Sylgard with a trough to fit the construct. 75 – 100 µl of Ringer's buffer containing 300 or 500 pmol siRNA or 2 µm FITC-labelled control oligos was pipetted into the trough, covering the construct. The electroporation apparatus was arranged so that electrodes were on either sides of the width of the construct without any contact. Electrical current of 20 V for 50 ms was applied twice with normal polarity and repeated twice with reverse polarity. Each construct was treated at 4 points evenly along the construct. Constructs were then placed in a well containing complete medium and incubated for 24 hours at 37°C, 5% CO_2. **(C)** Constructs were stained with propidium iodide and imaged for cell death and oligo uptake. **(D)** qPCR analysis of Arhgap28 mRNA level. Fold changes in mRNA levels were normalised to GAPDH ($2^{-\Delta\Delta Ct}$ values). Bars show SEM.

in vitro. Arhgap28 was further upregulated during the cellular tension-dependent improvement in the matrix mechanical properties, but downregulated when the matrix was no longer under tension. Expression of a C-terminal V5 fusion Arhgap28 protein caused a reduction in basal levels of active RhoA and disruption to stress fibres. These results indicate that Arhgap28 negatively regulates stress fibre assembly via inactivation of RhoA, providing a mechanism by which cellular tension is regulated in fibrous tissues. The development of mechanical integrity of the tendon matrix has been shown to be dependent on actomyosin machinery (Kalson *et al.*, 2010). In this study, remodelling of collagen matrices was found to be regulated by Rho signalling. These findings implicate Arhgap28 in the development of the tendon matrix, by suppressing over active cellular contractility.

Arhgap28 was identified in Chapter 3 as differentially upregulated in embryonic tendon tissue in a microarray comparing rat tail tendon tissue at different developmental stages. This upregulation was validated in the rat flexor tendon, mouse tail tendon, and in tendon constructs formed by hMSCs and embryonic chick tendon cells, suggesting that the role of Arhgap28 in the formation of an organised collagen ECM is highly conserved. Significant upregulation of Arhgap28 commenced from T0 in tendon constructs form by chick cells. This upregulation from T0 was concurrent with upregulation in gene expression of COL1A1, fibronectin and β1 integrin, which are required for collagen fibrillogenesis.

During the formation of tendon constructs, there was also an upregulation in cell-matrix adhesion proteins (tensin and α-actinin) and Rho GTPases (RhoA, Rac1, Cdc42 and RhoQ), which are involved in actin reorganisation and the assembly of contractile

stress fibres (discussed in the Introduction). As well as Arhgap28, the upregulation of previously characterised RhoGAPs, Arhgap6, Arhgap18 and DLC1, were also observed from T0 in tendon constructs. These RhoGAPs have been shown to regulate actin stress fibre assembly (Maeda *et al.*, 2011, Prakash *et al.*, 2000, Wong *et al.*, 2008, Zhou *et al.*, 2008). Together, these results suggest that major actin reorganisation events occur during tendon matrix assembly and development of mechanical properties, and that Rho GTPases signalling required cell contractility are tightly regulated by a number of RhoGAPs. Interestingly, Racgap1 was only significantly upregulated at d3 in fibrin gels, before the tendon constructs are formed. This is most likely because Racgap1, a GAP with specificity for Rac1 and Cdc42, and is associated with cell migration and invasion through ECM (Wang *et al.*, 2011).

Tensioning of the tendon matrix involves actomyosin-mediated cell contractility (Kalson *et al.*, 2010). Untensioning of tendon constructs did not affect the expression of Rho GTPases. However, Arhgap28, Arhgap6 and the adhesion proteins examined (vinculin, tensin and α-actinin) were all significantly downregulated after 24 hours, suggesting that these molecules are involved in the tensioning of the tendon matrix. Cellular tension is generated by actin stress fibres (Burridge and Chrzanowska-Wodnicka, 1996). In this context, the closely related Arhgap6 and Arhgap18 regulate the formation actin stress fibres via RhoA (Prakash *et al.*, 2000, Maeda *et al.*, 2011). In this study, overexpression of Arhgap28-V5 caused a reduction in RhoA activity, loss of stress fibres, which is similar to the effects observed for Arhgap6 and Arhgap18 (Prakash *et al.*, 2000, Maeda *et al.*, 2011). Overexpression of Arhgap28-V5 also caused an increase in occurrence of membrane protrusions and ruffling. Sustained RhoA activity has inhibitory effects on Rac1- and Cdc42-activated lamellipodia and filopodia

formation (Arthur and Burridge, 2001, Cox *et al.*, 2001), which explains the appearance of actin microspikes and membrane ruffles in Arhgap28-overexpressing cells. Assays assessing levels of active Rac1 and Cdc42 in cells overexpressing Arhgap28-V5 would confirm this. These data suggest that Arhgap28 negatively regulates RhoA signalling in embryonic tendon cells, which could be critical for responding to tensile stresses.

Collagen gel remodelling by fibroblasts is regulated by Rho-ROCK-generated cellular tension (Grinnell *et al.*, 2003). Here, modulating Rho-ROCK signalling via treatment with LPA and the ROCK inhibitor Y27632 confirmed that Rho signalling is required for collagen ECM remodelling. Unlike collagen gels, where there is a meshwork of fibrils, the collagen fibrils in embryonic tendon are highly organised in parallel bundles. LPA and Y27632 treatment of tendon constructs confirmed that contraction of tendon-like ECM is also regulated by Rho signalling. In migratory cells, RhoA signalling mediates the retraction of the tail to allow the cell to move forward (Worthylake *et al.*, 2001). However, fibroblasts in normal tissues are non-migratory. It has been demonstrated that stress fibre contraction in non-migratory cells lead to stronger focal adhesions (Chrzanowska-Wodnicka and Burridge, 1996). These data suggest that tendon cells are in contact with the ECM via cell-matrix adhesions, which are linked to contractile stress fibres.

RhoA-mediated stress fibre contraction has been shown to be required for the stretching of fibronectin molecules (Yoneda *et al.*, 2007, Zhong *et al.*, 1998). However, Arhgap28 and Arhgap6 upregulation during collagen fibrillogenesis in tendon constructs suggest that the actomyosin-mediated contractility is tightly regulated. It would be interesting to explore further the role of RhoA signalling and actin stress

fibre on the mechanical integrity and organisation of tendon ECM. One reason why it would be important to regulate stress fibres during the establishment of a strong tendon ECM is for alignment of collagen fibrils. For example, the purpose of stress fibres in myofibroblasts is to remodel the collagen fibres at the wound site into parallel bundles along the long axis (Hinz *et al.*, 2001). A similar mechanism might be involved during the remodelling of collagen fibrils in tendon tissue.

In summary, Arhgap28 is a RhoGAP that regulates RhoA and stress fibre formation during the assembly of a strong, organised collagen ECM. RhoA signalling is required for remodelling of collagen matrices, via contractile stress fibres and cell-matrix adhesions. Therefore, in tendon tissues, Arhgap28 is predicted to be important for the alignment of collagen fibrils in the ECM and improve its tensile properties. In future work, it will be interesting to explore if modulating RhoA signalling by knockdown of Arhgap28, perhaps by lentiviral-delivery of shRNAs, affects collagen fibril organisation and cell-matrix adhesions.

CHAPTER 5

STUDY OF ARHGAP28 FUNCTION IN THE *ARHGAP28*^{GT} REPORTER MOUSE AND *ARHGAP28*^{DEL} KNOCKOUT MOUSE

5. Study of Arhgap28 Function in the *Arhgap28^{gt}* Reporter Mouse and *Arhgap28^{del}* Knockout Mouse

5.1 Chapter introduction

In Chapter 4, Arhgap28 was shown to regulate RhoA and assembly of stress fibres, which are required for the generation of cellular tension in tendon tissues. To complement the *in vitro* overexpression studies, a knockout approach was taken to study the function of Arhgap28 in ECM organisation *in vivo*. Chapter 5 describes two mouse models for the disruption of the Arhgap28 gene – using a gene trap approach (*Arhgap28^{gt}* mouse) and cross breeding this *Arhgap28^{gt}* mouse with a *Cre* transgenic mouse to produce the *Arhgap28^{del}* mouse, where exons 7-9 were excised from the Arhgap28 gene. The gene trap approach was unsuccessful at disrupting the expression of wild type Arhgap28 transcript, but the *Arhgap28^{gt}* mouse was used to report the spatial and temporal activation of the Arhgap28 gene. Development of tendon appeared to be unaffected in Arhgap28-deficient, *Arhgap28$^{del/del}$* mice. However, as will be discussed below, RNA analysis suggests that upregulation of Arhgap6 might compensate for the lack of Arhgap28 in *Arhgap28$^{del/del}$* mice. The reporter mouse showed that Arhgap28 expression was activated prominently in bone from E18.5. Data obtained at the end of the PhD period of study from a microarray comparison of P0 wild type and *Arhgap28$^{del/del}$* bone tissues showed a downregulation in genes that are linked to bone dysplasia. This data might suggest that the Arhgap28-null mice have a bone ECM phenotype.

5.2 Results

5.2.1 Targeted disruption of the mouse Arhgap28 gene by gene trapping

Arhgap28 gene trap (*Arhgap28*^{gt}) mice were generated as described in section 2.9.1 using ES cells containing the L1L2_Bact_P targeting gene trap cassette (including the genes encoding β-galactosidase and neomycin) introduced into intron 6 of the Arhgap28 gene. The ES cells were purchased from KOMP (NIH Knockout Mouse Project; see Fig. 24). The insertion of the gene trap at this position is predicted to disrupt expression of the endogenous Arhgap28 transcript and instead a β-galactosidase fusion transcript will be expressed under the control of the endogenous promoter of the Arhgap28 gene. A PCR strategy was devised to confirm the genotypes (wild type, heterozygous or homozygous) of pups in a single reaction (see Fig. 24). A forward primer and a reverse primer that span intron 6 were used so that a 493 bp product confirmed the presence of the wild type allele. The same forward primer and an additional reverse primer that binds the 5' end on the gene trap cassette were used to produce a 354 bp product and confirmed the presence of the *Arhgap28*^{gt} allele.

5.2.2 *Arhgap28*$^{gt/gt}$ mice are viable

Mice heterozygous for the *Arhgap28*^{gt} allele were viable and fertile. Litters resulted from cross breeding heterozygotes were examined during embryonic development (at E12.5, E15.5 and E18.5) and a normal Mendelian distribution of genotypes was observed (see Table 7). Only 4 out of 39 embryos at E15.5 were resorbed. Pups aged between P0 and P7 from heterozygous breedings were also genotyped. Although *Arhgap28*$^{gt/gt}$ mice survived and were indistinguishable from their littermates, homozygotes accounted for 8 ± 3% of the genotypes, instead of the expected 25% (see Table 7). A possible explanation was that some homozygous pups were eaten by their

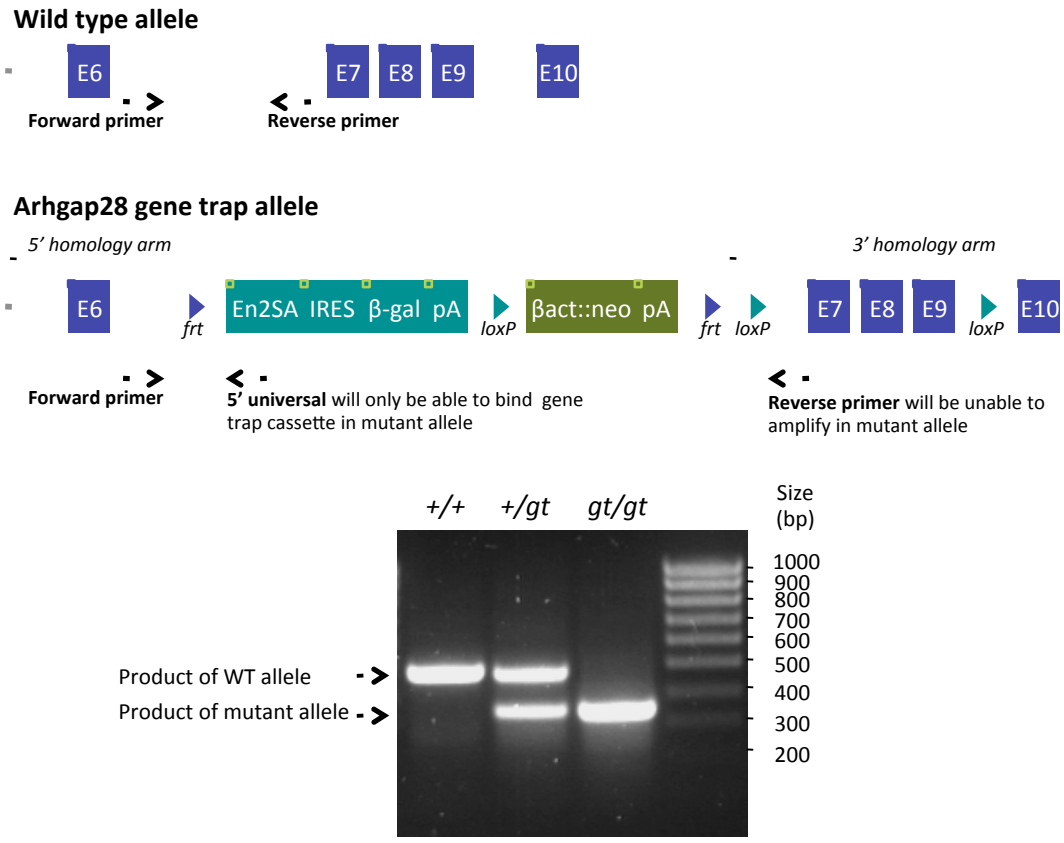

Figure 24
Genotyping for the *Arhgap28^{gt}* allele by PCR.
Schematic showing the genotyping strategy for identifying the presence of the gene trap cassette targeted to the Arhgap28 gene. Representative gel image of genotyping PCR products performed as described in section 2.9.2. DNA from wild type (+/+) animals will only produce a 493 bp product whereas DNA from homozygous (gt/gt) animals will only produce a 354 bp product and DNA from heterozygous (+/gt) animals will produce both bands.

Day of gestation	+/+	+/gt	gt/gt	resorbed
E12.5	2	5	3	0
E15.5	8	21	6	4
E18.5	2	7	2	0
Percentage ± SEM	**20 ± 4%**	**54 ± 5%**	**19 ± 6%**	**6 ± 6%**
Born	31	55	11	
Percentage ± SEM	**32 ± 6%**	**60 ± 5%**	**8 ± 3%**	

Table 7
Mendelian ratio of heterozygous *Arhgap28^{gt}* matings.
Percentage of wild type (+/+), heterozygous (+/gt) and homozygous (gt/gt) offspring.

mothers as no adult deaths were observed.

5.2.3 *Arhgap28*$^{gt/gt}$ mice do not display histological abnormalities

Arhgap28 is upregulated in tendon during embryonic development and detected in various tissues in newborn mice (see Chapter 4). To examine if limb development was affected by the mutant allele, *Arhgap28*$^{gt/gt}$ embryos were examined histologically. No apparent differences between wild type, *Arhgap28*$^{+/gt}$ and *Arhgap28*$^{gt/gt}$ embryos were observed (see Fig. 25A). Tail tendons from E15.5 embryos were examined by TEM to detect any changes during the establishment of the tendon ECM (see Fig. 25B). Features such as fibripositors, plasma membrane channels and narrow-diameter collagen fibrils were seen in tendons of wild type and homozygous embryos, with no apparent differences between them.

To investigate if expression of the Arhgap28 transcript in mice with the *Arhgap28*^{gt} allele was disrupted, RNA from tendons of P0 mice was isolated and analysed by RT-PCR. The genotypes of the mice were confirmed (see Fig. 25C). Analysis of gene expression using primers that span exon 6 to exon 11 would produce a 624 bp product if an intact Arhgap28 transcript were present. Surprisingly, intact Arhgap28 transcript was detected in tendon tissue isolated from *Arhgap28*$^{gt/gt}$ mice (see Fig. 25D). This result meant that the predicted splicing between exon 6 and the splice acceptor of the reporter gene did not occur. PCRs detecting expression of COL1A1 and GAPDH served as control reactions and no differences were observed between wild type and *Arhgap28*$^{gt/gt}$ mice (Fig. 25D). These data suggest that *Arhgap28*$^{gt/gt}$ mice develop normally because Arhgap28 gene was not sufficiently disrupted by the gene trap cassette.

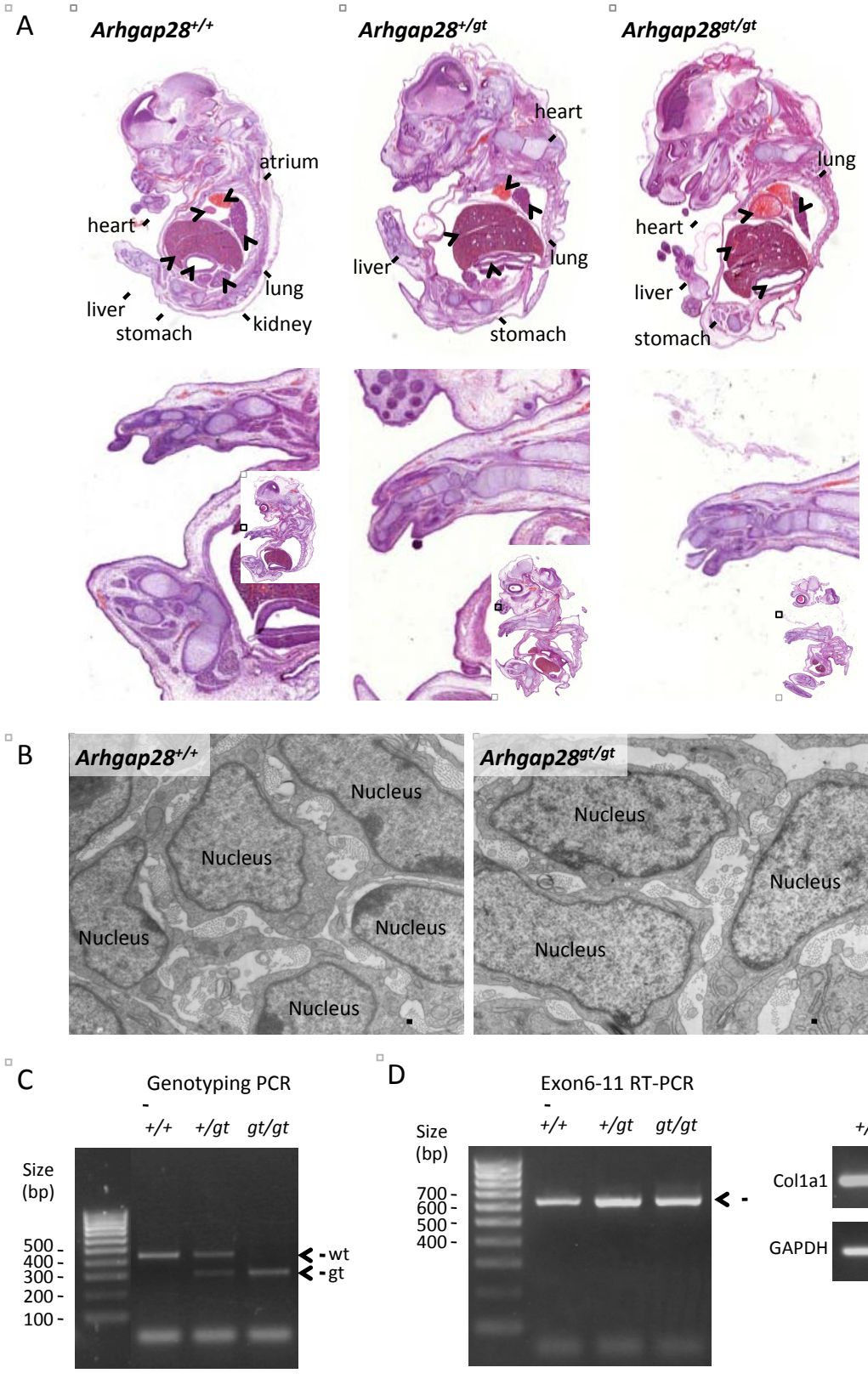

Figure 25

Mice homozygous for the *Arhgap28^{gt}* allele appear normal.

(A) Sagittal sections of wild type (*+/+*), heterozygous (*+/gt*) and homozygous *Arhgap28^{gt}*mutant (*gt/gt*) embryos at gestation day E15.5 stained with H&E and close-up of the limbs. **(B)** Representative micrographs of transverse sections of tail tendon from wild type and *Arhgap28$^{gt/gt}$* mutant E15.5 embryos examined by TEM. Bars = 1 µm. **(C)** DNA was isolated from wild type, *Arhgap28$^{+/gt}$* and *Arhgap28$^{gt/gt}$* mutant neonatal tail tendons cells to confirm genotypes. **(D)** RNA was also isolated RT-PCR was performed to detect the expression of Arhgap28 transcript spanning from exon 6 to 11, Col1a1 and GAPDHs.

5.2.4 Arhgap28 has a restricted expression pattern through embryonic development

The expression of the reporter gene, β-galactosidase, in the gene trap cassette is driven by the promoter of the Arhgap28 gene. Its expression was used to track the spatial and temporal expression of Arhgap28 during embryonic development. β-galactosidase activity was localised in embryos by X-gal staining. β-galactosidase activity had a restricted spatial pattern and could be detected from E11.5, the earliest time point examined, to E18.5, just before birth (see Fig. 26A). β-galactosidase activity was observed in what appeared to be mesenchymal progenitors and later, at E18.5, in bone tissues. E18.5 embryos were sectioned and counter stained with Alizarin red S to localise bone tissue. Cells stained positive for β-galactosidase activity were localised to the calcified portions of long bones and ribs (see Fig. 26B). Surprisingly, β-galactosidase activity was not observed in tendon tissues, which might suggest that the Arhgap28 promoter is not as active as in bone tissues during late-embryonic development.

5.2.5 Targeted disruption of the *Arhgap28^{gt}* allele by Cre recombinase

An alternative strategy to disrupt the Arhgap28 gene was to cross breed *Arhgap28$^{+/gt}$* mice with *Cre* transgenic mice (as described in section 2.9.1). In the gene trap cassette designed by KOMP, *loxP* sites flank exons 7 and 9 of the Arhgap28 gene. Therefore, expression of Cre recombinase would be expected to excise exons 7, 8 and 9, and produce mice harbouring an *Arhgap28^{del}* allele (see Fig. 27A). The absence of exons 7-9 would cause a shift in the coding sequence and if this mutant Arhgap28 transcript were stable and translated, it would produce a truncated (312 aa instead of 729 aa) protein without the RhoGAP domain, represented in Appendix 6. The PCR strategy described previously (section 5.2.1) was used to confirm genotypes (wild type,

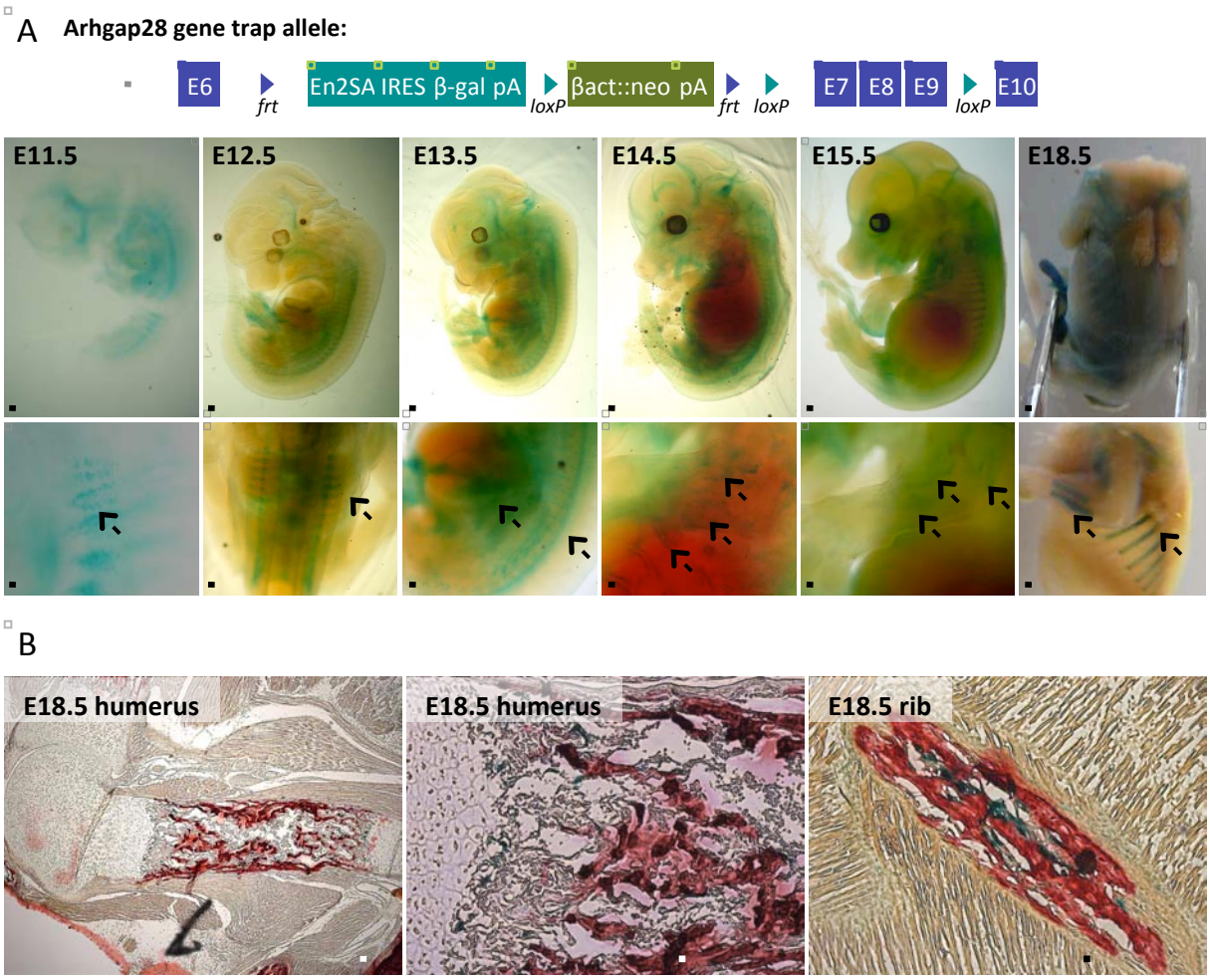

Figure 26
Spatial and temporal expression of Arhgap28 in *Arhgap28$^{gt/gt}$* reporter mice.
Embryos from time-mated heterozygous *Arhgap28^{gt}* mice were stained with X-gal and genotyped. **(A)** Embryos homozygous for the *Arhgap28^{gt}* allele were imaged. Wild type embryos acted as controls (not shown). Bars = 2 mm.**(B)** *Arhgap28$^{gt/gt}$* embryos from E18.5 litters were processed for wax embedding and sagittal sections were counterstained with Alizarin red S to stain for calcified matrix. Areas of where X-gal-positive cells are shown. Cells stained positive with X-gal are blue green and red shows tissues stained with Alizarin red S. Bars = 200 µm.

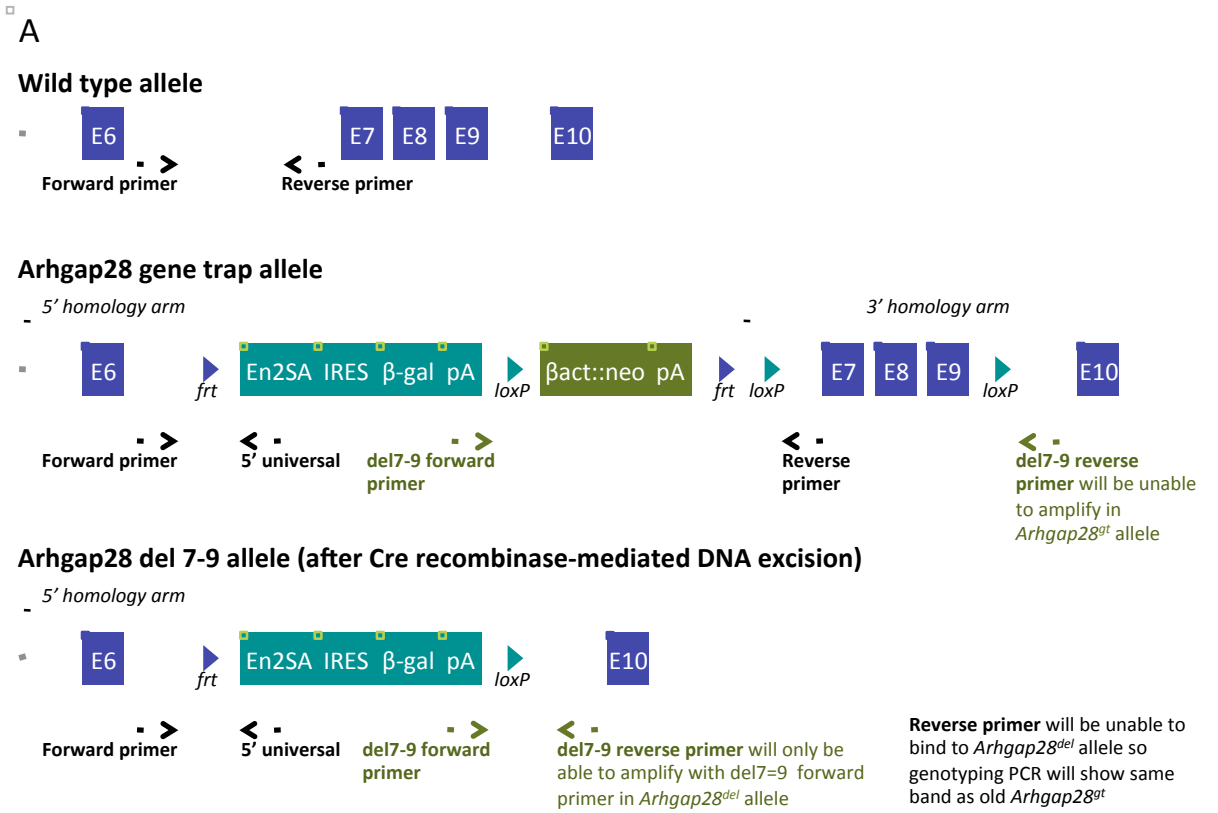

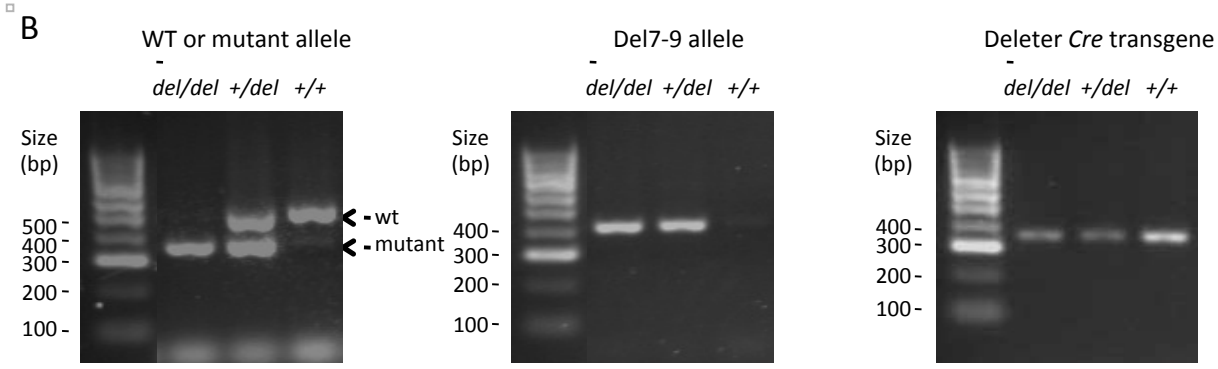

Figure 27
Genotyping for the *Arhgap28*^{del} allele by PCR.
(A) Schematic showing the genotyping strategy for identifying the presence of the gene trap cassette targeted to the Arhgap28 gene and for the detection of Arhgap28 del7-9 KO allele. **(B)** Representative gel image of genotyping PCR products performed as described in section 2.9.2. In the first genotyping PCR which distinguishes between wild type (493 bp) or mutant Arhgap28 allele (either the *Arhgap28*^{gt} or *Arhgap28*^{del} allele; 354 bp). The second genotyping PCR tests for the presence of the *Arhgap28*^{del} allele, the product of the mutant Arhgap28 allele after Cre recombinase-mediated DNA excision (400 bp). The third genotyping PCR tests for the presence of the deleter *Cre* transgene (350 bp).

heterozygous or homozygous) of pups in a single reaction (see Fig. 27B). A second PCR confirmed the presence of the new *Arhgap28*^{del} allele. A third PCR confirmed the presence of the *Cre* transgene. Mice heterozygous for the *Arhgap28*^{del} allele were viable and fertile. Litters resulted from cross breeding heterozygotes had a normal Mendelian distribution of genotypes: 30 ± 9% wild types; 49 ± 5% heterozygotes; and 22 ± 8% homozygotes (± SEM; from a total of 37 pups, in 8 litters).

5.2.6 *Arhgap28*$^{del/del}$ mice do not display histological abnormalities despite expression of a truncated Arhgap28 transcript

Arhgap28$^{del/del}$ embryos (E15.5) were examined histologically and no apparent differences were observed compared to wild types (see Fig. 28A). RT-PCR was performed on RNA isolated from neonatal tendon cells using primers that spanned exons 6 to exons 11, which would produce a 624 bp product if an intact Arhgap28 transcript were present. In cells isolated from wild types, expression of intact Arhgap28 transcript was confirmed (see Fig. 28B). In cells isolated from *Arhgap28*$^{+/del}$ and *Arhgap28*$^{del/del}$ mice, a PCR product of ~350 bp was amplified and confirmed by DNA sequencing to lack sequences encoded by exons 7-9 of the Arhgap28 transcript (see Fig. 27B). The predicted amino acid sequence that resulted from *Arhgap28*^{del} transcript was slightly longer than expected, 367 aa (instead of 312 aa), which was probably the result of altered intron-exon splicing, causing some foreign sequences to remain in the transcript (shown in Fig. 28B and Appendix 6).

5.2.7 *Arhgap28*$^{del/del}$ mice do not display tendon abnormalities

Tail tendons from E15.5 *Arhgap28*$^{del/del}$ embryos were examined by TEM to detect any changes during the establishment of the tendon ECM (see Fig. 29A). Features such as

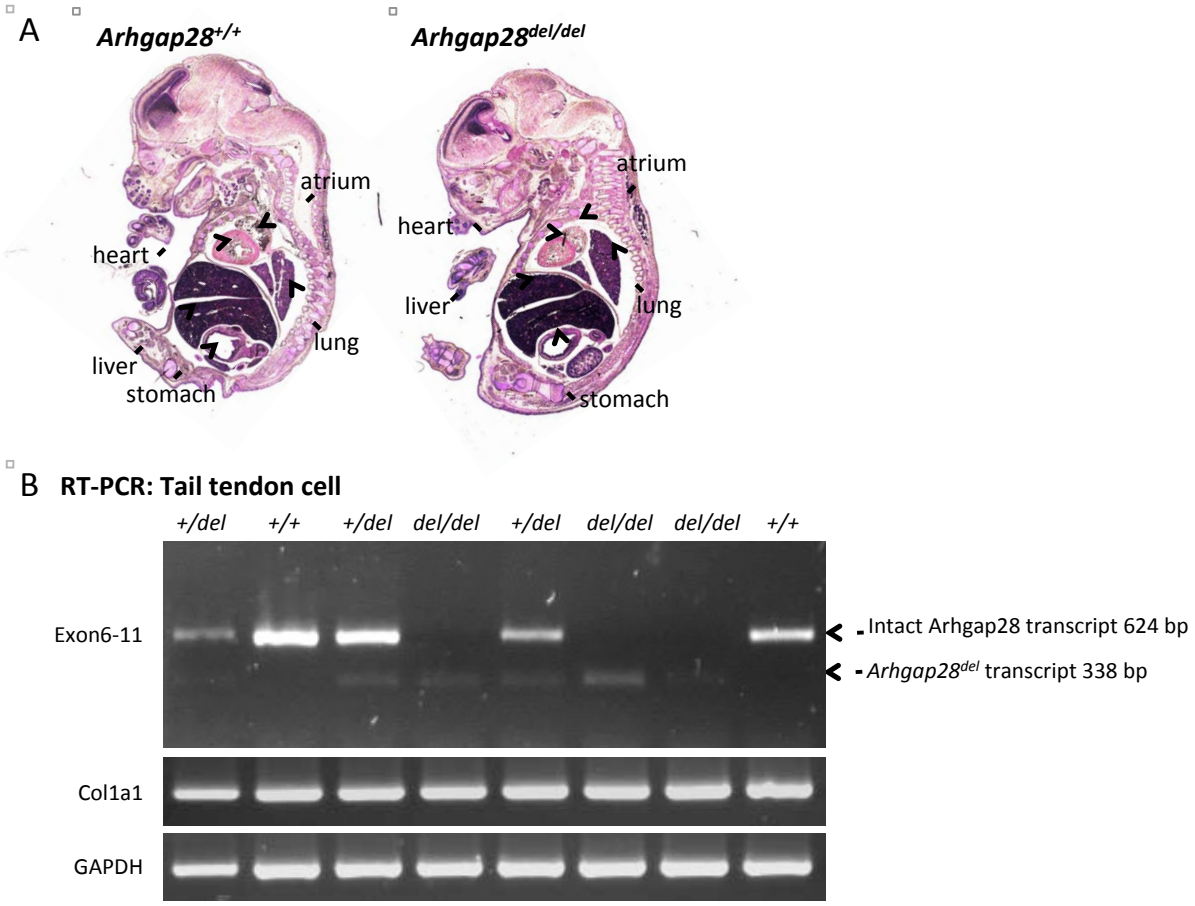

Figure 28
Mice homozygous for the *Arhgap28*^{del} allele appear normal.
(A) Sagittal sections of wild type (*+/+*) and homozygous Arhgap28 del7-9 mutant (*gt/gt*) embryos at gestation day E15.5 stained with H&E. **(B)** RNA was isolated from wild type, *Arhgap28*$^{+/del}$ and *Arhgap28*$^{del/del}$ mutant neonatal tail tendons cells and RT-PCR was used to detect expression of wild type and mutant Arhgap28 transcript spanning from exons 6 to 11. RT-PCRs for Col1a1 and GAPDH was used as loading controls. **(C)** The sequence of the mutant *Arhgap28*^{del} transcript is shown.

fibripositors, plasma membrane channels and narrow-diameter collagen fibrils were seen in tendons of wild type and *Arhgap28*$^{del/del}$ embryos, with no apparent differences between them. As an indication of mechanical strength, the elastic modulus of tail tendons isolated from 2-week-old pups was measured (as described in section 2.9.5; from a total of 14 pups, in 2 litters). No significant differences were found in the elastic modulus of tail tendons between wild type, heterozygous and homozygous *Arhgap28*^{del} mice (see Fig. 29B). These data suggest that Arhgap28 is not essential for the development of tendon tissue, albeit in the presence of potential compensating mechanisms.

The results in Chapter 4 implicated a role for Arhgap28 in regulating stress fibres. Tendon cells were isolated from P0 tail tendons of wild type, heterozygous and homozygous *Arhgap28*^{del} mice and the stress fibres were examined by phalloidin staining. Tendon cells of all genotypes were able to attach to tissue culture plastics and glass, and no apparent differences were observed in cell spreading and stress fibres in *Arhgap28*$^{del/del}$ tendon cells compared to wild types (see Fig. 29C). These observations suggest that Arhgap28 may not be the only RhoGAP regulating actin reorganisation in these cells.

5.2.8 Comparison of gene expression between bone tissues of wild type and *Arhga28*$^{del/del}$ mutant mice

Arhgap28 is prominently expressed in bone tissues from E18.5, as indicated by the β-galactosidase reporter assay (see Fig. 26). To understand the function of Arhgap28 *in vivo*, the effect of loss of Arhgap28 was further investigated in bone tissues. First, RNA was isolated from the tibia and fibula of P0 wild type and *Arhgap28*$^{del/del}$ mice, and

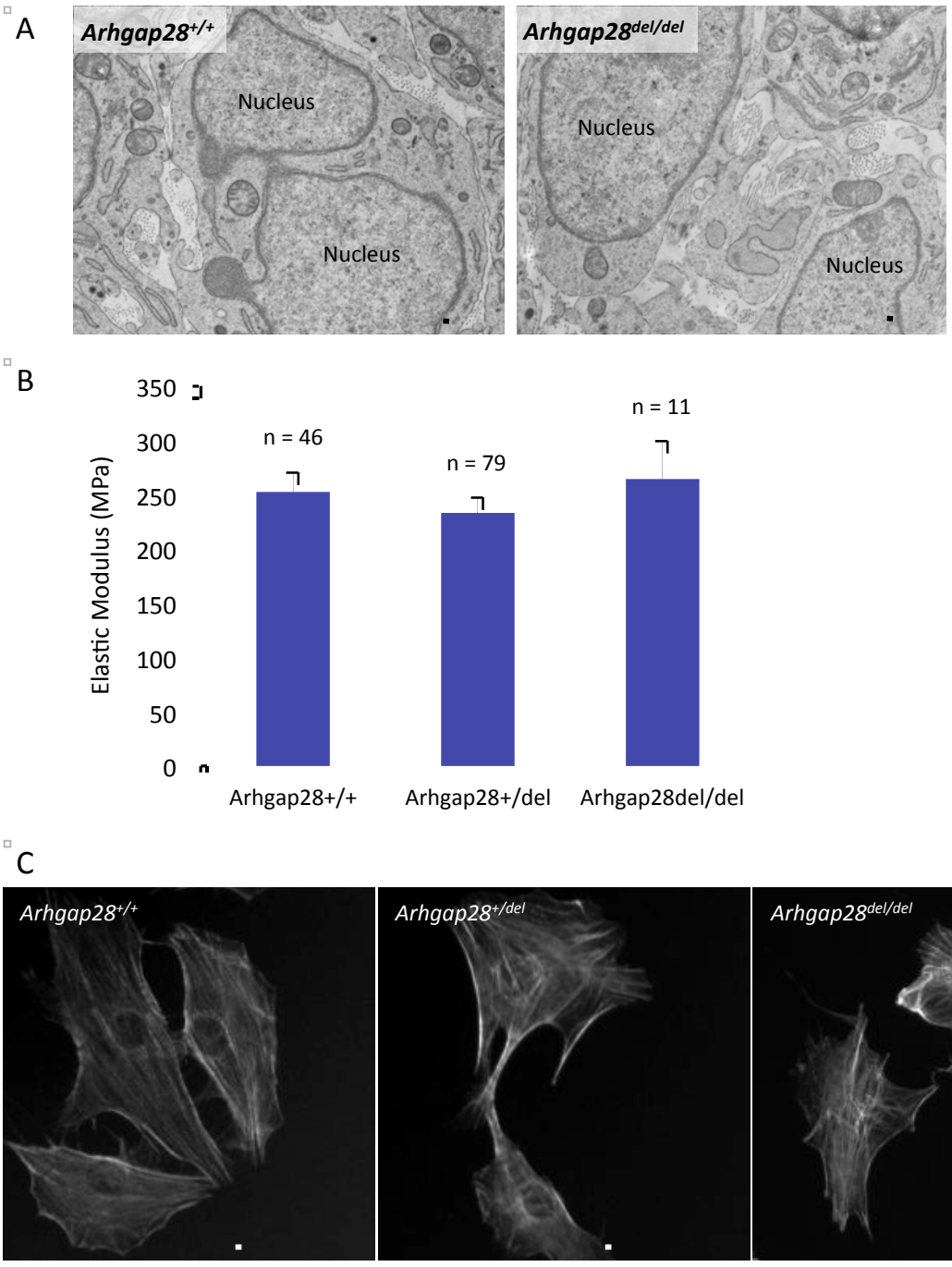

Figure 29
***Arhgap28*^{del} mice appear to have normal tendon development.**
(A) Representative micrographs of transverse sections of tail tendon from wild type and *Arhgap28*^{del} mutant E15.5 embryos examined by TEM. Bars = 1 µm. **(B)** Elastic modulus of tail tendons from P14 mice (p = 0.58). n indicates the number of tendons measured. **(C)** F-actin in primary tendon cells isolated from P0 mouse tails were visualised using phalloidin. Bars = 50 µm.

overlapping PCRs were performed to determine which Arhgap28 isoform was expressed in bone tissues and if the mutant transcript could be detected in mutant mice (Fig. 30A). The larger isoform of Arhgap28 was expressed in wild type bone tissues, which is the same isoform expressed in tendon tissues (see Fig. 29B). The overlapping PCRs confirmed that exons 7-9 were absent in the Arhgap28 transcript of *Arhgap28*$^{del/del}$ mutants (see Fig. 30B). The products of these reactions were sequenced and confirmed that the transcript expressed in *Arhgap28*$^{del/del}$ mutants would be translated into the 367 aa protein, lacking in a functional RhoGAP domain (for the sequences, see Appendix 6).

To investigate the possibility that other RhoGAPs can compensate for the absence of Arhgap28, such as Arhgap6, Arhgap18, DLC1 and Racgap1 (as discussed in Chapter 4), the expression of these genes was examined in wild type and *Arhgap28*$^{del/del}$ bone tissues by qPCR (Fig. 31). Arhgap28 expression was detectable in tissues from *Arhgap28*$^{del/del}$ mice, which was expected because the mutant transcript is stable (see Fig. 31A). However, it was clear that it was at significantly lower levels compared to expression in bone tissues from wild type mice ($p < 0.001$; Fig. 31A). Surprisingly, a significant 2-fold upregulation in Arhgap6 expression was detected in *Arhgap28*$^{del/del}$ tissues ($p < 0.001$), but no differences were found in the expression of Arhgap18, DLC1 and Racgap1 (see Fig. 31A and B). These data show that in tissues devoid of functional Arhgap28, there is compensatory upregulation of Arhgap6, which might indicate that the Arhgap6-Arhgap28 pair might co-regulate the same Rho signalling pathway for actin reorganisation. In addition to RhoGAPs, expression of Rho GTPases were also examined. A significant upregulation in RhoA expression, but not in expression of Rac1, Cdc42 or RhoQ, was found in *Arhgap28*$^{del/del}$ bone tissues compared to wild type ($p <$

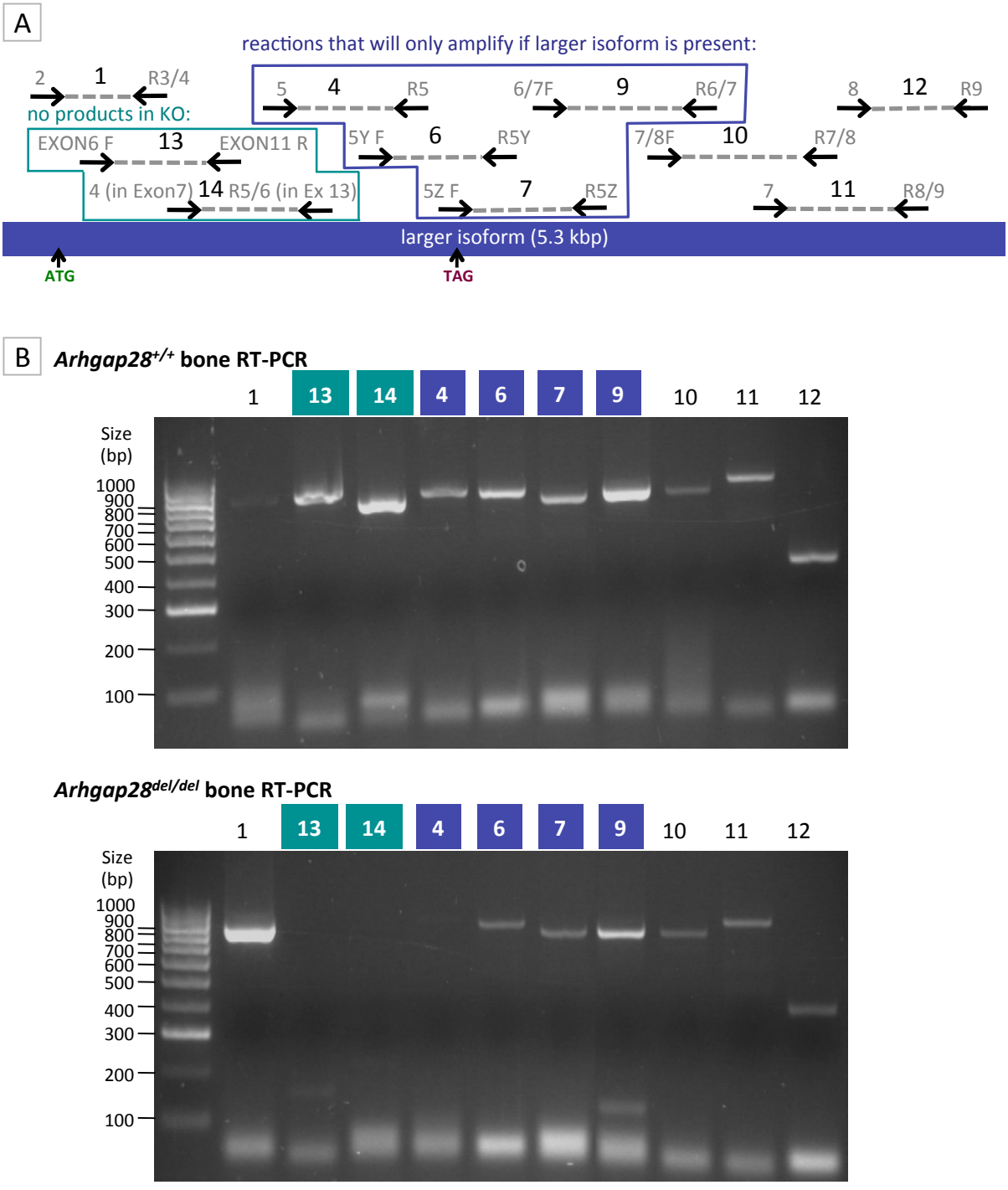

Figure 30

Comparison of the full length transcripts of wild type and *Arhgap28*^{del} alleles.

PCR strategy used to examine the Arhgap28 transcript expressed by wild type and *Arhgap28*$^{del/del}$ mice. **(A)** Overlapping products of PCR reactions 1, 4, 6-7, 9-14 by specific primers (numbers in grey) are sequenced. Reactions in the box will not produce a product with cDNA from *Arhgap28*$^{del/del}$. ATG and TAG indicates the start and stop codons, respectively. Diagram not drawn to scale. **(B)** RNA was isolated from the tibia and fibular of P0 mice, and the 10 overlapping RT-PCRs were performed and visualised by gel electrophoresis. Products were subsequently purified and confirmed by DNA sequencing.

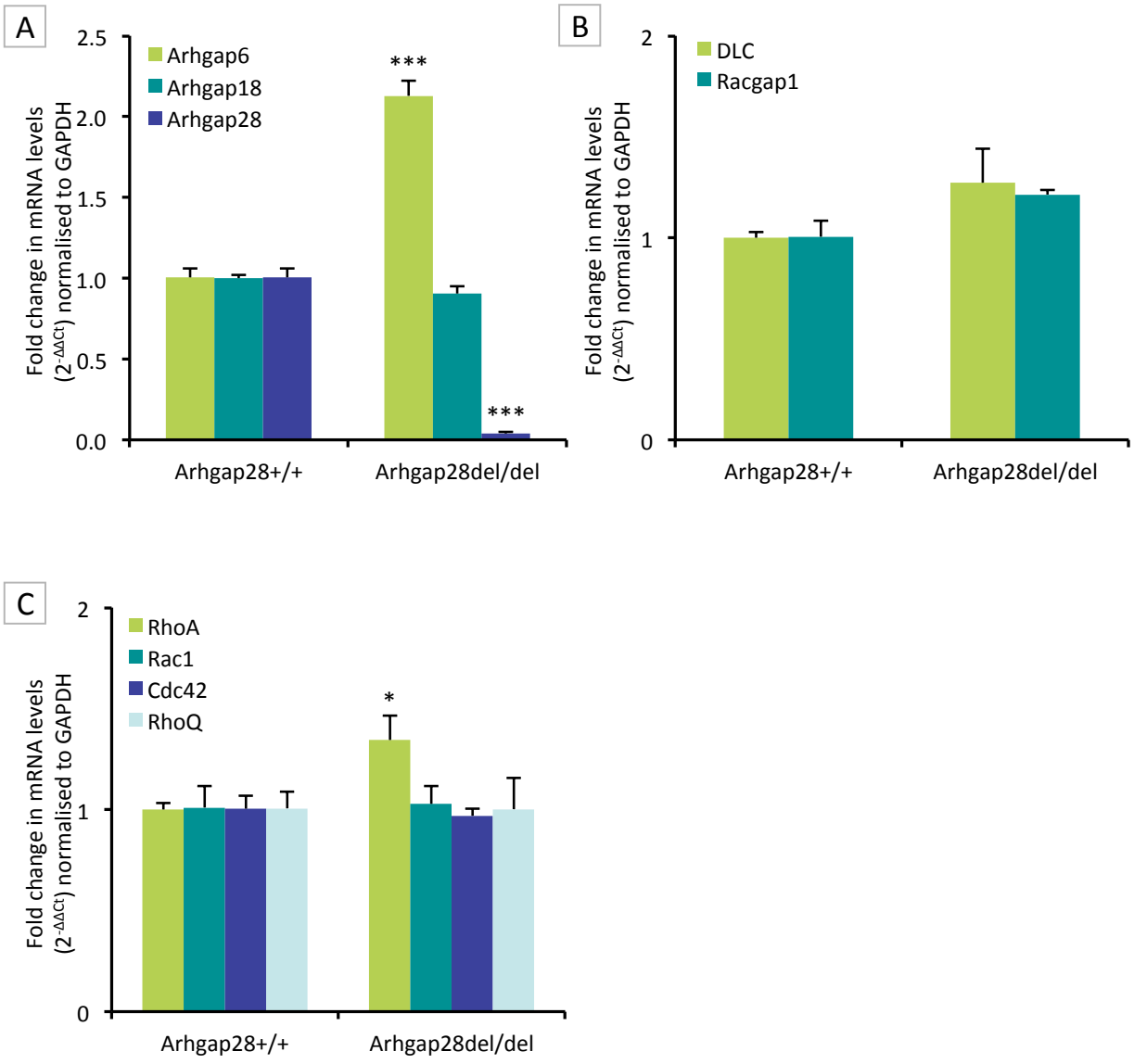

Figure 31

Expression of RhoGAPs and Rho GTPases in *Arhgap28*$^{del/del}$ bone tissues.

RNA was isolated from bone tissues (from tibia and fibula) of P0 wild type and *Arhgap28*$^{del/del}$ mice. **(A)** The expression of genes encoding Arhgap28 and related RhoGAPs, Arhgap6 and Arhgap18; **(B)** candidate RhoGAPs, DLC1 and Racgap1; and **(C)** Rho GTPases, RhoA, Rac1, Cdc42 and RhoQ was quantified by qPCR (n = 3). Fold changes in gene expression normalised to GAPDH ($2^{-\Delta\Delta Ct}$ values). Bars show SEM. *** and * indicate significant differences found when compared to wild type, $p < 0.001$ and $p < 0.05$, respectively.

0.05; see Fig. 31C). Again, these data were indicative of a role of Arhgap28 in RhoA regulation.

5.2.9 Comparative microarray and gene ontology analysis

To identify global changes in gene expression, microarray analysis was performed to compare RNA from bone tissues (tibia and fibula) of wild type and *Arhgap28*$^{del/del}$ mice. The integrity of the RNA samples isolated from wild type and *Arhgap28*$^{del/del}$ bone tissue was analysed by gel electrophoresis (Fig. 32A). The microarray readouts were analysed by dChip analysis and PCA, as described previously in section 3.2.2. PC #1 accounted for 46% of the total variability between samples, grouping the triplicates of wild type and Arhgap28-null bone tissues (see Fig. 32B). The data from dChip analysis is presented in Table 8. The median intensities of the arrays were between 137 and 184 (arbitrary units; see Table 8). Hybridisation to 60-63% of the probe sets was detected (see P call % in Table 8). Percentage of array and single outliers showed no anomalies in the readouts of individual probe sets and probes (see Table 8). A total of 45, 037 probe sets were detected. However, only 363 probe sets showed differential expression ≥ ± 2 fold difference. A heat map generated by hierarchical clustering of all the genes (or probe sets), based on similarities in the expression level and the expression profile is shown in Appendix 7.

The microarray readouts indicated that Arhgap28 expression was detected by 3 probe sets, which showed that Arhgap28 was downregulated in *Arhgap28*$^{del/del}$ bone by 1- to 2.5-fold (see Table 9). This was expected because a 3' microarray was used and the mutant *Arhgap28*^{del} transcript contains the endogenous 3'-end. In contrast to the qPCR analyses performed previously (see Fig. 31), readouts for Arhgap6 did not show a

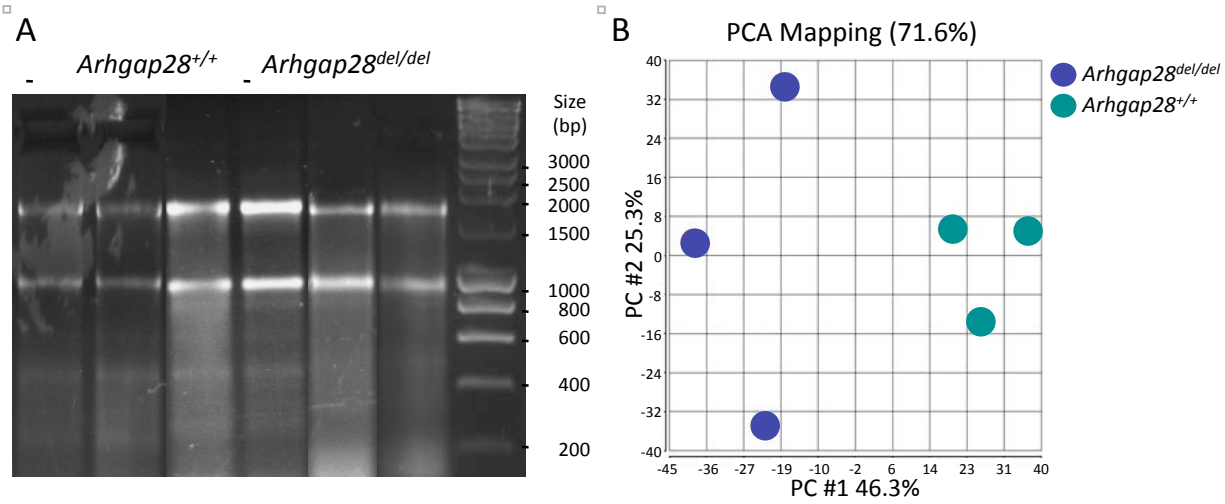

Figure 32
RNA isolated from *Arhgap28*$^{+/+}$ and *Arhgap28*$^{del/del}$ bone tissues for microarray.
(A) Agarose gel showing total RNA isolated from triplicate samples of P0 tibia and fibula tissues from wild type and *Arhgap28*$^{del/del}$ mice. **(B)** PCA mapping of variability between the array samples.

Array[A]	Median Intensity[B]	P call %[C]	% Array outlier[D]	% Single outlier[E]
wt_1	142	63.3	0.353	0.106
wt_2	184	61.2	0.081	0.037
wt_3	180	60.15	0.184	0.072
del_1	137	61.7	0.339	0.091
del_2	143	61.6	0.306	0.100
del_3	139	63.4	0.554	0.158

Table 8
dChip analysis of microarray data sets.
(A) Triplicate samples of RNA from tibia and fibula of P0 *Arhgap28*$^{+/+}$ (wt) and *Arhgap28*$^{del/del}$ (del) mice indicated by the number at the end of each array name. **(B)** Median intensity of microarray chip for each triplicate of each experimental group. **(C)** Present (P) call percentage indicates the percentage of total probe sets detected. **(D)** Array outlier percentage indicates the percentage of probe sets that have outliers in the average readout profile of each probe within a probe set. **(E)** Percentage single outlier indicates the percentage of probes that do not have the same intensity pattern of other probes within the probe set.

Gene	Gene symbol	Wild type	*Arhgap28*$^{del/del}$	Fold change	*q* value
RhoGAP genes					
Arhgap28	Arhgap28	271.7	110.3	-2.5	0.037
		82.5	76.5	-1.1	0.345
		67.1	64.2	-1.0	0.466
Arhgap6	Arhgap6	62.2	62.1	-1.0	0.656
		271.4	275.8	1.0	0.607
		20.2	24.7	1.2	0.257
Arhgap18	Arhgap18	488.6	397.5	-1.2	0.106
		82.2	73.2	-1.1	0.356
Deleted in liver cancer 1	DLC1	48.6	52.3	1.1	0.413
Racgap1	Racgap1	7.8	8.3	1.1	0.439
		751.7	890.4	1.2	0.194
		414.0	511.0	1.2	0.123
Rho GTPases genes					
RhoA	RhoA	5112.5	5060.3	-1.0	0.627
		4777.4	4752.9	-1.0	0.643
		12.9	16.3	1.3	0.099
Rac1	Rac1	3672.1	3349.2	-1.1	0.254
		3591.8	3611.5	1.0	0.645
		14.5	18.0	1.2	0.085
Cdc42	Cdc42	239.8	190.0	-1.3	0.197
		4229.0	3745.1	-1.1	0.191
		3386.3	3059.5	-1.1	0.352
		8834.9	8114.0	-1.1	0.270
RhoQ	RhoQ	2126.4	2001.0	-1.1	0.520
actin genes					
alpha-skeletal actin	Acta1	334.1	94.0	-3.6	0.015
alpha-cardiac-actin	Actc1	687.1	223.8	-3.1	0.046
bone collagen genes					
collagen, type I, alpha 1	Col1a1	10217.8	10997.6	1.1	0.413
		10473.8	11427.3	1.1	0.528
collagen, type I, alpha 2	Coll1a2	321.6	767.0	2.4	0.163
		23205.8	24471.2	1.1	0.422
		19122.7	1024.8	1.1	0.444
collagen, type X, alpha 1	Col10a1	1917.6	1024.8	-1.9	0.056

Table 9
Expression of genes of interest in *Arhgap28*$^{del/del}$ bone tissues.
Comparison of gene expression in wild type and *Arhgap28*$^{del/del}$ bone tissues. Mean intensities from hybridisation of triplicate samples to probe set(s) for the genes listed.

differential expression (with a fold change ≥ ±2) in *Arhgap28*$^{del/del}$ bone (see Table 9). Expression of the RhoGAPs (Arhgap18, DLC1 and Racgap1) and Rho GTPases (RhoA, Rac1, Cdc42 and RhoQ) also showed no differential expression in *Arhgap28*$^{del/del}$ bone (see Table 9). The discrepancy between the microarray and the qPCR analyses could be because qPCR is a more quantitative and sensitive method of detecting gene expression. Interestingly, the actin genes detected by this microarray study, ACTA1 and ACTC1, were both downregulated by ~3-fold in the bone tissue of *Arhgap28*$^{del/del}$ mice (see Table 9).

DAVID online tool was used to perform gene ontology analyses on probe sets showing a differential expression ≥ 2-fold (as described in Chapter 3). After filtering the data, 57 probe sets detected genes that were downregulated in the mutant samples and 306 probe sets detected genes that were upregulated in the mutant samples. DAVID identified 10 functional annotation clusters in the genes that were downregulated. The top 3 annotation clusters and the genes that are over-represented in these clusters are listed in Table 10. All three clusters contained genes indicative of a cartilage ECM, for example, COL2A1, COL9A1, hyaluronan and proteoglycan link protein 1 (HAPLN1), matrillin 1 (MATN1) and MATN3, and some genes that are linked to negatively regulating bone mass, angiotensin II receptor, type 2 (AGTR2) and a transmembrane protein called delta-like 1 homolog (DLK1).

For genes that were upregulated in mutant bone tissue, 65 annotation clusters were identified and the top 3 clusters are listed in Table 11. The genes that were over-represented in the first cluster were genes involved in targeting proteins for ubiquitination. For example, this cluster contained 13 E3 ubiquitin protein ligases,

Cluster components[A]	*p* value[B]	Matched genes[C]	Gene names (if annotated) of corresponding probe IDs in the GO list[D]
Annotation cluster 1, Enrichment score 6.72			
SP_PIR_KEYWORDS secreted	4.13E-11	21	Egfl6, Hapln1, Mia1, Sfrp4, Ccl6, Col2a1, Lect1, Ptn, Matn3, Ecrg4, Matn3, Hapln1, Ccl12, Comp, C1qtnf3, Angptl1, Hapln1, Nts, Mfap5, Hapln1, Epyc, Ecrg4, Mmrn1, Cma1, Col9a1, Cxcl14
GO:0005576~ extracellular region	6.53E-10	22	Egfl6, Hapln1, Mia1, Sfrp4, Ccl6, Col2a1, Lect1, Ptn, Matn3, Ecrg4, Hapln1, Matn3, Ccl12, Comp, C1qtnf3, Angptl1, Hapln1, Nts, Mfap5, Matn1, Hapln1, Epyc, Ecrg4, Mmrn1, Cma1, Col9a1, Cxcl14
SP_PIR_KEYWORDS signal	1.06E-7	24	Egfl6, Mia1, Sfrp4, Ccl6, Col2a1, Snorc, Dlk1, Ptn, Matn3, Ecrg4, Matn3, Ccl12, Comp, C1qtnf3, Cd300ld, Angptl1, Nts, Mfap5, Matn1, Cpa3, Epyc, Ecrg4, Mmrn1, Cma1, Col9a1, Cxcl14
GO:0044421~ extracellular region part	1.57E-7	14	Hapln1, Hapln1, Angptl1, Egfl6, Dlk1, Mfap5, Matn1, Col2a1, Hapln1, Epyc, Ptn, Matn3, Hapln1, Matn3, Col9a1, Ccl12, Cxcl14, Comp
UP_SEQ_FEATURE signal peptide	7.64E-7	24	Egfl6, Mia1, Sfrp4, Ccl6, Col2a1, Snorc, Dlk1, Ptn, Matn3, Ecrg4, Matn3, Ccl12, Comp, C1qtnf3, Cd300ld, Angptl1, Nts, Mfap5, Matn1, Cpa3, Epyc, Ecrg4, Mmrn1, Cma1, Col9a1, Cxcl14
UP_SEQ_FEATURE disufide bond	1.86E-6	21	Egfl6, Hapln1, Mia1, Sfrp4, Ccl6, Lect1, Dlk1, Ptn, Matn3, Matn3, Hapln1, Ccl12, Comp, Agtr2, Cd300ld, Angptl1, Hapln1, Matn1, Cpa3, Hapln1, Epyc, Mmrn1, Cma1, Col9a1, Cxcl14
Annotation cluster 2, Enrichment score 3.78			
GO:0005578~ proteinaceous ECM	1.48E-7	10	Egfl6, Hapln1, Hapln1, Mfap5, Matn1, Col2a1, Hapln1, Epyc, Ptn, Matn3, Matn4, Hapln1, Col9a1, Comp
GO:0031012~ extracellular matrix	2.07E-7	10	Egfl6, Hapln1, Hapln1, Mfap5, Matn1, Col2a1, Hapln1, Epyc, Ptn, Matn3, Matn4, Hapln1, Col9a1, Comp
SP_PIR_KEYWORDS extracellular matrix	1.48E-5	7	Hapln1, Hapln1, Egfl6, Hapln1, Mfap5, Col9a1, Comp, Col2a1, Hapln1, Epyc
GO:0007155~ cell adhesion	7.13E-3	6	Hapln1, Hapln1, Egfl6, Mia1, Hapln1, Col9a1, Comp, Col2a1, Hapln1
GO:0022610~ biological adhesion	7.19E-3	6	Hapln1, Hapln1, Egfl6, Mia1, Hapln1, Col9a1, Comp, Col2a1, Hapln1
Annotation cluster 3, Enrichment score 2.24			
SP_PIR_KEYWORDS egf-like domain	2.32E-4	6	Egfl6, Matn3, Mmrn1, Comp, Matn1, Dlk1, Matn3

Table 10

Top 3 annotation clusters of genes downregulated in *Arhgap28*$^{del/del}$ bone.

Annotation cluster analysis of probe sets detecting a significant fold change greater than -2 from wild type to *Arhgap28*$^{del/del}$ produced 10 clusters. The top 3 annotation clusters with the highest enrichment score are listed here. **(A)** The top gene ontology components of the cluster. **(B)** The statistical significance of this grouping where the lower the score the more unlikely this clustering is due to chance. **(C)** The number of probe sets that recognise genes contributing to the GO term. **(D)** List of gene names of the Affymetrix Mouse Genome 430 2.0 array probe IDs.

including membrane-associated ring finger (C_3HC_4) 3 (MARCH3), MARCH5, MYC-binding protein 2 (MYBP2); 3 peptidases; and a gene, PSMD14, which encodes a regulatory subunit of 26S proteasome (see Table 11 for full list of genes). The second cluster contained genes that promote actin polymerisation, including platelet-activating factor acetyl-hydrolase 1b (PAFAH1B1), tropomodulin 1 (TMOD1) and Diap3 (also known as mDia2); actin nucleation (Spire1); and genes involved in linking the actin cytoskeleton to the plasma membrane, including utrophin (UTRN) and spectrin (SPNA1). The third cluster of over-represented genes that were upregulated in *Arhgap28*$^{del/del}$ bone tissue contained zinc finger proteins, which bind DNA or RNA. To summarise, these GO analyses data show that loss of Arhgap28-mediated RhoA signalling causes (i) downregulation of cartilage ECM genes; (ii) upregulation in genes involved in targeting proteins for degradation by ubiquitination; and (iii) upregulation of genes involved in anchorage of the actin cytoskeleton to the plasma membrane. Whether or not these effects are linked will require further investigation.

5.3 Discussion

The results show that loss of Arhgap28 did not appear to affect embryonic development, the formation of a mechanically strong tendon tissue or actin reorganisation in primary tendon cells. However, this lack of phenotype could be due to compensation in RhoGAP activity resulting from upregulation in Arhgap6 expression, which suggests a new Arhgap28 and Arhgap6 co-regulation of RhoA signalling in tissues. The results showed that expression of Arhgap28 was activated in bone tissues before birth. Microarray analysis on bone tissues from P0 wild type and *Arhgap28*$^{del/del}$ mice showed that in Arhgap28-null bone tissues, there was a downregulation of genes encoding cartilage ECM molecules, an upregulation of

Cluster components[A]	*p* value[B]	Matched genes[C]	Gene names (if annotated) of corresponding probe IDs in the GO list[D]
Annotation cluster 1, Enrichment score 5.02			
SP_PIR_KEYWORDS ubl conjugation pathway	1.47E-6	19	March3, Cblb, Herc4, Mycbp2, Ranbp2, March3, Rad18, Fbxl7, Mkrn1, Spopl, Usp7, March5, Phr1, Hip1, Fbxo30, Hace1, March3, Ube2o, Mycbp2, Dtl, Huwe1, Mkrn1, Psmd14, Usp25, Herc1
GO:0030163~ protein catabolic process	1.64E-6	21	March3, Cblb, Herc4, Mycbp2, Ranbp2, March3, Rad18, Fbxl7, Mkrn1, Spopl, Usp7, March5, Phr1, Hip1, Fbxo30, Usp32, Hace1, March3, Ybey, Usp32, Btrc, Ube2o, Mycbp2, Dtl, Ttll3, Huwe1, Mkrn1, Psmd14, Usp25, Herc1
GO:0019941~ modification-dependent protein catabolic process	1.72E-6	20	March3, Cblb, Herc4, Mycbp2, Ranbp2, March3, Rad18, Fbxl7, Mkrn1, Spopl, Usp7, March5, Phr1, Hip1, Fbxo30, Usp32, Hace1, March3, Ybey, Usp32, Ube2o, Mycbp2, Dtl, Ttll3, Huwe1, Mkrn1, Psmd14, Usp25, Herc1
GO:0009057~ macromolecule catabolic process	5.25E-6	22	March3, Cblb, Herc4, Mycbp2, Ranbp2, March3, Rad18, Fbxl7, Mkrn1, Spopl, Usp7, March5, Phr1, Pan3, Hip1, Fbxo30, Usp32, Hace1, March3, Ybey, Usp32, Btrc, Ube2o, Mycbp2, Dtl, Ttll3, Huwe1, Mkrn1, Psmd14, Usp25, Herc1
SP_PIR_KEYWORDS ligase	6.21E-6	11	Hace1, March3, Cblb, March3, Herc4, Mycbp2, Btrc, March3, Rad18, Ube2o, Mkrn1, Mycbp2, Huwe1, Mkrn1, March5, Phr1, Hip1
GO:0006508~ proteolysis	2.91E-3	22	Cblb, March3, Herc4, Mycbp2, Ranbp2, March3, Rad18, Fbxl7, Mkrn1, Spopl, Usp7, March5, Phr1, Hip1, Fbxo30, Usp32, Hace1, March3, Ybey, Usp32, Ube2o, Mycbp2, Dtl, Ttll3, Huwe1, Mkrn1, Psmd14, Kel, Metap2, Usp25, Herc1
Annotation cluster 2, Enrichment score 3.38			
GO:0003779~ actin binding	1.03E-4	13	Myo1D, Spna1, Myo1D, Epb4.1, Spna1, Spire1, Spire1, Utrn, Fhdc1, Trpm7, Tmod1, Mtss1, Epb4.9, Epb4.1, Slc4a1, Epb4.1, Diap3, Add1, Fhdc1
GO:0030036~ actin cytoskeleton organization	3.71E-4	9	Myo1D, Pafah1b1, Trpm7, Rictor, Fhdc1, Tmod1, Mtss1, Epb4.1, Sorbs1, Epb4.1, Sorbs1, Diap3, Fhdc1
GO:0007010~ cytoskeleton organization	7.02E-4	12	Myo1D, Pafah1b1, Stradb Trpm7, Rictor, Fhdc1, Tmod1, Mtss1, Epb4.9, Epb4.1, Sorbs1, Epb4.1, Sorbs1, Diap3, Cenpe, Fhdc1
GO:0008092~ cytoskeletal protein binding	8.28E-4	14	Myo1D, Spna1, Myo1D, Epb4.1, Pafah1b1, Spna1, Spire1, Spire1, Utrn, Fhdc1, Trpm7, Tmod1, Mtss1, Epb4.9, Epb4.1, Slc4a1, Epb4.1, Diap3, Fhdc1, Add1
Annotation cluster 3, Enrichment score 3.15			
UP_SEQ_FEATURE zinc finger region:RanBP2-type	1.09E-2	3	Rbm5, Neil3, Fus

Table 11

Top 3 annotation clusters of genes upregulated in *Arhgap28*$^{del/del}$ bone.

Annotation cluster analysis of probe sets detecting a significant fold change greater than 2 from wild type to *Arhgap28*$^{del/del}$ produced 65 clusters. The top 3 annotation clusters with the highest enrichment score are listed here. **(A)** The top gene ontology components of the cluster. **(B)** The statistical significance of this grouping where the lower the score the more unlikely this clustering is due to chance. **(C)** The number of probe sets that recognise genes contributing to the GO term. **(D)** List of gene names of the Affymetrix Mouse Genome 430 2.0 array probe IDs.

molecules involved in ubiquitination and molecules involved in stabilising actin polymerisation and anchorage to the plasma membrane. These new findings reveal possible insights in the critical regulation of RhoA signalling during tissue development.

To knockout Arhgap28, a mouse model based on gene trapping that is designed to target the disruption of the Arhgap28 gene was investigated. However, results from RNA analysis suggested that the reporter gene was not spliced to the targeted exon, which meant that this approach was not able to disrupt the expression of the endogenous Arhgap28 transcript. Cross breeding the *Arhgap28*^{gt} mouse and a mouse expressing *Cre* recombinase resulted in the *Arhgap28*^{del} mouse. RNA analysis confirmed that Arhgap28 transcript lacking exons 7-9 was expressed in the *Arhgap28*^{del} mouse. Sequencing this transcript confirmed that a shift in the reading frame so that if it were translated, the protein would lack the RhoGAP domain (see Appendix 6).

Despite the lack of expression of Arhgap28 containing the RhoGAP domain in *Arhgap28*$^{del/del}$ embryos, the mice appear to develop normally. Examination of tendon tissue by TEM and mechanical testing also showed that tendon development was not affected by loss of Arhgap28 function. Although the previous chapter showed that overexpression of Arhgap28 was able to disrupt actin stress fibres, no obvious changes in actin reorganisation was observed in primary tendon cells lacking Arhgap28. Data from Chapter 4 showed that Arhgap6 was also upregulated during the assembly of a tensioned tendon matrix. Knockout of Arhgap6 does not cause abnormalities in mice (Prakash *et al.*, 2000). Due to the large family of mammalian RhoGAPs (discussed in the Introduction; see Fig. 9), it was predicted that Arhgap28 deficiency might be compensated for by functional redundancy between Arhgap28 and other RhoGAPs. To

this end, qPCR analysis performed on wild type and *Arhgap28*$^{del/del}$ bone tissues, because Arhgap28 transcription was prominently activated in this tissue just before birth. Of all the RhoGAPs examined, compensatory upregulation was only observed in the expression of Arhgap6. It was surprising that Arhgap18 was not upregulated in *Arhga28*$^{del/del}$ bone tissues because Arhgap6 and Arhgap18 have both been shown to negatively regulate RhoA and actin stress fibres (Prakash *et al.*, 2000, Maeda *et al.*, 2011). These results reveal the potential of a novel co-regulatory mechanism for RhoA signalling and actin stress fibres by Arhgap6 and Arhgap28.

RhoA expression detected by qPCR was also significantly upregulated in bone tissues of Arhgap28-null mice. RhoA expression is activated by transcription factor Myc (Chan *et al.*, 2010). In the microarray comparison between wild type and *Arhgap28*$^{del/del}$ bone tissues, Myc was not differentially regulated. An alternative explanation is that RhoA mRNA in *Arhgap28*$^{del/del}$ is more stable than in wild type tissues. It has been documented that overexpression of RhoA and other Rho GTPases is linked to cancer and the stability of RhoA transcripts in cancer cells has been shown to be a result of altered polyadenylation signals (Moscow *et al.*, 1994, and for a review on RhoGTPases and cancer, see Ellenbroek and Collard, 2007). These results further suggest why it would be biologically important to have more than one RhoGAP regulating RhoA.

Detection of β-galactosidase activity resulting from *Arhgap28* gene activation in *Arhgap28*$^{gt/gt}$ mice showed that Arhgap28 expression is activated in bone tissue just before birth. Histological analysis of bone showed that β-galactosidase activity was restricted to cells found in the calcified portion of the bone, where type I collagen is expressed. A microarray comparison of the gene expression between bone tissues of

P0 wild type and Arhgap28-null mice did not detect any changes in expression of genes encoding COL1A1 or COL1A2. This was expected because tendon tissue from *Arhga28*$^{del/del}$ mouse did not exhibit any significant differences in mechanical strength, which is largely attributed to the content of type I collagen in the tissue. No changes were observed in expression of RhoGAPs of interest or Rho GTPases.

Interestingly, the microarray study revealed downregulation in ACTA1 and ACTC1 genes in Arhgap28-null bone tissue, which encode isoforms of actin found most abundantly in muscle. Downregulation in both these genes has also been observed in a microarray study of chondrocyte differentiation *in vitro* (James *et al.*, 2005). Downregulation of ACTA1 was observed in bone in response to mechanical loading (Mantila Roosa *et al.*, 2011). Together, these data are suggestive of change in the cells of *Arhgap28*$^{del/del}$ bone tissues. Gene ontology analysis revealed an enrichment of genes that encode ECM molecules associated with a cartilage tissue (including COL2A1, COL9A1, MATN3 and COMP) were downregulated in Arhgap28-null bone tissues. However, because Arhgap28 expression was not localised to cartilage, the downregulation of these genes might be an indicator of a bone ECM phenotype. Mutations in these genes are associated with bone dysplasia (for reviews, see Francomano *et al.*, 1996, Briggs and Chapman, 2002, Jackson *et al.*, 2012).

As a preliminary analysis, litters from cross breeding *Arhgap28*$^{+/del}$ mice were examined by x-ray at P7 (see Fig. 33A). The lengths of the tibia and femur were measured (from a total 12 pups, in 3 litters). No significant differences were found between the bone lengths of heterozygous and wild type mice (see Fig. 33B). However, the *Arhgap28*$^{del/del}$ mouse examined had tibias that were 15% shorter, and femurs that

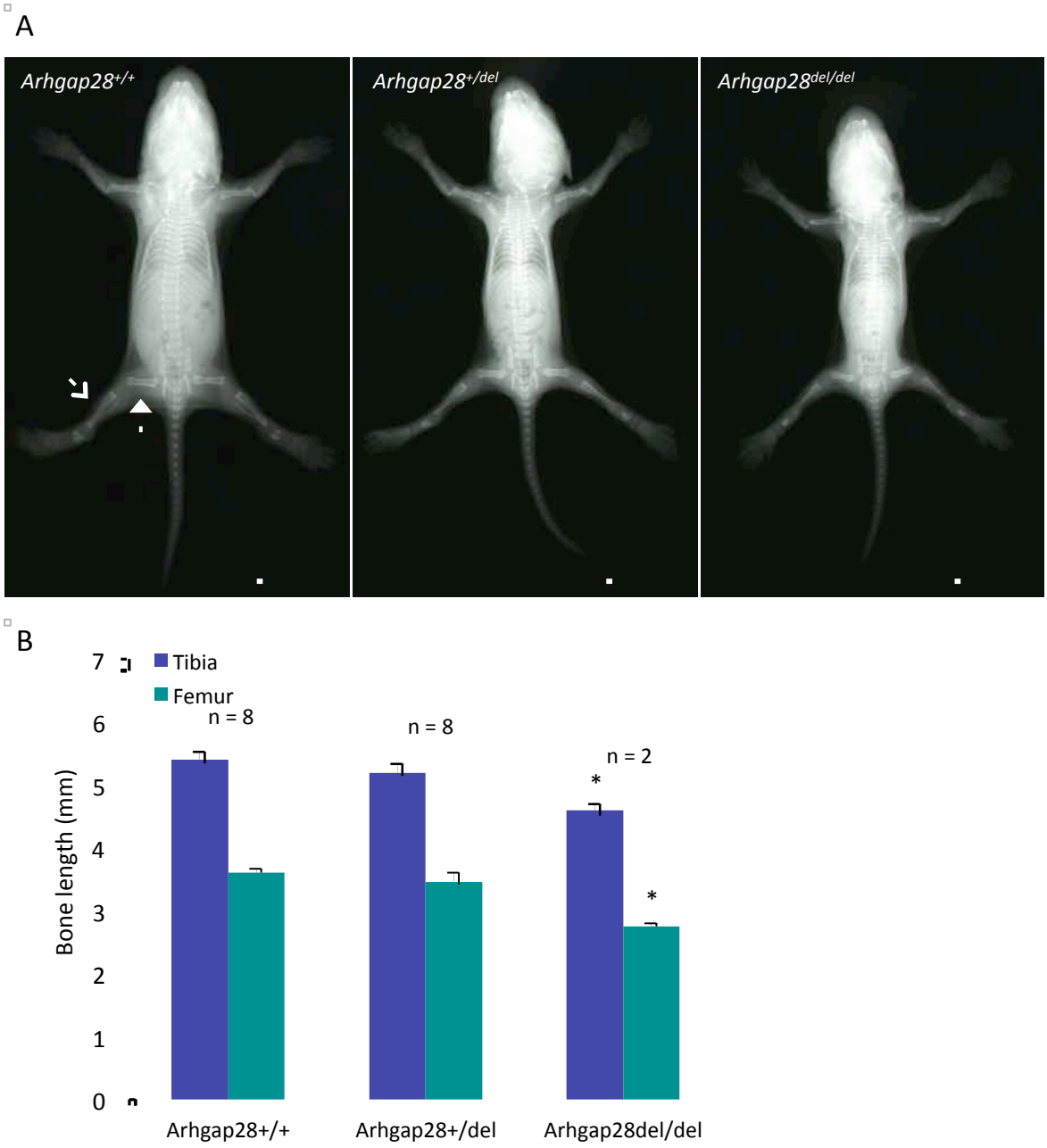

Figure 33
Preliminary analysis of bone length of the *Arhgap28*$^{del/del}$ mouse.
(A) Representative image of x-rays of wild type (n = 4), *Arhgap28*$^{+/del}$ (n = 4) and *Arhgap28*$^{del/del}$ (n = 1) P4 mice (from a total of 12 pups, in 3 litters). Bars = 10 mm. Open arrow points to the tibia and closed arrow points to the femur. **(B)** Length of tibia and femur measured from the x-ray images. * indicates significant differences found when compared to wild type, $p < 0.05$. n indicates the number of bones measured.

were 20% shorter than the wild type bones (Fig. 33B). Although a more extensive examination of more mice is required, together with the microarray data, this preliminary finding suggests that a bone length phenotype can be expected in the Arhgap28-null mouse.

Intriguingly, bone tissues from *Arhgap28*$^{del/del}$ mice show an upregulation of genes involved in ubiquitination and actin reorganisation compared to wild type. Most of the genes enriched in the top cluster were E3 ubiquitin ligases, which mediate the specificity of the ubiquitination pathway (reviewed by Deshaies and Joazeiro, 2009). The target for many of these E3 ligases is unknown. The genes that stand out include HACE1, which catalyses the ubiquitination of Rac1 (Torrino *et al.*, 2011), MYCBP2, which can bind Myc (Guo *et al.*, 1998) but whether or not it is inhibitory or enhancing for RhoA transcription is unknown. The second cluster contained genes that bind to actin for polymerisation, stabilisation and linkage to the plasma membrane. The upregulation of these genes may be a response to the altered RhoA signalling in Arhgap28-deficient bone tissue.

In summary, Arhgap28 is a RhoGAP dispensable for embryonic development, which might be due to compensatory upregulation of Arhgap6 expression. Arhgap28 expression is localised to bone tissues and loss of Arhgap28 causes a downregulation in genes that are linked to bone dysplasia. Therefore, it is likely that Arhgap28-null mice have a bone phenotype. In future work, it will be interesting to explore if Arhgap28 and Arhgap6 co-regulate RhoA signalling, and if a double knockout mutant produces a tendon phenotype.

CHAPTER 6

CONCLUDING REMARKS

6. Concluding Remarks

The mechanical stiffness of musculoskeletal tissues is directly related to the organisation of collagen fibrils in the ECM. For example, the strongest tensile tissues such as tendon and ligament have collagen fibrils arranged in strict parallel register, which presumably is the best organisation to resist uniaxial force. As another example, skin is able to resist planar forces because the collagen fibrils in the dermis are arranged in a lattice weave. Conversely, tissues with the least tensile strength, for example vitreous humour, have disorganised collagen fibrils. Furthermore, the collagen fibrils are pre-stressed by cells to ensure that tissues can respond directly to applied forces. It is poorly understood how the tissue-specific arrangement and pre-stressing of collagen fibrils is achieved.

In previous work done by Canty and colleagues (2004, 2006), the parallel fibrils in embryonic tendon were shown to be co-aligned with the actin cytoskeleton of the tendon fibroblasts. Building on these observations, this PhD thesis hypothesised that organisation of actin filaments inside the cell leads to the tensioning and alignment of collagen fibrils outside the cell. The work presented in this thesis identified a novel RhoGAP called Arhgap28 that is highly expressed during embryonic tendon tissue morphogenesis. Findings from *in vitro* studies showed that Arhgap28 is responsible for negative regulation of RhoA signalling and assembly of actin stress fibres needed for tensioning the collagen-rich ECM. In a knockout mouse model, Arhgap28 was dispensable for tendon development due to possible compensation from Arhgap6. Furthermore, data from a microarray study suggested that absence of Arhgap28 in bone tissue might lead to a bone growth defect. In conclusion, Arhgap28 is a potential regulator of RhoA-generated stress fibres.

It has been shown that cells respond to stiff/rigid ECM via Rho-activated actin stress fibres (Matthews *et al.*, 2006, Keung *et al.*, 2011, Bordeleau *et al.*, 2012). However, how a cell exerts tension and stiffens the ECM is not well understood. This thesis proposes that it is via the actin cytoskeleton and that its regulation by RhoGAP has a prominent involvement. It is known that overactive RhoA signalling is linked to cancer (for review, see Ellenbroek and Collard, 2007) and loss of RhoGAPs that regulated RhoA, such as DLC1, is also associated with cancer (Kim *et al.*, 2007), further suggesting that RhoA signalling affects cell fate. The data from this thesis suggest that Arhgap28 might play the role of a rheostat in RhoA-mediated actin contraction, acting as a balancer required to control cell fate (for example, cartilage or bone) during tissue formation. This proposed role for Arhgap28 illustrated in the model in Figure 34.

There are a few studies that show that the differentiation of mesenchymal stem cells into an osteogenic lineage can be influenced by Rho/ROCK signalling. Mechanical stimulation by fluid flow induces RhoA/ROCKII-dependent osteogenic differentiation (Arnsdorf *et al.*, 2009), osteogenic differentiation induced by bone-morphogenetic protein is also dependent on ROCK signalling and cellular tension, which positively feeds back onto the BMP-induced signalling (Chen *et al.*, 2011, Wang *et al.*, 2012). Surprisingly, mice expressing a dominant-negative RhoA have a bone sclerotic phenotype, which suggests that lack of RhoA signalling enhances mineralisation (Negishi-Koga *et al.*, 2011). These disagreements linking Rho/ROCK and bone development could be due to need for a balanced signal and crosstalk between Rho/ROCK and growth factors rather an all or nothing response.

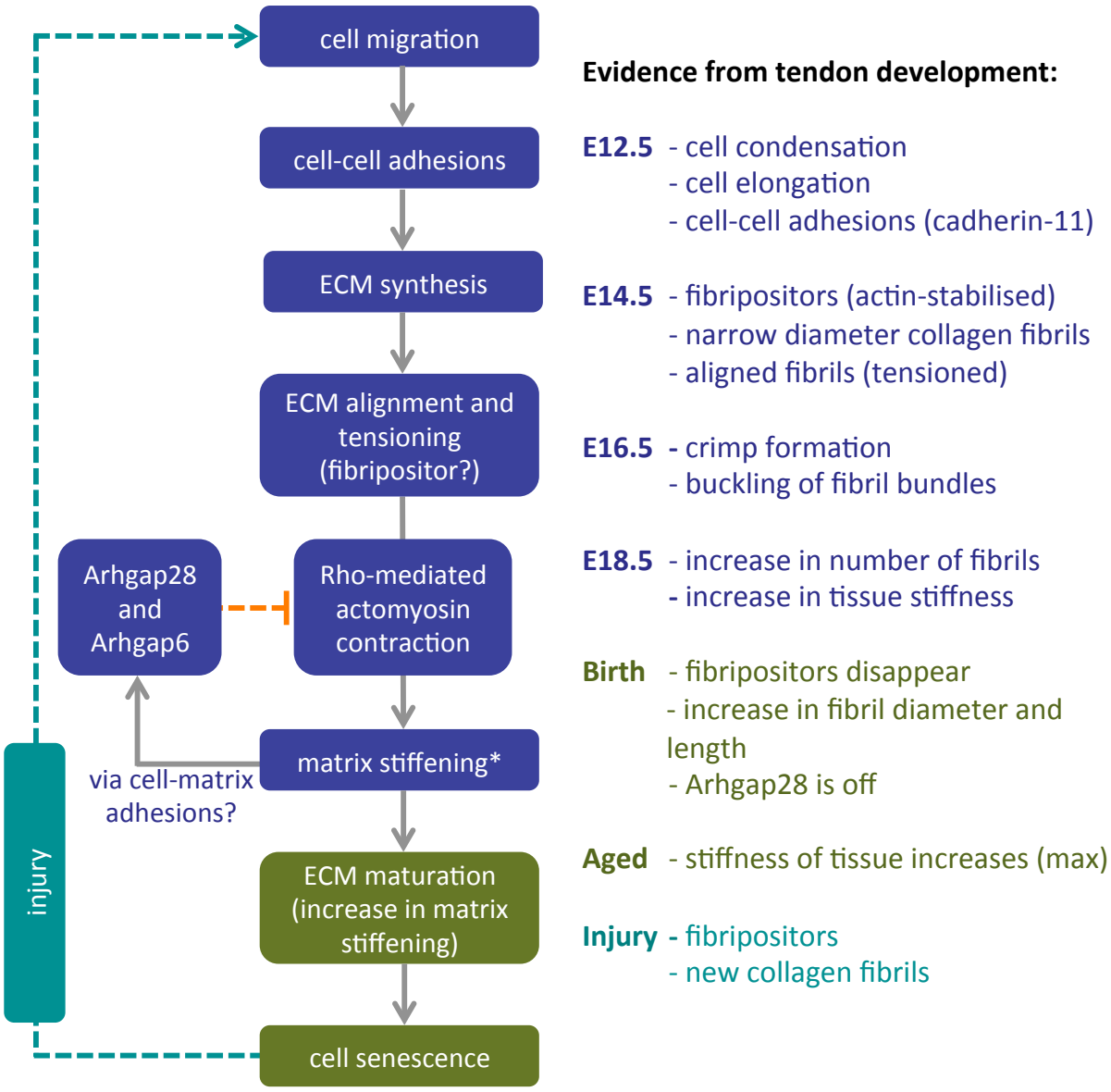

Figure 34
Proposed model of a role for Arhgap28 in regulation of tensional homeostasis in tissue formation. In embryonic tendon, cells use RhoA-regulated stress fibres to generate pulling forces to tension the collagen fibrils in the matrix. Arhgap28 is upregulated during embryonic development and acts as a rheostat to fine tune the tensional homeostasis by inhibiting RhoA activation and actin stress fibres. It is hypothesised that this 'Arhgap28 loop' regulates the stiffening of the embryonic ECM and that mature tendon tissue is regulated by alternative mechanisms as Arhgap28 expression is switched off after birth. *Failure to achieve the optimal tissue tension could lead to abnormal cell differentiation and/or poor organisation of ECM.

Future studies of the role of Arhgap28 in RhoA-mediated tissue stiffening could be focused on investigating the link between tension and Arhgap28 expression. The results in this thesis correlated Arhgap28 expression with tendon constructs under tension. It would be important to test this hypothesis by examining the expression of Arhgap28 in after treatment of tendon constructs with reagents such as blebbistatin or Y27632, which inhibit cell-generated forces, or beta-aminopropionitrile, which reduces cross-links between collagens and thus reduces tissue stiffness/tension. RhoA mediates tail retraction in migratory cells (Worthylake *et al.*, 2001) and live cell imaging combined with the expression of fluorescent-tagged Arhgap28 would help determine its localisation and effect of overexpression during cell migration. An antibody specific to Arhgap28 would enable the localisation in various tissues and allow further studies of Arhgap28 function in different cell types.

Another area of further research into Arhgap28 function would be to determine the signalling cues that activate Arhgap28 during the patterning of ECM. Matrix assembly and detection of the ECM occurs at cell-matrix adhesion sites, therefore it is hypothesised that Arhgap28 is activated by signals downstream of cell-matrix adhesions in similar mechanisms described for other RhoGAPs. For examples, upon activation of integrin β1, p190RhoGAP is activated via tyrosine phosphorylation at the N-terminus by Src (Roof *et al.* 1998), and more recently, the identification of protein-protein interaction domains within DLC1 suggest direction interaction between DLC1 and cell-matrix adhesion proteins tensin, talin and focal adhesion kinase (Cao *et al.*, 2012, Li *et al.*, 2011).

The most recent results from the *Arhgap28*^{del} mouse show compensatory upregulation in Arhgap6 expression. Interestingly, the Arhgap6 knockout mouse is also non-lethal and does not have an apparent phenotype (Prakash *et al.*, 2000). This Arhgap6 knockout mouse model provides an opportunity to explore the possibility of a mutual RhoA regulation by Arhgap6 and Arhgap28. These Arhgap6 knockout mice, a generous gift from Professor Igna van den Veyver (Baylor College of Medicine, Houston, TX, USA), are now within the animal facilities at the University of Manchester. The *Arhgap6/Arhgap28* double knockout mice are expected to either have a pronounced phenotype or further compensation by Arhgap18.

The future direction of research aimed at understanding the function of Arhgap28 will be largely influenced by the phenotype of the *Arhgap28* knockout mouse and of the *Arhgap6/Arhgap28* double knockout mouse. If the mice exhibit a short statue, RhoGAP proteins could become new candidates for genes that cause chondrodysplasias. Likewise, if mechanical measurements on the mice show that Arhgap6 and/or Arhgap28 determine tissue stiffness, research could focus on the roles of these RhoA regulators in tissue stiffness, which has been shown to affect cell fate, cancer and tissue morphogenesis (for examples, see Huang and Ingber, 2005, Engler *et al.*, 2006, Goffin *et al.*, 2006, Vargo-Gogola *et al.*, 2006).

REFERENCES

REFERENCES

ABDUL-MANAN, N., AGHAZADEH, B., LIU, G. A., MAJUMDAR, A., OUERFELLI, O., SIMINOVITCH, K. A. & ROSEN, M. K. 1999. Structure of Cdc42 in complex with the GTPase-binding domain of the 'Wiskott-Aldrich syndrome' protein. *Nature,* **399,** 379-83.

ABRAMOFF, M. D., MAGELHAES, P. J. & RAM, S. J. 2004. Image Processing with ImageJ. *Biophotonics Int,* **11,** 36-42.

ADAMS, J. C. & SCHWARTZ, M. A. 2000. Stimulation of fascin spikes by thrombospondin-1 is mediated by the GTPases Rac and Cdc42. *J Cell Biol,* **150,** 807-22.

ANRAKU, M., CAMERON, M. J., WADDELL, T. K., LIU, M., ARENOVICH, T., SATO, M., CYPEL, M., PIERRE, A. F., DE PERROT, M., KELVIN, D. J. & KESHAVJEE, S. 2008. Impact of human donor lung gene expression profiles on survival after lung transplantation: a case-control study. *Am J Transplant,* **8,** 2140-8.

ANSORGE, H. L., ADAMS, S., BIRK, D. E. & SOSLOWSKY, L. J. 2011. Mechanical, compositional, and structural properties of the post-natal mouse Achilles tendon. *Ann Biomed Eng,* **39,** 1904-13.

ARNSDORF, E. J., TUMMALA, P., KWON, R. Y. & JACOBS, C. R. 2009. Mechanically induced osteogenic differentiation - the role of RhoA, ROCKII and cytoskeletal dynamics. *J Cell Sci,* **122,** 546-53.

ARTHUR, W. T. & BURRIDGE, K. 2001. RhoA inactivation by p190RhoGAP regulates cell spreading and migration by promoting membrane protrusion and polarity. *Mol Biol Cell,* **12,** 2711-20.

ASKARI, J. A., BUCKLEY, P. A., MOULD, A. P. & HUMPHRIES, M. J. 2009. Linking integrin conformation to function. *J Cell Sci,* **122,** 165-70.

ASPENSTROM, P., FRANSSON, A. & SARAS, J. 2004. Rho GTPases have diverse effects on the organization of the actin filament system. *Biochem J,* **377,** 327-37.

BARRETT, T., XIAO, B., DODSON, E. J., DODSON, G., LUDBROOK, S. B., NURMAHOMED, K., GAMBLIN, S. J., MUSACCHIO, A., SMERDON, S. J. & ECCLESTON, J. F. 1997. The structure of the GTPase-activating domain from p50rhoGAP. *Nature,* **385,** 458-61.

BAYER, M. L., YEUNG, C. Y., KADLER, K. E., QVORTRUP, K., BAAR, K., SVENSSON, R. B., MAGNUSSON, S. P., KROGSGAARD, M., KOCH, M. & KJAER, M. 2010. The initiation of embryonic-like collagen fibrillogenesis by adult human tendon fibroblasts when cultured under tension. *Biomaterials,* **31,** 4889-97.

BIRK, D. E. & TRELSTAD, R. L. 1985. Fibroblasts create compartments in the extracellular space where collagen polymerizes into fibrils and fibrils associate into bundles. *Ann N Y Acad Sci,* **460,** 258-66.

BIRK, D. E. & TRELSTAD, R. L. 1986. Extracellular compartments in tendon morphogenesis: collagen fibril, bundle, and macroaggregate formation. *J Cell Biol,* **103,** 231-40.

BONEV, B., PISCO, A. & PAPALOPULU, N. 2011. MicroRNA-9 reveals regional diversity of neural progenitors along the anterior-posterior axis. *Dev Cell,* **20,** 19-32.

BORDELEAU, F., MYRAND LAPIERRE, M. E., SHENG, Y. & MARCEAU, N. 2012. Keratin 8/18 regulation of cell stiffness-extracellular matrix interplay through modulation of Rho-mediated actin cytoskeleton dynamics. *PLoS One,* **7,** e38780.

BOS, J. L., REHMANN, H. & WITTINGHOFER, A. 2007. GEFs and GAPs: critical elements in the control of small G proteins. *Cell,* **129,** 865-77.

BRIGGS, M. D. & CHAPMAN, K. L. 2002. Pseudoachondroplasia and multiple epiphyseal dysplasia: mutation review, molecular interactions, and genotype to phenotype correlations. *Hum Mutat,* **19,** 465-78.

BURRIDGE, K. & CHRZANOWSKA-WODNICKA, M. 1996. Focal adhesions, contractility, and signaling. *Annu Rev Cell Dev Biol,* **12,** 463-518.

BUSTOS, R. I., FORGET, M. A., SETTLEMAN, J. E. & HANSEN, S. H. 2008. Coordination of Rho and Rac GTPase function via p190B RhoGAP. *Curr Biol,* **18,** 1606-11.

CANTY, E. G., LU, Y., MEADOWS, R. S., SHAW, M. K., HOLMES, D. F. & KADLER, K. E. 2004. Coalignment of plasma membrane channels and protrusions (fibripositors) specifies the parallelism of tendon. *J Cell Biol,* **165,** 553-63.

CANTY, E. G., STARBORG, T., LU, Y., HUMPHRIES, S. M., HOLMES, D. F., MEADOWS, R. S., HUFFMAN, A., O'TOOLE, E. T. & KADLER, K. E. 2006. Actin filaments are required for fibripositor-mediated collagen fibril alignment in tendon. *J Biol Chem,* **281,** 38592-8.

CAO, X., VOSS, C., ZHAO, B., KANEKO, T. & LI, S. S. 2012. Differential regulation of the activity of deleted in liver cancer 1 (DLC1) by tensins controls cell migration and transformation. *Proc Natl Acad Sci U S A,* **109,** 1455-60.

CHAN, C. H., LEE, S. W., LI, C. F., WANG, J., YANG, W. L., WU, C. Y., WU, J., NAKAYAMA, K. I., KANG, H. Y., HUANG, H. Y., HUNG, M. C., PANDOLFI, P. P. & LIN, H. K. 2010. Deciphering the transcriptional complex critical for RhoA gene expression and cancer metastasis. *Nat Cell Biol,* **12,** 457-67.

CHAN, D., DELBES, G., LANDRY, M., ROBAIRE, B. & TRASLER, J. M. 2012. Epigenetic alterations in sperm DNA associated with testicular cancer treatment. *Toxicol Sci,* **125,** 532-43.

CHANG, F. & PETER, M. 2002. Formins set the record straight. *Science,* **297,** 531-2.

CHEN, Z., WANG, X., SHAO, Y., SHI, D., CHEN, T., CUI, D. & JIANG, X. 2011. Synthetic osteogenic growth peptide promotes differentiation of human bone marrow mesenchymal stem cells to osteoblasts via RhoA/ROCK pathway. *Mol Cell Biochem,* **358,** 221-7.

CHING, Y. P., WONG, C. M., CHAN, S. F., LEUNG, T. H., NG, D. C., JIN, D. Y. & NG, I. O. 2003. Deleted in liver cancer (DLC) 2 encodes a RhoGAP protein with growth suppressor function and is underexpressed in hepatocellular carcinoma. *J Biol Chem,* **278,** 10824-30.

CHOI, C. K., VICENTE-MANZANARES, M., ZARENO, J., WHITMORE, L. A., MOGILNER, A. & HORWITZ, A. R. 2008. Actin and alpha-actinin orchestrate the assembly and maturation of nascent adhesions in a myosin II motor-independent manner. *Nat Cell Biol,* **10,** 1039-50.

CHRZANOWSKA-WODNICKA, M. & BURRIDGE, K. 1996. Rho-stimulated contractility drives the formation of stress fibers and focal adhesions. *J Cell Biol,* **133,** 1403-15.

CLARK, K., HOWE, J. D., PULLAR, C. E., GREEN, J. A., ARTYM, V. V., YAMADA, K. M. & CRITCHLEY, D. R. 2010. Tensin 2 modulates cell contractility in 3D collagen gels through the RhoGAP DLC1. *J Cell Biochem,* **109,** 808-17.

COLEMAN, D. E., BERGHUIS, A. M., LEE, E., LINDER, M. E., GILMAN, A. G. & SPRANG, S. R. 1994. Structures of active conformations of Gi alpha 1 and the mechanism of GTP hydrolysis. *Science,* **265,** 1405-12.

COX, E. A., SASTRY, S. K. & HUTTENLOCHER, A. 2001. Integrin-mediated adhesion regulates cell polarity and membrane protrusion through the Rho family of GTPases. *Mol Biol Cell,* **12,** 265-77.

CUKIERMAN, E., PANKOV, R., STEVENS, D. R. & YAMADA, K. M. 2001. Taking cell-matrix adhesions to the third dimension. *Science,* **294,** 1708-12.

CUKIERMAN, E., PANKOV, R. & YAMADA, K. M. 2002. Cell interactions with three-dimensional matrices. *Curr Opin Cell Biol,* **14,** 633-9.

DAVIS, S., LU, M. L., LO, S. H., LIN, S., BUTLER, J. A., DRUKER, B. J., ROBERTS, T. M., AN, Q. & CHEN, L. B. 1991. Presence of an SH2 domain in the actin-binding protein tensin. *Science,* **252,** 712-5.

DESHAIES, R. J. & JOAZEIRO, C. A. 2009. RING domain E3 ubiquitin ligases. *Ann Rev Biochem,* **78,** 399-434.

DOHERTY, G. J., AHLUND, M. K., HOWES, M. T., MOREN, B., PARTON, R. G., MCMAHON, H. T. & LUNDMARK, R. 2011. The endocytic protein GRAF1 is directed to cell-matrix adhesion sites and regulates cell spreading. *Mol Biol Cell,* **22,** 4380-9.

DURKIN, M. E., AVNER, M. R., HUH, C. G., YUAN, B. Z., THORGEIRSSON, S. S. & POPESCU, N. C. 2005. DLC-1, a Rho GTPase-activating protein with tumor suppressor function, is essential for embryonic development. *FEBS Lett,* **579,** 1191-6.

DURKIN, M. E., ULLMANNOVA, V., GUAN, M. & POPESCU, N. C. 2007. Deleted in liver cancer 3 (DLC-3), a novel Rho GTPase-activating protein, is downregulated in cancer and inhibits tumor cell growth. *Oncogene,* **26,** 4580-9.

EDWARDS, D. C., SANDERS, L. C., BOKOCH, G. M. & GILL, G. N. 1999. Activation of LIM-kinase by Pak1 couples Rac/Cdc42 GTPase signalling to actin cytoskeletal dynamics. *Nat Cell Biol,* **1,** 253-9.

ELLENBROEK, S. I. & COLLARD, J. G. 2007. Rho GTPases: functions and association with cancer. *Clin Exp Metastasis,* **24,** 657-72.

ENGLER, A. J., SEN, S., SWEENEY, H. L. & DISCHER, D. E. 2006. Matrix elasticity directs stem cell lineage specification. *Cell,* **126,** 677-89.

FÈVRE-MONTANGE, M., CHAMPIER, J., DURAND, A., WIERINCKX, A., HONNORAT, J., GUYOTAT, J. & JOUVET, A. 2009. Microarray gene expression profiling in meningiomas: differential expression according to grade or histopathological subtype. *Int J Oncol,* **35,** 1395-407.

FLOYD, H. S., CHEN, L. C., VALLANAT, B. & DREHER, K. 2009. Fine ambient air particulate matter exposure induces molecular alterations associated with vascular disease progression within plaques of atherosclerotic susceptible mice. *Inhal Toxicol,* **21,** 394-403.

FRANCOMANO, C. A., MCINTOSH, I. & WILKIN, D. J. 1996. Bone dysplasias in man: molecular insights. *Curr Opin Genet Dev,* **6,** 301-8.

FURUKAWA, Y., KAWASOE, T., DAIGO, Y., NISHIWAKI, T., ISHIGURO, H., TAKAHASHI, M., KITAYAMA, J. & NAKAMURA, Y. 2001. Isolation of a novel human gene, ARHGAP9, encoding a rho-GTPase activating protein. *Biochem Biophys Res Commun,* **284,** 643-9.

GARCIA-MATA, R., BOULTER, E. & BURRIDGE, K. 2011. The 'invisible hand': regulation of RHO GTPases by RHOGDIs. *Nat Rev Mol Cell Biol,* **12,** 493-504.

GEWURZ, B. E., TOWFIC, F., MAR, J. C., SHINNERS, N. P., TAKASAKI, K., ZHAO, B., CAHIR-MCFARLAND, E. D., QUACKENBUSH, J., XAVIER, R. J. & KIEFF, E. 2012. Genome-wide siRNA screen for mediators of NF-kappaB activation. *Proc Natl Acad Sci U S A,* **109,** 2467-72.

GOFFIN, J. M., PITTET, P., CSUCS, G., LUSSI, J. W., MEISTER, J. J. & HINZ, B. 2006. Focal adhesion size controls tension-dependent recruitment of alpha-smooth muscle actin to stress fibers. *J Cell Biol,* **172,** 259-68.

GREEN, J. A. & YAMADA, K. M. 2007. Three-dimensional microenvironments modulate fibroblast signaling responses. *Adv Drug Deliv Rev,* **59,** 1293-8.

GRINNELL, F., HO, C. H., TAMARIZ, E., LEE, D. J. & SKUTA, G. 2003. Dendritic fibroblasts in three-dimensional collagen matrices. *Mol Biol Cell,* **14,** 384-95.

GROSS, J., HIGHBERGER, J. H. & SCHMITT, F. O. 1952. Some factors involved in the fibrogenesis of collagen *in vitro*. *Proc Soc Exp Biol Med,* **80,** 462-5.

GUEGAN, F., TATIN, F., LESTE-LASSERRE, T., DRUTEL, G., GENOT, E. & MOREAU, V. 2008. p190B RhoGAP regulates endothelial-cell-associated proteolysis through MT1-MMP and MMP2. *J Cell Sci,* **121,** 2054-61.

GUO, Q., XIE, J., DANG, C. V., LIU, E. T. & BISHOP, J. M. 1998. Identification of a large Myc-binding protein that contains RCC1-like repeats. *Proc Natl Acad Sci U S A,* **95,** 9172-7.

HADJ-HAMOU, N. S., LAE, M., ALMEIDA, A., GRANGE, P. D., KIROVA, Y., SASTRE-GARAU, X. & MALFOY, B. 2012. A transcriptome signature of endothelial lymphatic cells coexists with the chronic oxidative stress signature in radiation-induced post-radiotherapy breast angiosarcomas. *Carcinogenesis*.

HARDEN, N., LEE, J., LOH, H. Y., ONG, Y. M., TAN, I., LEUNG, T., MANSER, E. & LIM, L. 1996. A Drosophila homolog of the Rac- and Cdc42-activated serine/threonine kinase PAK is a potential focal adhesion and focal complex protein that colocalizes with dynamic actin structures. *Mol Cell Biol,* **16,** 1896-908.

HASHIMOTO, J. G., FORQUER, M. R., TANCHUCK, M. A., FINN, D. A. & WIREN, K. M. 2011. Importance of genetic background for risk of relapse shown in altered prefrontal cortex gene expression during abstinence following chronic alcohol intoxication. *Neuroscience,* **173,** 57-75.

HEASMAN, S. J. & RIDLEY, A. J. 2008. Mammalian Rho GTPases: new insights into their functions from in vivo studies. *Nat Rev Mol Cell Biol,* **9,** 690-701.

HINZ, B., MASTRANGELO, D., ISELIN, C. E., CHAPONNIER, C. & GABBIANI, G. 2001. Mechanical tension controls granulation tissue contractile activity and myofibroblast differentiation. *Am J Pathol,* **159,** 1009-20.

HIROSE, M., ISHIZAKI, T., WATANABE, N., UEHATA, M., KRANENBURG, O., MOOLENAAR, W. H., MATSUMURA, F., MAEKAWA, M., BITO, H. & NARUMIYA, S. 1998. Molecular dissection of the Rho-associated protein kinase (p160ROCK)-regulated neurite remodeling in neuroblastoma N1E-115 cells. *J Cell Biol,* **141,** 1625-36.

HUANG DA, W., SHERMAN, B. T. & LEMPICKI, R. A. 2009. Systematic and integrative analysis of large gene lists using DAVID bioinformatics resources. *Nature protocols,* **4,** 44-57.

HUANG, S. & INGBER, D. E. 2005. Cell tension, matrix mechanics, and cancer development. *Cancer Cell,* **8,** 175-6.

HUMPHRIES, J. D., WANG, P., STREULI, C., GEIGER, B., HUMPHRIES, M. J. & BALLESTREM, C. 2007. Vinculin controls focal adhesion formation by direct interactions with talin and actin. *J Cell Biol,* **179,** 1043-57.

HUMPHRIES, S. M., LU, Y., CANTY, E. G. & KADLER, K. E. 2008. Active negative control of collagen fibrillogenesis in vivo. Intracellular cleavage of the type I procollagen propeptides in tendon fibroblasts without intracellular fibrils. *J Biol Chem,* **283,** 12129-35.

I, S. T., NIE, Z., STEWART, A., NAJDOVSKA, M., HALL, N. E., HE, H., RANDAZZO, P. A. & LOCK, P. 2004. ARAP3 is transiently tyrosine phosphorylated in cells attaching to fibronectin and inhibits cell spreading in a RhoGAP-dependent manner. *J Cell Sci,* **117,** 6071-84.

IRIZARRY, R. A., BOLSTAD, B. M., COLLIN, F., COPE, L. M., HOBBS, B. & SPEED, T. P. 2003. Summaries of Affymetrix GeneChip probe level data. *Nucleic Acids Res,* **31,** e15.

ISHIZAKI, T., NAITO, M., FUJISAWA, K., MAEKAWA, M., WATANABE, N., SAITO, Y. & NARUMIYA, S. 1997. p160ROCK, a Rho-associated coiled-coil forming protein kinase, works downstream of Rho and induces focal adhesions. *FEBS Lett,* **404,** 118-24.

JACKSON, D. S. & FESSLER, J. H. 1955. Isolation and properties of a collagen soluble in salt solution at neutral pH. *Nature,* **176,** 69-70.

JACKSON, G. C., MITTAZ-CRETTOL, L., TAYLOR, J. A., MORTIER, G. R., SPRANGER, J., ZABEL, B., LE MERRER, M., CORMIER-DAIRE, V., HALL, C. M., OFFIAH, A., WRIGHT, M. J., SAVARIRAYAN, R., NISHIMURA, G., RAMSDEN, S. C., ELLES, R., BONAFE, L., SUPERTI-FURGA, A., UNGER, S., ZANKL, A. & BRIGGS, M. D. 2012. Pseudoachondroplasia and multiple epiphyseal dysplasia: a 7-year comprehensive analysis of the known disease genes identify novel and recurrent mutations and provides an accurate assessment of their relative contribution. *Hum Mutat,* **33,** 144-57.

JAMES, C. G., APPLETON, C. T., ULICI, V., UNDERHILL, T. M. & BEIER, F. 2005. Microarray analyses of gene expression during chondrocyte differentiation identifies novel regulators of hypertrophy. *Mol Biol Cell,* **16,** 5316-33.

KADLER, K. E., HILL, A. & CANTY-LAIRD, E. G. 2008. Collagen fibrillogenesis: fibronectin, integrins, and minor collagens as organizers and nucleators. *Curr Opin Cell Biol,* **20,** 495-501.

KADLER, K. E., HOLMES, D. F., TROTTER, J. A. & CHAPMAN, J. A. 1996. Collagen fibril formation. *Biochem J,* **316 (Pt 1),** 1-11.

KAIBUCHI, K., KURODA, S. & AMANO, M. 1999. Regulation of the cytoskeleton and cell adhesion by the Rho family GTPases in mammalian cells. *Annu Rev Biochem,* **68,** 459-86.

KALSON, N. S., HOLMES, D. F., KAPACEE, Z., OTERMIN, I., LU, Y., ENNOS, R. A., CANTY-LAIRD, E. G. & KADLER, K. E. 2010. An experimental model for studying the biomechanics of embryonic tendon: Evidence that the development of mechanical properties depends on the actinomyosin machinery. *Matrix Biol,* **29,** 678-89.

KAPACEE, Z., RICHARDSON, S. H., LU, Y., STARBORG, T., HOLMES, D. F., BAAR, K. & KADLER, K. E. 2008. Tension is required for fibripositor formation. *Matrix Biol,* **27,** 371-5.

KAPACEE, Z., YEUNG, C. Y., LU, Y., CRABTREE, D., HOLMES, D. F. & KADLER, K. E. 2010. Synthesis of embryonic tendon-like tissue by human marrow stromal/mesenchymal stem cells requires a three-dimensional environment and transforming growth factor beta3. *Matrix Biol,* **29,** 668-77.

KASHEF, J., KOHLER, A., KURIYAMA, S., ALFANDARI, D., MAYOR, R. & WEDLICH, D. 2009. Cadherin-11 regulates protrusive activity in Xenopus cranial neural crest cells upstream of Trio and the small GTPases. *Genes Dev,* **23,** 1393-8.

KASTELIC, J., GALESKI, A. & BAER, E. 1978. The multicomposite structure of tendon. *Connect Tissue Res,* **6,** 11-23.

KAWAI, K., KIYOTA, M., SEIKE, J., DEKI, Y. & YAGISAWA, H. 2007. START-GAP3/DLC3 is a GAP for RhoA and Cdc42 and is localized in focal adhesions regulating cell morphology. *Biochem Biophys Res Commun,* **364,** 783-9.

KEUNG, A. J., DE JUAN-PARDO, E. M., SCHAFFER, D. V. & KUMAR, S. 2011. Rho GTPases mediate the mechanosensitive lineage commitment of neural stem cells. *Stem Cells,* **29,** 1886-97.

KIM, T. Y., LEE, J. W., KIM, H. P., JONG, H. S., JUNG, M. & BANG, Y. J. 2007. DLC-1, a GTPase-activating protein for Rho, is associated with cell proliferation, morphology, and migration in human hepatocellular carcinoma. *Biochem Biophys Res Commun,* **355,** 72-7.

KNAUS, U. G., WANG, Y., REILLY, A. M., WARNOCK, D. & JACKSON, J. H. 1998. Structural requirements for PAK activation by Rac GTPases. *J Biol Chem,* **273,** 21512-8.

KOLODNEY, M. S. & ELSON, E. L. 1993. Correlation of myosin light chain phosphorylation with isometric contraction of fibroblasts. *J Biol Chem,* **268,** 23850-5.

LAUKAITIS, C. M., WEBB, D. J., DONAIS, K. & HORWITZ, A. F. 2001. Differential dynamics of alpha5 integrin, paxillin, and alpha-actinin during formation and disassembly of adhesions in migrating cells. *J Cell Biol,* **153,** 1427-40.

LI, C. & WONG, W. H. 2001. Model-based analysis of oligonucleotide arrays: expression index computation and outlier detection. *Proc Natl Acad Sci U S A,* **98,** 31-6.

LI, G., DU, X., VASS, W. C., PAPAGEORGE, A. G., LOWY, D. R. & QIAN, X. 2011. Full activity of the deleted in liver cancer 1 (DLC1) tumor suppressor depends on an LD-like motif that binds talin and focal adhesion kinase (FAK). *Proc Natl Acad Sci U S A,* **108,** 17129-34.

LI, S., VAN DEN DIEPSTRATEN, C., D'SOUZA, S. J., CHAN, B. M. & PICKERING, J. G. 2003. Vascular smooth muscle cells orchestrate the assembly of type I collagen via alpha2beta1 integrin, RhoA, and fibronectin polymerization. *Am J Pathol,* **163,** 1045-56.

LI, X., BU, X., LU, B., AVRAHAM, H., FLAVELL, R. A. & LIM, B. 2002. The hematopoiesis-specific GTP-binding protein RhoH is GTPase deficient and modulates activities of other Rho GTPases by an inhibitory function. *Mol Cell Biol,* **22,** 1158-71.

LIPPI, G., STEINERT, J. R., MARCZYLO, E. L., D'ORO, S., FIORE, R., FORSYTHE, I. D., SCHRATT, G., ZOLI, M., NICOTERA, P. & YOUNG, K. W. 2011. Targeting of the Arpc3 actin nucleation factor by miR-29a/b regulates dendritic spine morphology. *J Cell Biol,* **194,** 889-904.

LIVAK, K. J. & SCHMITTGEN, T. D. 2001. Analysis of relative gene expression data using real-time quantitative PCR and the 2(-Delta Delta C(T)) Method. *Methods,* **25,** 402-8.

LO, S. H., JANMEY, P. A., HARTWIG, J. H. & CHEN, L. B. 1994. Interactions of tensin with actin and identification of its three distinct actin-binding domains. *J Cell Biol,* **125,** 1067-75.

MAEDA, M., HASEGAWA, H., HYODO, T., ITO, S., ASANO, E., YUANG, H., FUNASAKA, K., SHIMOKATA, K., HASEGAWA, Y., HAMAGUCHI, M. & SENGA, T. 2011. ARHGAP18, a GTPase-activating protein for RhoA, controls cell shape, spreading, and motility. *Mol Biol Cell,* **22,** 3840-52.

MAEKAWA, M., ISHIZAKI, T., BOKU, S., WATANABE, N., FUJITA, A., IWAMATSU, A., OBINATA, T., OHASHI, K., MIZUNO, K. & NARUMIYA, S. 1999. Signaling from Rho to the actin cytoskeleton through protein kinases ROCK and LIM-kinase. *Science,* **285,** 895-8.

MANTILA ROOSA, S. M., LIU, Y. & TURNER, C. H. 2011. Gene expression patterns in bone following mechanical loading. *J Bone Miner Res,* **26,** 100-12.

MARCHLER-BAUER, A., LU, S., ANDERSON, J. B., CHITSAZ, F., DERBYSHIRE, M. K., DEWEESE-SCOTT, C., FONG, J. H., GEER, L. Y., GEER, R. C., GONZALES, N. R., GWADZ, M., HURWITZ, D. I., JACKSON, J. D., KE, Z., LANCZYCKI, C. J., LU, F., MARCHLER, G. H., MULLOKANDOV, M., OMELCHENKO, M. V., ROBERTSON, C. L., SONG, J. S., THANKI, N., YAMASHITA, R. A., ZHANG, D., ZHANG, N., ZHENG, C. & BRYANT, S. H. 2011. CDD: a Conserved Domain Database for the functional annotation of proteins. *Nucleic Acids Res,* **39,** D225-9.

MATTHEWS, B. D., OVERBY, D. R., MANNIX, R. & INGBER, D. E. 2006. Cellular adaptation to mechanical stress: role of integrins, Rho, cytoskeletal tension and mechanosensitive ion channels. *J Cell Sci,* **119,** 508-18.

MCHENRY, P. R., SEARS, J. C., HERRICK, M. P., CHANG, P., HECKMAN-STODDARD, B. M., RYBARCZYK, M., CHODOSH, L. A., GUNTHER, E. J., HILSENBECK, S. G., ROSEN, J. M. & VARGO-GOGOLA, T. 2010. P190B RhoGAP has pro-tumorigenic functions during MMTV-Neu mammary tumorigenesis and metastasis. *Breast Cancer Res,* **12,** R73.

MIERKE, C. T., KOLLMANNSBERGER, P., ZITTERBART, D. P., DIEZ, G., KOCH, T. M., MARG, S., ZIEGLER, W. H., GOLDMANN, W. H. & FABRY, B. 2010. Vinculin facilitates cell invasion into three-dimensional collagen matrices. *J Biol Chem,* **285,** 13121-30.

MIERKE, C. T., KOLLMANNSBERGER, P., ZITTERBART, D. P., SMITH, J., FABRY, B. & GOLDMANN, W. H. 2008. Mechano-coupling and regulation of contractility by the vinculin tail domain. *Biophys J,* **94,** 661-70.

MIKI, H., YAMAGUCHI, H., SUETSUGU, S. & TAKENAWA, T. 2000. IRSp53 is an essential intermediate between Rac and WAVE in the regulation of membrane ruffling. *Nature,* **408,** 732-5.

MIYAMOTO, S., AKIYAMA, S. K. & YAMADA, K. M. 1995. Synergistic roles for receptor occupancy and aggregation in integrin transmembrane function. *Science,* **267,** 883-85.

MOSCOW, J. A., HE, R., GUDAS, J. M. & COWAN, K. H. 1994. Utilization of multiple polyadenylation signals in the human RHOA protooncogene. *Gene,* **144,** 229-36.

NAKAHARA, H., MUELLER, S. C., NOMIZU, M., YAMADA, Y., YEH, Y. & CHEN, W. T. 1998. Activation of beta1 integrin signaling stimulates tyrosine phosphorylation of p190RhoGAP and membrane-protrusive activities at invadopodia. *J Biol Chem,* **273,** 9-12.

NEGISHI-KOGA, T., SHINOHARA, M., KOMATSU, N., BITO, H., KODAMA, T., FRIEDEL, R. H. & TAKAYANAGI, H. 2011. Suppression of bone formation by osteoclastic expression of semaphorin 4D. *Nat Med,* **17,** 1473-80.

NG, I. O., LIANG, Z. D., CAO, L. & LEE, T. K. 2000. DLC-1 is deleted in primary hepatocellular carcinoma and exerts inhibitory effects on the proliferation of hepatoma cell lines with deleted DLC-1. *Cancer Res,* **60,** 6581-4.

NODA, M., YASUDA-FUKAZAWA, C., MORIISHI, K., KATO, T., OKUDA, T., KUROKAWA, K. & TAKUWA, Y. 1995. Involvement of rho in GTP gamma S-induced enhancement of phosphorylation of 20 kDa myosin light chain in vascular smooth muscle cells: inhibition of phosphatase activity. *FEBS Lett,* **367,** 246-50.

OAKES, P. W., BECKHAM, Y., STRICKER, J. & GARDEL, M. L. 2012. Tension is required but not sufficient for focal adhesion maturation without a stress fiber template. *J Cell Biol,* **196,** 363-74.

OHASHI, T., KIEHART, D. P. & ERICKSON, H. P. 2002. Dual labelling of the fibronectin matrix and actin cytoskeleton with green fluorescent protein. *J Cell Sci,* **115,** 1221-1229.

PANKOV, R., CUKIERMAN, E., KATZ, B. Z., MATSUMOTO, K., LIN, D. C., LIN, S., HAHN, C. & YAMADA, K. M. 2000. Integrin dynamics and matrix assembly: Tensin-dependent translocation of alpha(5)beta(1) integrins promotes early fibronectin fibrillogenesis. *J Cell Biol,* **148,** 1075-90.

PARAMANIK, V. & THAKUR, M. K. 2012. Estrogen receptor beta and its domains interact with casein kinase 2, phosphokinase C, and N-myristoylation sites of mitochondrial and nuclear proteins in mouse brain. *J Biol Chem,* **287,** 22305-16.

PARRY, D. A., BARNES, G. R. & CRAIG, A. S. 1978. A comparison of the size distribution of collagen fibrils in connective tissues as a function of age and a possible relation between fibril size distribution and mechanical properties. *Proc R Soc B,* **203,** 305-21.

PECK, J., DOUGLAS, G. T., WU, C. H. & BURBELO, P. D. 2002. Human RhoGAP domain-containing proteins: structure, function and evolutionary relationships. *FEBS Lett,* **528,** 27-34.

PRADAT, P. F., DUBOURG, O., DE TAPIA, M., DI SCALA, F., DUPUIS, L., LENGLET, T., BRUNETEAU, G., SALACHAS, F., LACOMBLEZ, L., CORVOL, J. C., DEMOUGIN, P., PRIMIG, M., MEININGER, V., LOEFFLER, J. P. & GONZALEZ DE AGUILAR, J. L. 2012. Muscle gene expression is a marker of amyotrophic lateral sclerosis severity. *Neurodegener Dis,* **9,** 38-52.

PRAKASH, S. K., PAYLOR, R., JENNA, S., LAMARCHE-VANE, N., ARMSTRONG, D. L., XU, B., MANCINI, M. A. & ZOGHBI, H. Y. 2000. Functional analysis of ARHGAP6, a novel GTPase-activating protein for RhoA. *Hum Mol Genet,* **9,** 477-88.

RICHARDSON, S. H., STARBORG, T., LU, Y., HUMPHRIES, S. M., MEADOWS, R. S. & KADLER, K. E. 2007. Tendon development requires regulation of cell condensation and cell shape via cadherin-11-mediated cell-cell junctions. *Mol Cell Biol,* **27,** 6218-28.

RIDLEY, A. J. & HALL, A. 1992. The small GTP-binding protein rho regulates the assembly of focal adhesions and actin stress fibers in response to growth factors. *Cell,* **70,** 389-99.

RIDLEY, A. J., SELF, A. J., KASMI, F., PATERSON, H. F., HALL, A., MARSHALL, C. J. & ELLIS, C. 1993. Rho family GTPase activating proteins p190, bcr and rhoGAP show distinct specificities in vitro and in vivo. *EMBO J,* **12,** 5151-60.

RINGNÉR, M. 2008. What is principal component analysis? *Nat Biotechnol,* **26,** 303-4.

RITTINGER, K., WALKER, P. A., ECCLESTON, J. F., NURMAHOMED, K., OWEN, D., LAUE, E., GAMBLIN, S. J. & SMERDON, S. J. 1997a. Crystal structure of a small G protein in complex with the GTPase-activating protein rhoGAP. *Nature,* **388,** 693-7.

RITTINGER, K., WALKER, P. A., ECCLESTON, J. F., SMERDON, S. J. & GAMBLIN, S. J. 1997b. Structure at 1.65 A of RhoA and its GTPase-activating protein in complex with a transition-state analogue. *Nature,* **389,** 758-62.

RIVELINE, D., ZAMIR, E., BALABAN, N. Q., SCHWARZ, U. S., ISHIZAKI, T., NARUMIYA, S., KAM, Z., GEIGER, B. & BERSHADSKY, A. D. 2001. Focal contacts as mechanosensors: externally applied local mechanical force induces growth of focal contacts by an mDia1-dependent and ROCK-independent mechanism. *J Cell Biol,* **153,** 1175-86.

ROBERTS, P. J., MITIN, N., KELLER, P. J., CHENETTE, E. J., MADIGAN, J. P., CURRIN, R. O., COX, A. D., WILSON, O., KIRSCHMEIER, P. & DER, C. J. 2008. Rho Family GTPase modification and dependence on CAAX motif-signaled posttranslational modification. *J Biol Chem,* **283,** 25150-63.

ROOF, R. W., HASKELL, M. D., DUKES, B. D., SHERMAN, N., KINTER, M. & PARSONS, S. J. 1998. Phosphotyrosine (p-Tyr)-dependent and -independent mechanisms of p190 RhoGAP-p120 RasGAP interaction: Tyr 1105 of p190, a substrate for c-Src, is the sole p-Tyr mediator of complex formation. *Mol Cell Biol,* **18,** 7052-63.

ROZEN, S. & SKALETSKY, H. 2000. Primer3 on the WWW for general users and for biologist programmers. *Methods Mol Biol,* **132,** 365-86.

SANDERS, L. C., MATSUMURA, F., BOKOCH, G. M. & DE LANEROLLE, P. 1999. Inhibition of myosin light chain kinase by p21-activated kinase. *Science,* **283,** 2083-5.

SCHILLING, T., KUFFNER, R., KLEIN-HITPASS, L., ZIMMER, R., JAKOB, F. & SCHUTZE, N. 2008. Microarray analyses of transdifferentiated mesenchymal stem cells. *J Cell Biochem,* **103,** 413-33.

SELLS, M. A., KNAUS, U. G., BAGRODIA, S., AMBROSE, D. M., BOKOCH, G. M. & CHERNOFF, J. 1997. Human p21-activated kinase (Pak1) regulates actin organization in mammalian cells. *Curr Biol,* **7,** 202-10.

SOTTILE, J., SHI, F., RUBLYEVSKA, I., CHIANG, H. Y., LUST, J. & CHANDLER, J. 2007. Fibronectin-dependent collagen I deposition modulates the cell response to fibronectin. *Am J Physiol Cell Physiol,* **293,** C1934-46.

STRADAL, T. E., ROTTNER, K., DISANZA, A., CONFALONIERI, S., INNOCENTI, M. & SCITA, G. 2004. Regulation of actin dynamics by WASP and WAVE family proteins. *Trends Cell Biol,* **14,** 303-11.

SYMONS, M., DERRY, J. M., KARLAK, B., JIANG, S., LEMAHIEU, V., MCCORMICK, F., FRANCKE, U. & ABO, A. 1996. Wiskott-Aldrich syndrome protein, a novel effector for the GTPase CDC42Hs, is implicated in actin polymerization. *Cell,* **84,** 723-34.

TAN, J. L., RAVID, S. & SPUDICH, J. A. 1992. Control of nonmuscle myosins by phosphorylation. *Annu Rev Biochem,* **61,** 721-59.

TCHERKEZIAN, J. & LAMARCHE-VANE, N. 2007. Current knowledge of the large RhoGAP family of proteins. *Biol Cell,* **99,** 67-86.

THE ROYAL COLLEGE OF SURGEONS OF ENGLAND 2010. Surgical Research Report 2010-2011.

TORRINO, S., VISVIKIS, O., DOYE, A., BOYER, L., STEFANI, C., MUNRO, P., BERTOGLIO, J., GACON, G., METTOUCHI, A. & LEMICHEZ, E. 2011. The E3 ubiquitin-ligase HACE1 catalyzes the ubiquitylation of active Rac1. *Dev Cell,* **21,** 959-65.

TRELSTAD, R. L. & HAYASHI, K. 1979. Tendon collagen fibrillogenesis: intracellular subassemblies and cell surface changes associated with fibril growth. *Dev Biol,* **71,** 228-42.

VARGO-GOGOLA, T., HECKMAN, B. M., GUNTHER, E. J., CHODOSH, L. A. & ROSEN, J. M. 2006. P190-B Rho GTPase-activating protein overexpression disrupts ductal morphogenesis and induces hyperplastic lesions in the developing mammary gland. *Mol Endocrinol,* **20,** 1391-405.

VELLING, T., RISTELI, J., WENNERBERG, K., MOSHER, D. F. & JOHANSSON, S. 2002. Polymerization of type I and III collagens is dependent on fibronectin and enhanced by integrins alpha11beta1 and alpha2beta1. *J Biol Chem,* **277,** 37377-81.

VETTER, I. R. & WITTINGHOFER, A. 2001. The guanine nucleotide-binding switch in three dimensions. *Science,* **294,** 1299-304.

VIGNJEVIC, D., KOJIMA, S., ARATYN, Y., DANCIU, O., SVITKINA, T. & BORISY, G. G. 2006. Role of fascin in filopodial protrusion. *J Cell Biol,* **174,** 863-75.

WANG, S. M., OOI, L. L. & HUI, K. M. 2011. Upregulation of Rac GTPase-activating protein 1 is significantly associated with the early recurrence of human hepatocellular carcinoma. *Clin Cancer Res,* **17,** 6040-51.

WANG, Y. K., YU, X., COHEN, D. M., WOZNIAK, M. A., YANG, M. T., GAO, L., EYCKMANS, J. & CHEN, C. S. 2012. Bone morphogenetic protein-2-induced signaling and osteogenesis is regulated by cell shape, RhoA/ROCK, and cytoskeletal tension. *Stem Cells Dev,* **21,** 1176-86.

WANSBURY, O., MACKAY, A., KOGATA, N., MITSOPOULOS, C., KENDRICK, H., DAVIDSON, K., RUHRBERG, C., REIS-FILHO, J. S., SMALLEY, M. J., ZVELEBIL, M. & HOWARD, B. A. 2011. Transcriptome analysis of embryonic mammary cells reveals insights into mammary lineage establishment. *Breast Cancer Res,* **13,** R79.

WATANABE, N., MADAULE, P., REID, T., ISHIZAKI, T., WATANABE, G., KAKIZUKA, A., SAITO, Y., NAKAO, K., JOCKUSCH, B. M. & NARUMIYA, S. 1997. p140mDia, a mammalian homolog of Drosophila diaphanous, is a target protein for Rho small GTPase and is a ligand for profilin. *EMBO J,* **16,** 3044-56.

WENNERBERG, K., FORGET, M. A., ELLERBROEK, S. M., ARTHUR, W. T., BURRIDGE, K., SETTLEMAN, J., DER, C. J. & HANSEN, S. H. 2003. Rnd proteins function as RhoA antagonists by activating p190 RhoGAP. *Curr Biol,* **13,** 1106-15.

WENNERBERG, K., ROSSMAN, K. L. & DER, C. J. 2005. The Ras superfamily at a glance. *J Cell Sci,* **118,** 843-6.

WETMORE, B. A., BREES, D. J., SINGH, R., WATKINS, P. B., ANDERSEN, M. E., LOY, J. & THOMAS, R. S. 2010. Quantitative analyses and transcriptomic profiling of circulating messenger RNAs as biomarkers of rat liver injury. *Hepatology,* **51,** 2127-39.

WONG, C. C., WONG, C. M., KO, F. C., CHAN, L. K., CHING, Y. P., YAM, J. W. & NG, I. O. 2008. Deleted in liver cancer 1 (DLC1) negatively regulates Rho/ROCK/MLC pathway in hepatocellular carcinoma. *PLoS One,* **3,** e2779.

WONG, J. K., LUI, Y. H., KAPACEE, Z., KADLER, K. E., FERGUSON, M. W. & MCGROUTHER, D. A. 2009. The cellular biology of flexor tendon adhesion formation: an old problem in a new paradigm. *Am J Pathol,* **175,** 1938-51.

WORTHYLAKE, R. A., LEMOINE, S., WATSON, J. M. & BURRIDGE, K. 2001. RhoA is required for monocyte tail retraction during transendothelial migration. *J Cell Biol,* **154,** 147-60.

WOZNIAK, M. A. & CHEN, C. S. 2009. Mechanotransduction in development: a growing role for contractility. *Nat Rev Mol Cell Biol,* **10,** 34-43.

YAMAZAKI, D., OIKAWA, T. & TAKENAWA, T. 2007. Rac-WAVE-mediated actin reorganization is required for organization and maintenance of cell-cell adhesion. *J Cell Sci,* **120,** 86-100.

YANG, Y. P., CHANG, Y. L., HUANG, P. I., CHIOU, G. Y., TSENG, L. M., CHIOU, S. H., CHEN, M. H., CHEN, M. T., SHIH, Y. H., CHANG, C. H., HSU, C. C., MA, H. I., WANG, C. T., TSAI, L. L., YU, C. C. & CHANG, C. J. 2012. Resveratrol suppresses tumorigenicity and enhances radiosensitivity in primary glioblastoma tumor initiating cells by inhibiting the STAT3 axis. *J Cell Physiol,* **227,** 976-93.

YONEDA, A., USHAKOV, D., MULTHAUPT, H. A. & COUCHMAN, J. R. 2007. Fibronectin matrix assembly requires distinct contributions from Rho kinases I and -II. *Mol Biol Cell,* **18,** 66-75.

YUAN, B. Z., ZHOU, X., DURKIN, M. E., ZIMONJIC, D. B., GUMUNDSDOTTIR, K., EYFJORD, J. E., THORGEIRSSON, S. S. & POPESCU, N. C. 2003. DLC-1 gene inhibits human breast cancer cell growth and in vivo tumorigenicity. *Oncogene,* **22,** 445-50.

ZAIDEL-BAR, R., BALLESTREM, C., KAM, Z. & GEIGER, B. 2003. Early molecular events in the assembly of matrix adhesions at the leading edge of migrating cells. *J Cell Sci,* **116,** 4605-13.

ZAMIR, E., KATZ, B. Z., AOTA, S., YAMADA, K. M., GEIGER, B. & KAM, Z. 1999. Molecular diversity of cell-matrix adhesions. *J Cell Sci,* **112 (Pt 11),** 1655-69.

ZAMIR, E., KATZ, M., POSEN, Y., EREZ, N., YAMADA, K. M., KATZ, B. Z., LIN, S., LIN, D. C., BERSHADSKY, A., KAM, Z. & GEIGER, B. 2000. Dynamics and segregation of cell-matrix adhesions in cultured fibroblasts. *Nat Cell Biol,* **2,** 191-6.

ZHAO, H., RAMOS, C. F., BROOKS, J. D. & PEEHL, D. M. 2007. Distinctive gene expression of prostatic stromal cells cultured from diseased versus normal tissues. *J Cell Physiol,* **210,** 111-21.

ZHONG, C., CHRZANOWSKA-WODNICKA, M., BROWN, J., SHAUB, A., BELKIN, A. M. & BURRIDGE, K. 1998. Rho-mediated contractility exposes a cryptic site in fibronectin and induces fibronectin matrix assembly. *J Cell Biol,* **141,** 539-51.

ZHOU, X., ZIMONJIC, D. B., PARK, S. W., YANG, X. Y., DURKIN, M. E. & POPESCU, N. C. 2008. DLC1 suppresses distant dissemination of human hepatocellular carcinoma cells in nude mice through reduction of RhoA GTPase activity, actin cytoskeletal disruption and down-regulation of genes involved in metastasis. *Int J Oncol,* **32,** 1285-91.

ZHU, X., OZTURK, F., PANDEY, S., GUDA, C. B. & NAWSHAD, A. 2012. Implications of TGFbeta on transcriptome and cellular biofunctions of palatal mesenchyme. *Front Physiol,* **3,** 85.

APPENDICES

Smaller isoform cDNA clone in pSPORT1 vector (BC066788.1, Source BioScience Geneservice)

Double digest with EcroRI and BsmBI to produce 1123 bp containing 5' portion of Arhgap28 clone

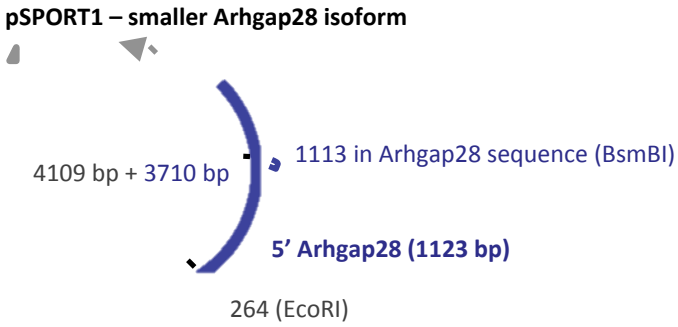

2. Amplify 3' end of endogenous mouse Arhgap28 transcript by PCR

PCR from endogenous BsmBI site to new BstBI site just before stop codon to produce 1209 bp product

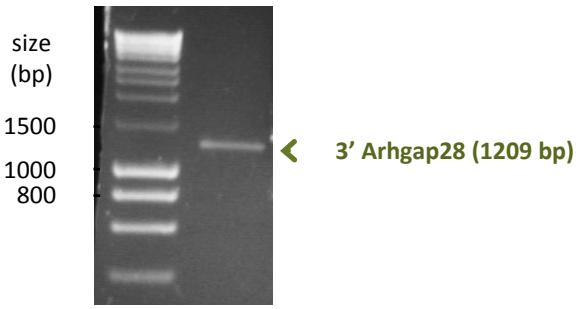

3. pcDNA6/V5-His vector C (invitrogen)

Double digest with EcroRI and BstBI to linearise vector

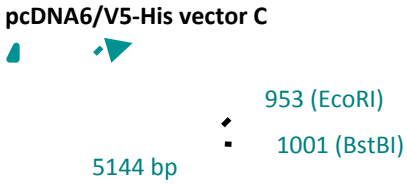

4. Ligation of all 3 gel-purified fragments together

Linearised pcDNA/V5-His + 5' end of Arhgap28 + 3' end of endogenously expressed Arhgap28

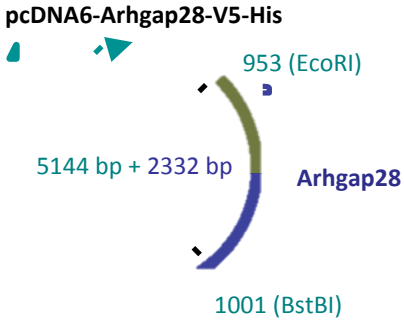

Appendix 1
Cloning of pcDNA6-Arhgap28-V5-His.
As described in section 2.5.

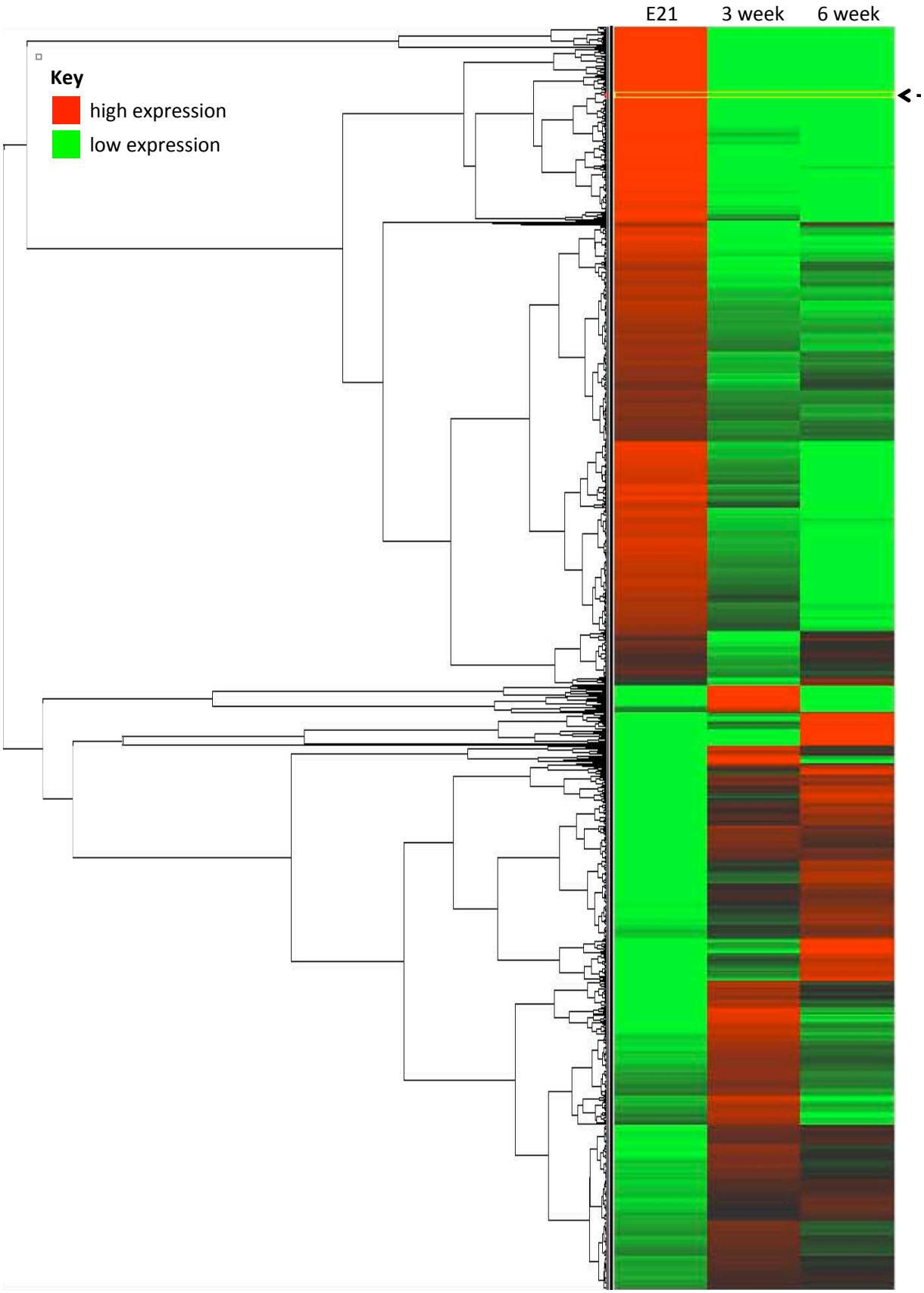

Appendix 2

Gene expression changes between embryonic and postnatal tendons.

Two-dimensional hierarchical cluster heat map analysis of the microarray readouts showing fold changes greater than 2 between E21 and 3 weeks postnatal. This type of clustering is based on similarities in the expression profiles and expression levels. Arrow points to the location of Arhgap28 Hierarchical clustering was performed using Cluster 3.0 software and visualised using Java TreeView.

Cluster components[A]	*p* value[B]	Matched genes[C]	Gene names (if annotated) of corresponding probe IDs in the GO list[D]
Annotation cluster 1, Enrichment score 13.26			
GO:0043228~ non-membrane-bounded organelle	1.90E-16	170	P2rx2, Mapk1, *1371450_AT*, Spag5, Sox11, *1396539_AT*, *1392742_AT*, Tpr, Ncaph, *1380653_AT*, Tmpo, Polr1a, Tobp1, *1377175_AT*, Epb4.1l3, Pold1, *1379116_AT*, Smc4, Cdk5rap2, Hnrnpa1, *1397481_AT*, RGD1561360, Ophn1, Chek1, Ncapd2, Fbxo5, Kif20a, Hmgb2, Ka15, Cgnl1, Rbm4b, *1390723_AT*, Utx, Rbm39, Smc1a, Nol8, Dlgap1, Ndn, *1396420_AT*, Tuba4a, Actn1, Cdca1, Klhdc3, Top2a, Krt5, *1383332_AT*, Mki67, *1371756_AT*, Espl1, Krt10, P2rx2, Lmnb1, *1372708_AT*, Dsp, Tnks2, Atp1b4, *1397489_AT*, Zwint, Fancd2, Krt1-14, *1372777_AT*, Ikbkap, Xpo1, LOC685179, RGD1305846, Cenpe, Chd1, Srpk2, *1381590_AT*, RGD1561740, *1396437_AT*, *1395613_AT*, *1393649_AT*, *1396641_AT*, Lmnb2, Incenp, Spbc25, Ckap5, RGD1565341, Nefh, Atrx, Timeless, Igf2bp2, Cenpn, *1398695_AT*, Myh10, *1394646_AT*, Pdcd6ip, *1381517_AT*, *1379830_AT*, Kif20b, Nol5, Myh3, *1378671_AT*, *1375518_AT*, LOC290704, *1376405_AT*, Epb4.1l3, Dlgap1, Mdc1, Smarca4, LOC690123, Stfa3, Tacc3, Rad51, *1375661_AT*, *1397779_AT*, *1388944_AT*, Ka17, Kif15, *1398000_AT*, Fntb, *1392607_AT*, Igf2bp2, Kif2c, Anln, Krt1-12, Actr10, Utx, Nol5, Decr2, Adarb1, Cenpj, Phr1, Ncor1, Pspc1, Rif1, *1380087_AT*, *1397449_AT*, Aspm, Krt1, Sept6, Rhoq, Krt78, Chd1, Numa1, Suv39h2, Sept6, Mad2l1, Bub1b, Tobp1, Aurkb, Smc3, *1397745_AT*, *1382229_AT*, Nup160, Nfib, Hells, *1381141_AT*, Cenpq, Ccnb1, Satb1, *1390737_AT*, Rif1, Recc1, *1395092_AT*, Baz1b, *1380763_AT*, *1376374_AT*, Nolc1, RGD1310778, RGD1563577, Map2, Cnfn, *1389955_AT*, Pola1, Hspa9, Kif1b, RGD1560863, Mpdz, *1372874_AT*, Dlg7, Zfp57, Baz1b, Sox11, Dscc1, Myc, *1376005_AT*, *1391373_AT*, *1385944_AT*, Top2a, Csnk2a1, Blm, *1382587_AT*, *1397240_AT*, Cdc45l, Kif11, *1375404_AT*, Cep250, Fam33a, Cenpt, Tnnt2, *1391464_AT*, Freq, Lor, Dnmt1, *1397324_AT*, Satb1, Actc1, *1380807_AT*, *1392311_AT*, Mcm2, *1396017_AT*, LOC690043, Prpf4b, C2cd3, Mcm3, Hipk2, Bub1
GO:0043232~ intracellular non-membrane-bounded organelle	1.90E-16	170	P2rx2, Mapk1, *1371450_AT*, Spag5, Sox11, *1396539_AT*, *1392742_AT*, Tpr, Ncaph, *1380653_AT*, Tmpo, Polr1a, Tobp1, *1377175_AT*, Epb4.1l3, Pold1, *1379116_AT*, Smc4, Cdk5rap2, Hnrnpa1, *1397481_AT*, RGD1561360, Ophn1, Chek1, Ncapd2, Fbxo5, Kif20a, Hmgb2, Ka15, Cgnl1, Rbm4b, *1390723_AT*, Utx, Rbm39, Smc1a, Nol8, Dlgap1, Ndn, *1396420_AT*, Tuba4a, Actn1, Cdca1, Klhdc3, Top2a, Krt5, *1383332_AT*, Mki67, *1371756_AT*, Espl1, Krt10, P2rx2, Lmnb1, *1372708_AT*, Dsp, Tnks2, Atp1b4, *1397489_AT*, Zwint, Fancd2, Krt1-14, *1372777_AT*, Ikbkap, Xpo1, LOC685179, RGD1305846, Cenpe, Chd1, Srpk2, *1381590_AT*, RGD1561740, *1396437_AT*, *1395613_AT*, *1393649_AT*, *1396641_AT*, Lmnb2, Incenp, Spbc25, Ckap5, RGD1565341, Nefh, Atrx, Timeless, Igf2bp2, Cenpn, *1398695_AT*, Myh10, *1394646_AT*, Pdcd6ip, *1381517_AT*, *1379830_AT*, Kif20b, Nol5, Myh3, *1378671_AT*, *1375518_AT*, LOC290704, *1376405_AT*, Epb4.1l3, Dlgap1, Mdc1, Smarca4, LOC690123, Stfa3, Tacc3, Rad51, *1375661_AT*, *1397779_AT*, *1388944_AT*, Ka17, Kif15, *1398000_AT*, Fntb, *1392607_AT*, Igf2bp2, Kif2c, Anln, Krt1-12, Actr10, Utx, Nol5, Decr2, Adarb1, Cenpj, Phr1, Ncor1, Pspc1, Rif1, *1380087_AT*, *1397449_AT*, Aspm, Krt1, Sept6, Rhoq, Krt78, Chd1, Numa1, Suv39h2, Sept6, Mad2l1, Bub1b, Tobp1, Aurkb, Smc3, *1397745_AT*, *1382229_AT*, Nup160, Nfib, Hells, *1381141_AT*, Cenpq, Ccnb1, Satb1, *1390737_AT*, Rif1, Recc1, *1395092_AT*, Baz1b, *1380763_AT*, *1376374_AT*, Nolc1, RGD1310778, RGD1563577, Map2, Cnfn, *1389955_AT*, Pola1, Hspa9, Kif1b, RGD1560863, Mpdz, *1372874_AT*, Dlg7, Zfp57, Baz1b, Sox11, Dscc1, Myc, *1376005_AT*, *1391373_AT*, *1385944_AT*, Top2a, Csnk2a1, Blm, *1382587_AT*, *1397240_AT*, Cdc45l, Kif11, *1375404_AT*, Cep250, Fam33a, Cenpt, Tnnt2, *1391464_AT*, Freq, Lor, Dnmt1, *1397324_AT*, Satb1, Actc1, *1380807_AT*, *1392311_AT*, Mcm2, *1396017_AT*, LOC690043, Prpf4b, C2cd3, Mcm3, Hipk2, Bub1
GO:0005856~ cytoskeleton	2.37E-12	99	*1383997_AT*, P2rx2, Spag5, *1396539_AT*, *1392742_AT*, *1380653_AT*, Ka17, Kif15, *1398000_AT*, Fntb, *1392607_AT*, Epb4.1l3, Igf2bp2, *1379116_AT*, Cdk5rap2, Kif2c, Anln, Krt1-12, Actr10, *1397481_AT*, Ophn1, Fbxo5, Kif20a, Ka15, Cgnl1, Cenpj, Ncor1, Phr1, *1390723_AT*, Rbm39, Dlgap1, Ndn, *1397449_AT*, Aspm, Tuba4a, Krt1, Sept6, Rhoq, Actn1, LOC685672, Numa1, Krt78, Top2a, Krt5, *1383332_AT*, Mad2l1, *1371756_AT*, Espl1, Krt10, P2rx2, Aurkb, Lmnb1, Smc3, *1397745_AT*, Dsp, *1382229_AT*, Tnks2, *1397489_AT*, *1381141*_AT, Ccnb1, Krt1-14, *1390737_AT*, *1372777_AT*, Cenpe, *1395092_AT*, *1381590_AT*, RGD1561740, *1396437_AT*, *1380763_AT*, *1395613_AT*, *1376374_AT*, Cnfn, Ophn1, Map2, Lmnb2, Incenp, Ckap5, Kif1b, Nefh, Mpdz, *1372874_AT*, Igf2bp2, Dlg7, Myc, *1398695_AT*, *1376005_AT*, Myh10, *1391373_AT*, *1385944_AT*, Top2a, *1382587_AT*, Pdcd6ip, *1397240_AT*, Cdc45l, Kif11, *1381517_AT*, *1375404_AT*, Kif20b, Cep250, Myh3, Fam33a, Tnnt2, Freq, Lor, *1376405_AT*, *1397324_AT*, LOC290704, Actc1, *1380807_AT*, *1392311_AT*, Epb4.1l3, Dlgap1, *1396017_AT*, Mdc1, C2cd3, Mcm3, Hipk2, Stfa3, Tacc3
GO:0044430~ cytoskeletal part	4.34E-11	78	*1381141_AT*, P2rx2, Sapg5, Ccnb1, Krt1-14, *1396539_AT*, *1390737_AT*, *1392742_AT*, Cenpe, *1380653_AT*, Ka17, Kif15, *1381590_AT*, RGD1561740, Fntb, Igf2bp2, *1396437_AT*, *1395613_AT*, *1376374_AT*, Cdk5rap2, Kif2c, Map2, Anln, Lmnb2, Incenp, Actr10, Krt1-12, *1397481_AT*, Kif1b, Nefh, Fbxo5, Kif20a, Mpdz, Ka15, *1372874_AT*, Igfbp2, Dlg7, Cenpj, Ncor1, Myc, *1398695_AT*, *1376005_AT*, Myh10, *1391373_AT*, *1385944_AT*, Top2a, Dlgap1, Ndn, *1382587_AT*, Pdcd6ip, *1397449_AT*, Aspm, *1397240_AT*, Tuba4a, Cdc45l, Krt1, *1381517_AT*, Kif11, Sept6, Actn1, Rhoq, Kif20b, Krt78, Cep250, Myh3, Numa1, Fam33a, Tnnt2, Freq, Sept6, Top2a, Krt5, *1383332_AT*, Mad2l1, *1371756_AT*, LOC290704, *1376405_AT*, Krt10, Espl1, Actc1, *1380807_AT*, Aurkb, P2rx2, Lmnb1, Dlgap1, Smc3, *1397745_AT*, C2cd3, Mcm3, Hipk2, Tnks2, *1397489_AT*, Tacc3

Appendix 3

Genes of the top annotation cluster produced by gene ontology analysis.

Annotation cluster analysis of probe sets detecting a significant fold change greater than -2 from E21 to 3 weeks postnatal ($q < 0.01$) produced 243 clusters. The top annotation cluster with the highest enrichment score is shown here. **(A)** The top gene ontology components of this cluster. **(B)** The statistical significance of this grouping where the lower the score the more unlikely this clustering is due to chance. **(C)** The number of probe sets that recognise genes contributing to the gene ontology term. **(D)** List of gene names of the Affymetrix Rat Genome 230 2.0 array probe IDs. Where genes have not been annotated, the probe ID is set in italic.

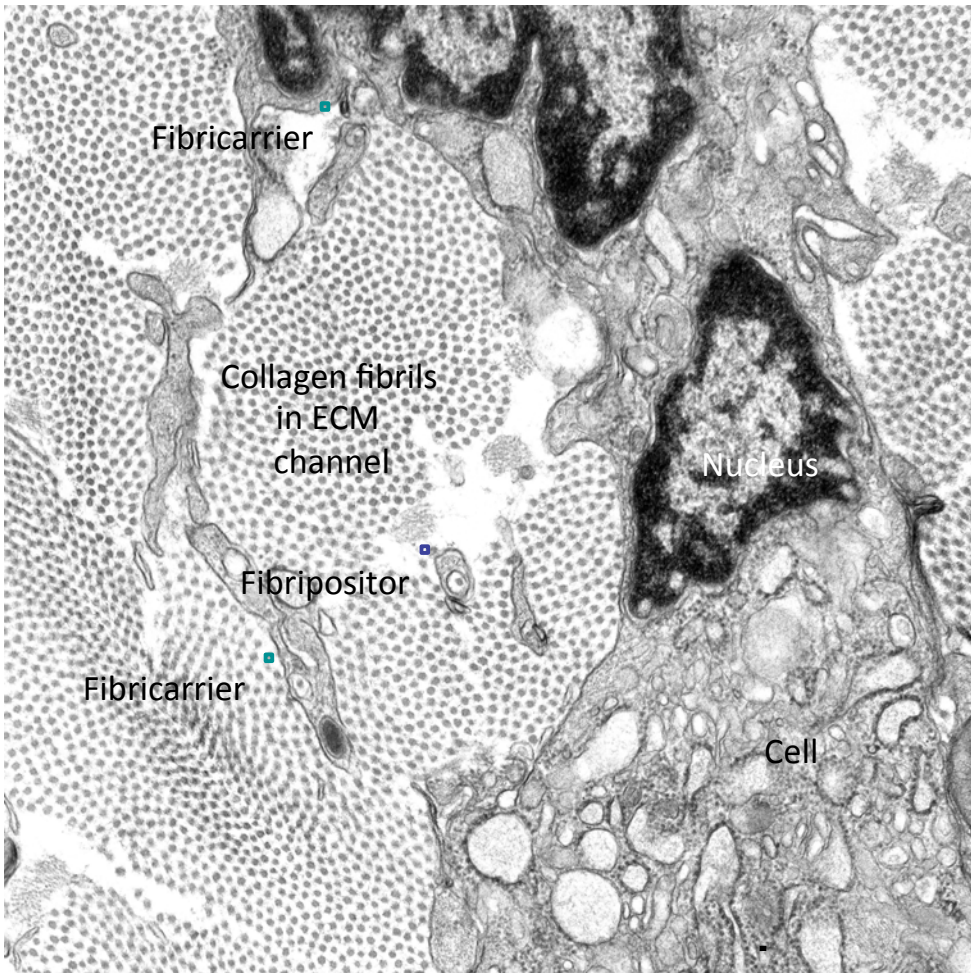

Appendix 4
P0 mouse tail tendon retain embryonic characteristics.
Representative micrograph of a transverse section of P0 mouse tail tendon examined by TEM. Bars= 1 µm.

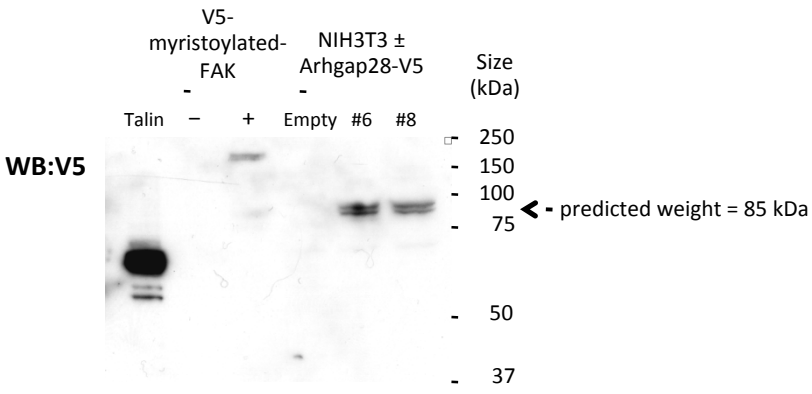

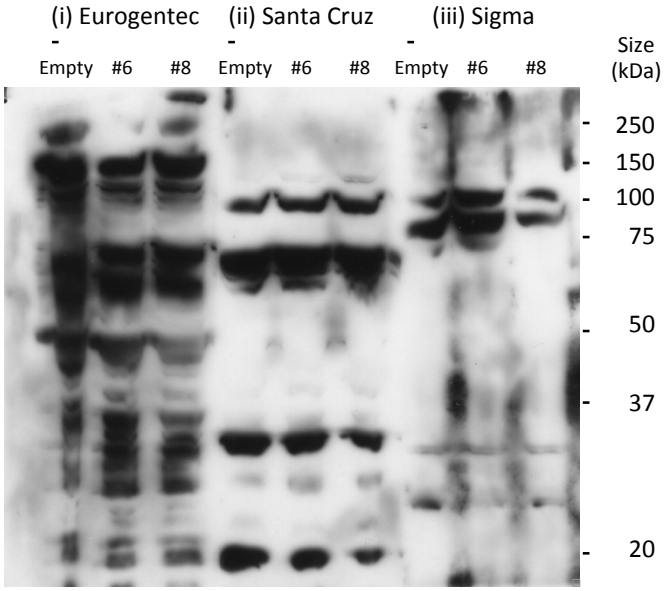

Appendix 5

Arhgap28 antibodies tested are not specific.

Lysates isolated from NIH3T3 cells transiently transfected with empty vector or murine Arhgap28-V5 clone (replicates #6 and #8) were analysed by western blotting. Antibodies to V5 detected a band of the predicted molecular weight only in lysates from the replicates #6 and #8 (from Figure 16C). The lysates were also blotted with antibodies diluted 1:1000 following methods described in section 2.6.3:

(i) custom made, affinity purified rabbit polyclonal antibody raised to MPDRNKWKKSDIKKE (residues 303-317, 633 aa residues before the start of the RhoGAP domain) of murine Arhgap28 (Eurogentec),

(ii) commercially available, rabbit polyclonal antibody raised to an internal region of Arhgap28 of human origin (SC-84697, Santa Cruz Biotechnology), or

(iii) commercially available, rabbit polyclonal antibody raised to KEGSFAVPRSDSVAILETIPVLPVHSNGS PEPGQPVQNAISDDDFLEKNI(residues 71-120) of human Arhgap28 (SAB2103052; Sigma).

```
          1                                                          50
 Wild Type MEVEDSGGVV LTAYHSHARS QPQGAEPRCA SRASHPLSRK SIPRCRRINR
 Predicted MEVEDSGGVV LTAYHSHARS QPQGAEPRCA SRASHPLSRK SIPRCRRINR
Arhgap28del MEVEDSGGVV LTAYHSHARS QPQGAEPRCA SRASHPLSRK SIPRCRRINR

         51                                                         100
 Wild Type MLSNESLHPP SFSRSNSQAS VDSSASMEEF LREIESIKES SVGASQEQPP
 Predicted MLSNESLHPP SFSRSNSQAS VDSSASMEEF LREIESIKES SVGASQEQPP
Arhgap28del MLSNESLHPP SFSRSNSQAS VDSSASMEEF LREIESIKES SVGASQEQPP

        101                                                         150
 Wild Type TAAAAAAEVK PVDEGELEAE WLQDVGLSTL ISGNEEEDGK ALLSTLTRTQ
 Predicted TAAAAAAEVK PVDEGELEAE WLQDVGLSTL ISGNEEEDGK ALLSTLTRTQ
Arhgap28del TAAAAAAEVK PVDEGELEAE WLQDVGLSTL ISGNEEEDGK ALLSTLTRTQ

        151                                                         200
 Wild Type AAAVKKRYNT YTQTLRKKNK QPVRDVRDIF GVSESPPSDS CEHATQLDGT
 Predicted AAAVKKRYNT YTQTLRKKNK QPVRDVRDIF GVSESPPSDS CEHATQLDGT
Arhgap28del AAAVKKRYNT YTQTLRKKNK QPVRDVRDIF GVSESPPSDS CEHATQLDGT

        201                                                         250
 Wild Type KEEKDLPGVT KTSRPLPDDA SLSSTTLSNG AQDEEGGFVA LQSGSVSILE
 Predicted KEEKDLPGVT KTSRPLPDDA SLSSTTLSNG AQDEEGGFVA LQSGSVSILE
Arhgap28del KEEKDLPGVT KTSRPLPDDA SLSSTTLSNG AQDEEGGFVA LQSGSVSILE

        251              end of EXON 6↓                             300
 Wild Type AIPDIAVHTN GSADAEQSVQ STLSDDDYHG KNVPAEAEEL SFEVSYSEMV
 Predicted AIPDIAVHTN GSADAEQSVQ STLSVFSESR GIRSGIGRNF STLGMYCQSQ
Arhgap28del AIPDIAVHTN GSADAEQSVQ STLSGPRSRK PKKKNPNKED KRPRTAFTAE

        301                                                         350
 Wild Type TEMPDRNKWK KSDIKKEDYV LTKFIIQKTR FGLTETGDLS VEDMKKIRHL
 Predicted AVPRRTGCQV QC-
Arhgap28del QLQRLKAEFQ TNSFFRKSRN QVWNRKEFFD SRDVLPKSSS TAKNWMPGSM

        351                                  ↓start of GAP domain 400
 Wild Type SLIELTAFFD AFGIQLKRNK TERVRGRDNG IFGVPLTVLL DNDRKKDPAV
Arhgap28del LTSSSGTRCV TEKLRSC-

        401                                                         450
 Wild Type KVPLVLQKFF QKVEESGLES EGIFRLSGCT AKVKQYREEL DARFNADKFK

        451                                                         500
 Wild Type WDKMCHREAA VMLKAFFREL PTSLFPVEYI PAFISLMERG PDIKVQFQAL

        501                                                         550
 Wild Type HLMVMALPDA NRDTAQALMA FFNKVIANES KNRMNLWNIS TVMAPNLFFS

        551                                                         600
 Wild Type RSKHSDCEEL LLANTATHII RLMLKYQKIL WKVPSFLITQ VRRMNEATML

        601                                                         650
 Wild Type LKKQLPSMKK LLRRKTLDRE VSILKTSKVP QKSPSSRRMS DVPEGVIRVH

        651                                                         700
 Wild Type APLLSKVSMA IQLNSQTKAK DILAKFQYEN SHGSSEHIKM QNQRLYEVGG

        701                                  729
 Wild Type NIGQHCLDPD AYILDVYHIN PHAEWVIKP-
```

Appendix 6

Sequences of Arhgap28 transcripts.

Predicted amino acid sequences of Arhgap28 from wild type, predicted *Arhgap28^{del}*, actual *Arhgap28^{del}* transcripts. Sequence in blue a result of remainder sequence from Cre-medated recombination. Sequence in green is the RhoGAP domain.

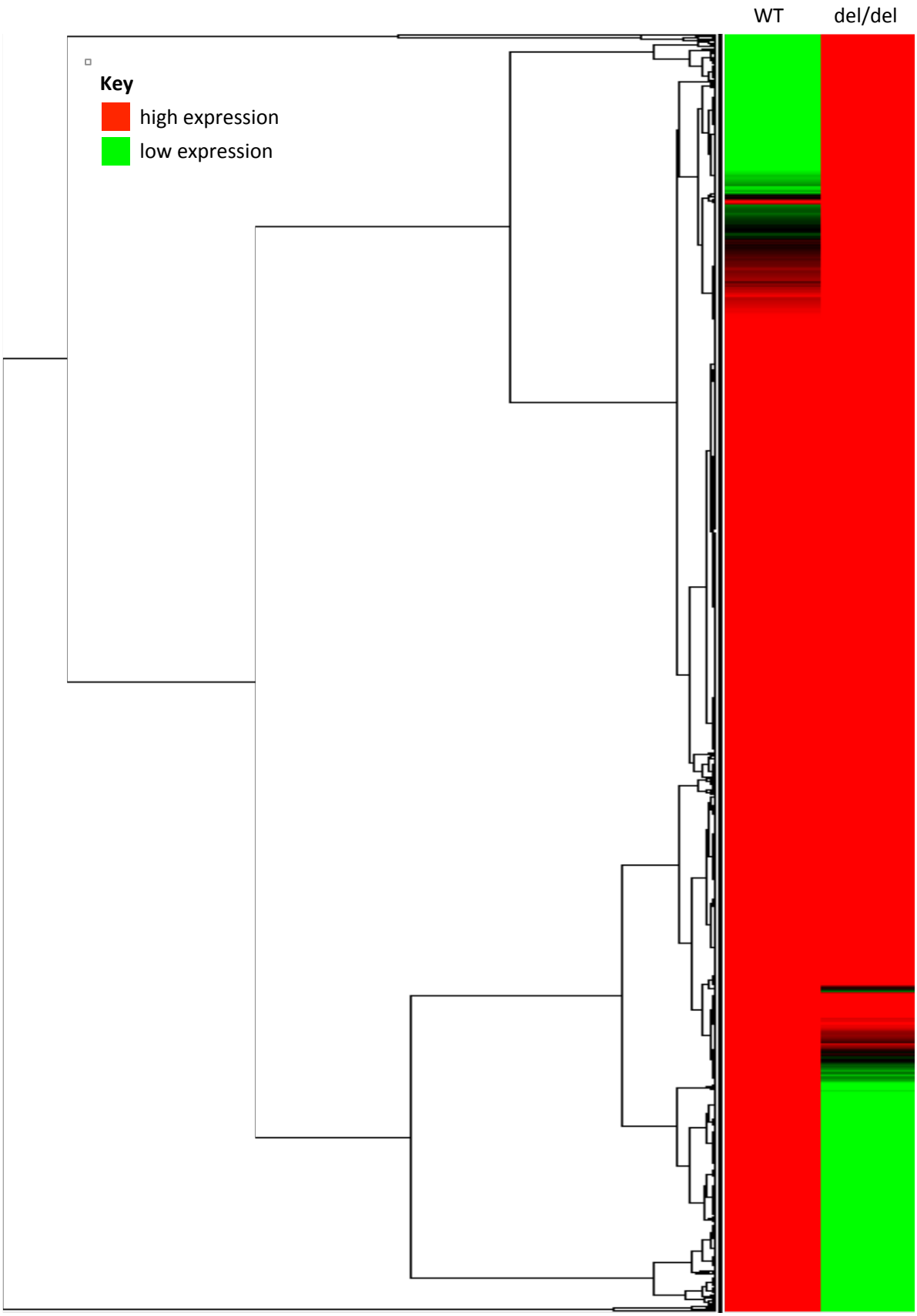

Appendix 7

Gene expression changes between P0 wild type and *Arhgap28*$^{del/del}$ bones.

Two-dimensional hierarchical cluster heat map analysis of the microarray readouts for all probe sets. This type of clustering is based on similarities in the expression profiles and expression levels. Hierarchical clustering was performed using Cluster 3.0 software and visualised using Java TreeView.